2019 Fall

"Advanced Physical Metallurgy"

- Non-equilibrium Solidification -

12.10.2019

Eun Soo Park

Office: 33-313
Telephone: 880-7221
Email: espark@snu.ac.kr
Office hours: by appointment

Deformation modes

Plastic deformation

(γ', τ, T)

F. Spaepen : Free volume theory

Homogeneous flow @ <u>steady state</u>

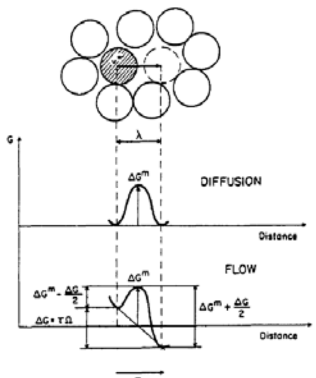

Inhomogeneous flow @ <u>steady state</u>

Competition of shear-induced disordering and a diffusion controlled reordering;

creation of FV vs. relaxation

$\Delta v_f^+ = \Delta v_f^-$

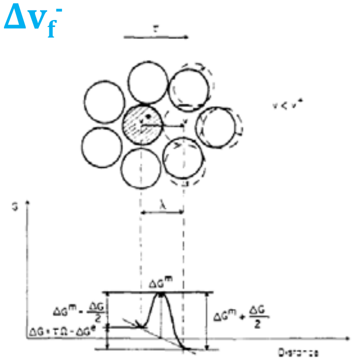

A. S. Argon / C. A. Schuh: STZ model

Homogeneous plastic flow

Viscous flow of a SCL

Steady-state flow

Structural disordering과 ordering,
즉 free volume creation과 annihilation 사이의 균형.
$\Delta v_f^+ = \Delta v_f^-$
Local diffusive jump 또는 STZ operation이 stress를 분산시키고, dilatation을 통해 free volume을 만들지만 동시에 relaxation이 진행되어 free volume을 없앤다.
Structural maintanance

Non-steady-state flow

Structural transience가 일어남.
균형이 이루어지지 않아 net gain / loss of free volume이 일어날 수 있다.
"overshoot" "undershoot"

Inhomogeneous plastic flow

Localization → Shear band formation
local production of FV (dilatation)
local evolution of structural order due to STZ operation
redistribution of internal stresses

Deformation mode of bulk metallic glasses

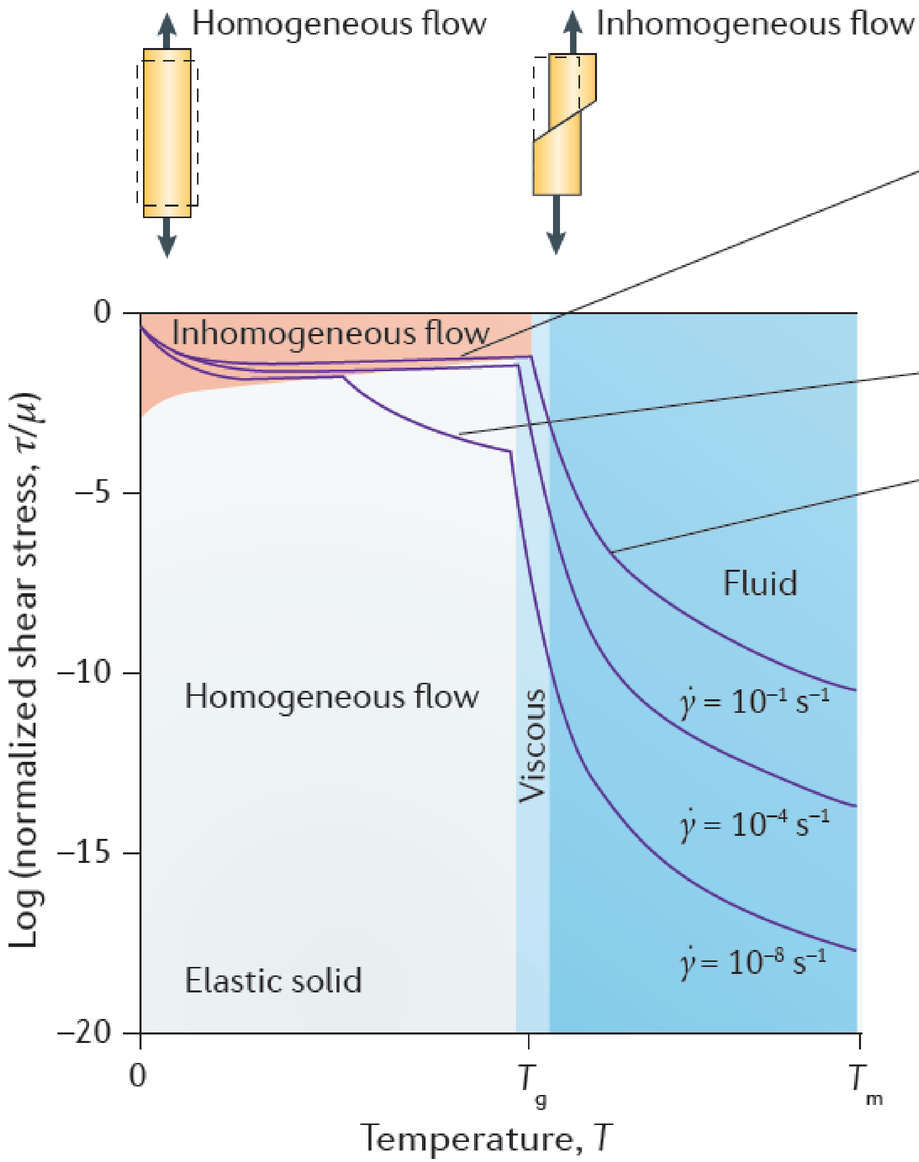

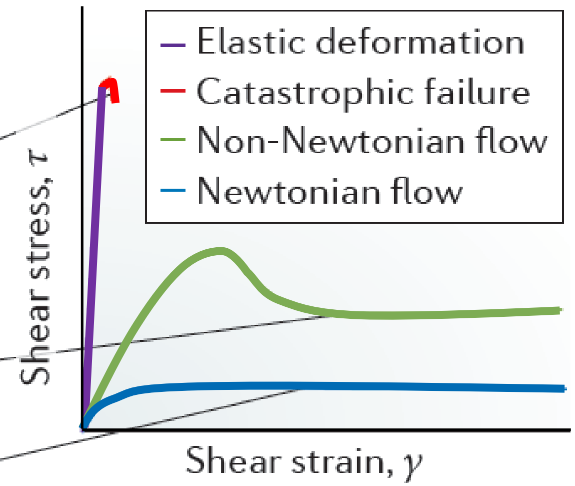

(1) Elastic deformation

- Elastic + anelastic component

(2) Homogeneous deformation

- Newtonian flow
- Non-Newtonian flow

(3) Inhomogeneous deformation

- ‘Shear banding’ or shear localization

Spaepen, Acta Metall. 25 (1977) 407.
Sun et al., Nature Rev. Mater. 1 (2016) 16039.

Deformation behavior of nanoscale metallic glass

Bulk metallic glass

(Brittleness, Strength ~*0.02E*)

Nanoscale metallic glass

(The smaller is the stronger,
and be also more ductile!)

▸ **Sample size effect on the strength and elastic limit of metallic glasses**

Wang et al., Acta. Mater. 60 (2012) 5370.

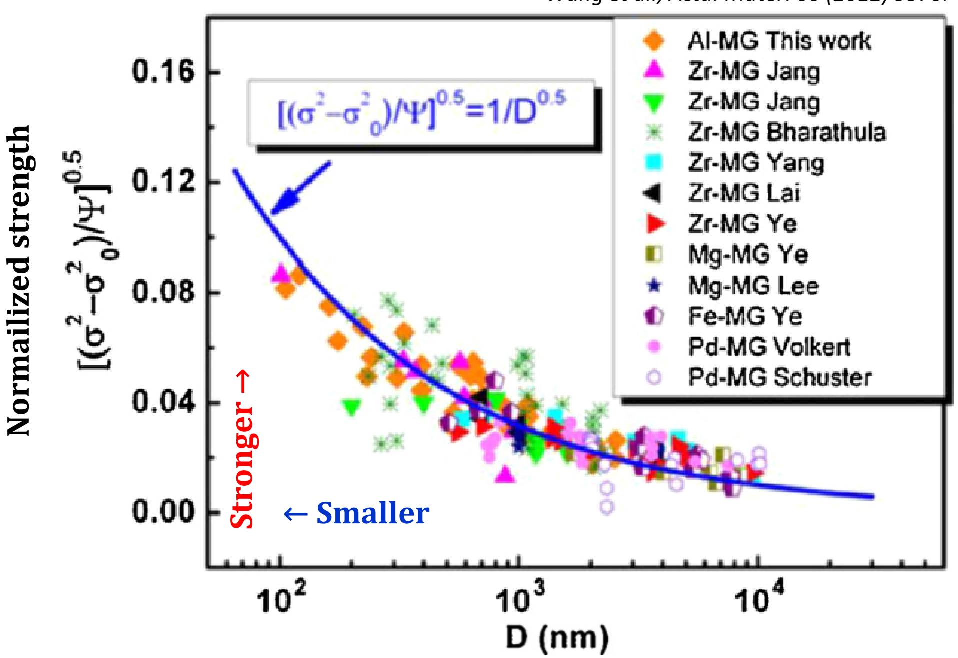

Tian et al., Nature Comm. 3 (2012) 609.

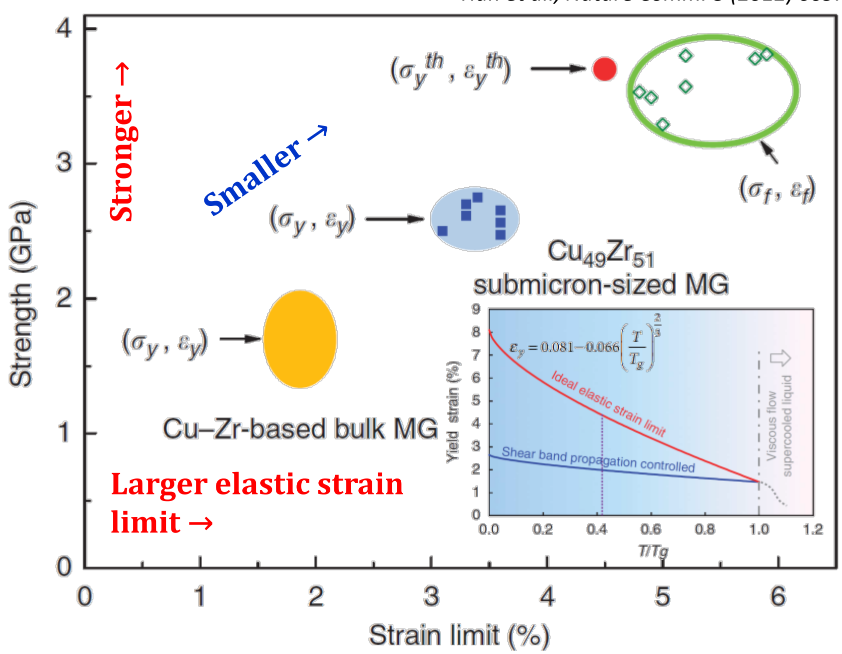

III. Construction of deformation map of nanoscale metallic glasses

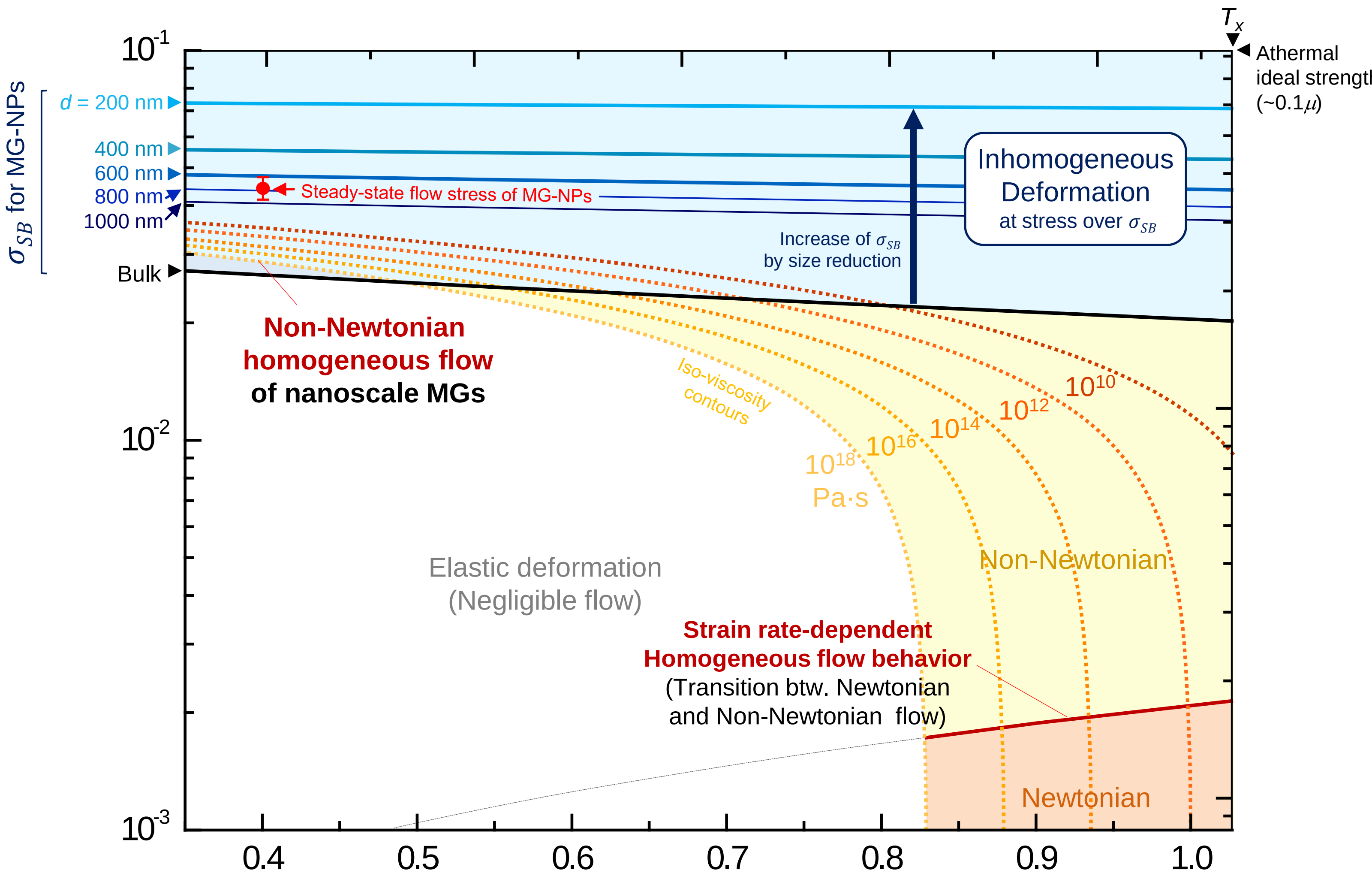

Limited Plasticity by shear softening and shear band

- **Microscopically brittle fracture**

  ➡ **Death of a material for structural applications**

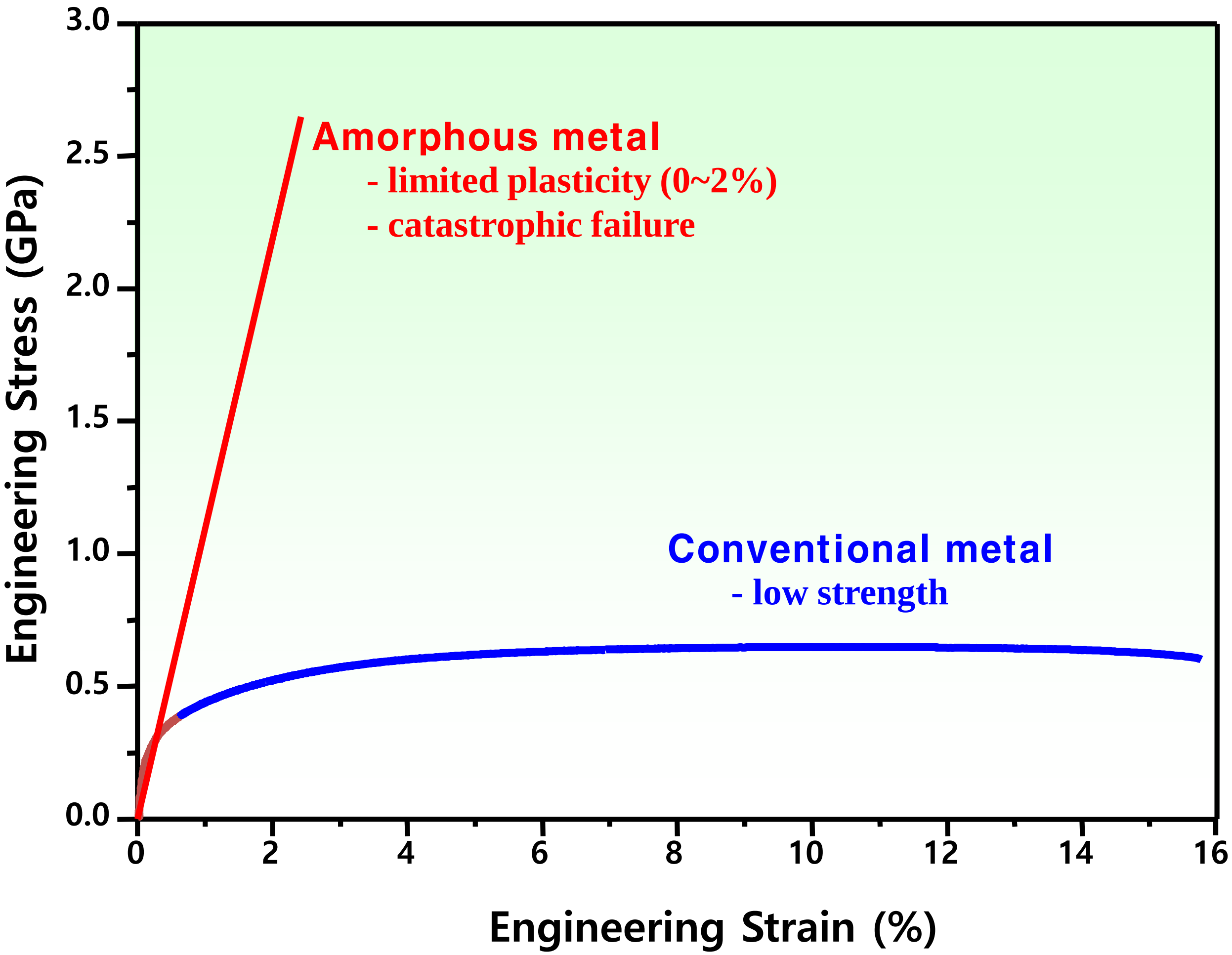

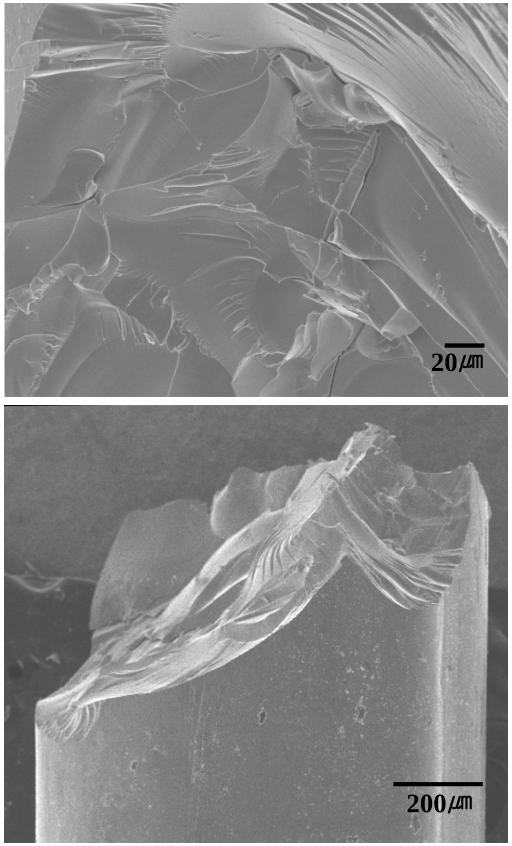

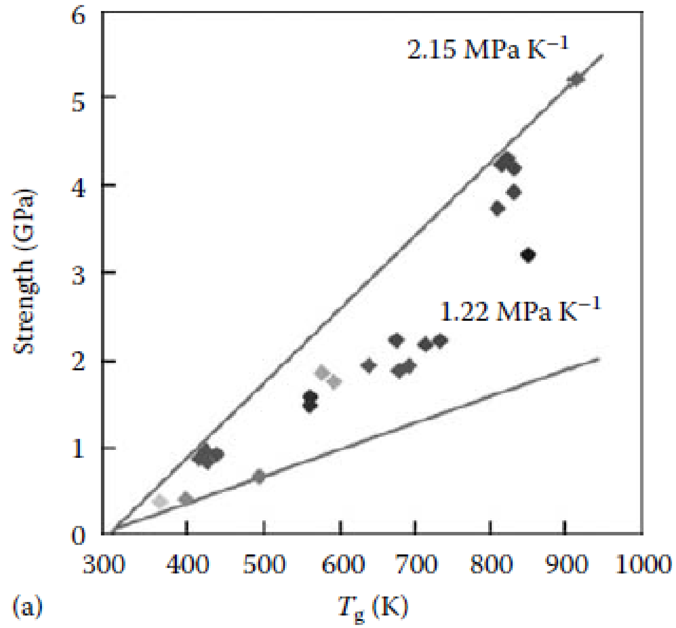

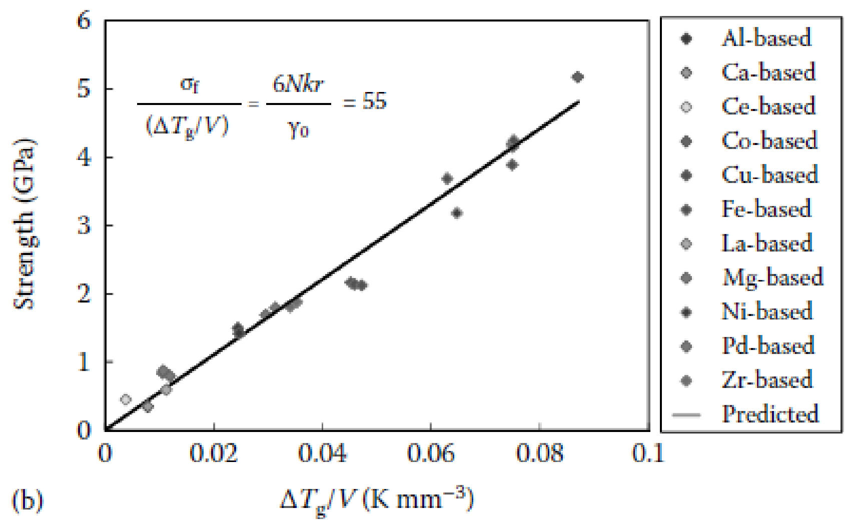

FIGURE 8.11
(a) Variation of strength with glass transition temperature, T_g for a number of BMGs. (b) Relationship between the calculated fracture strength from a free-volume model and the ratio of $\Delta T_g/V$ for a variety of BMGs. (Reprinted from Yang, B. et al., *Appl. Phys. Lett.*, 88, 221911-1, 2006. With permission.)

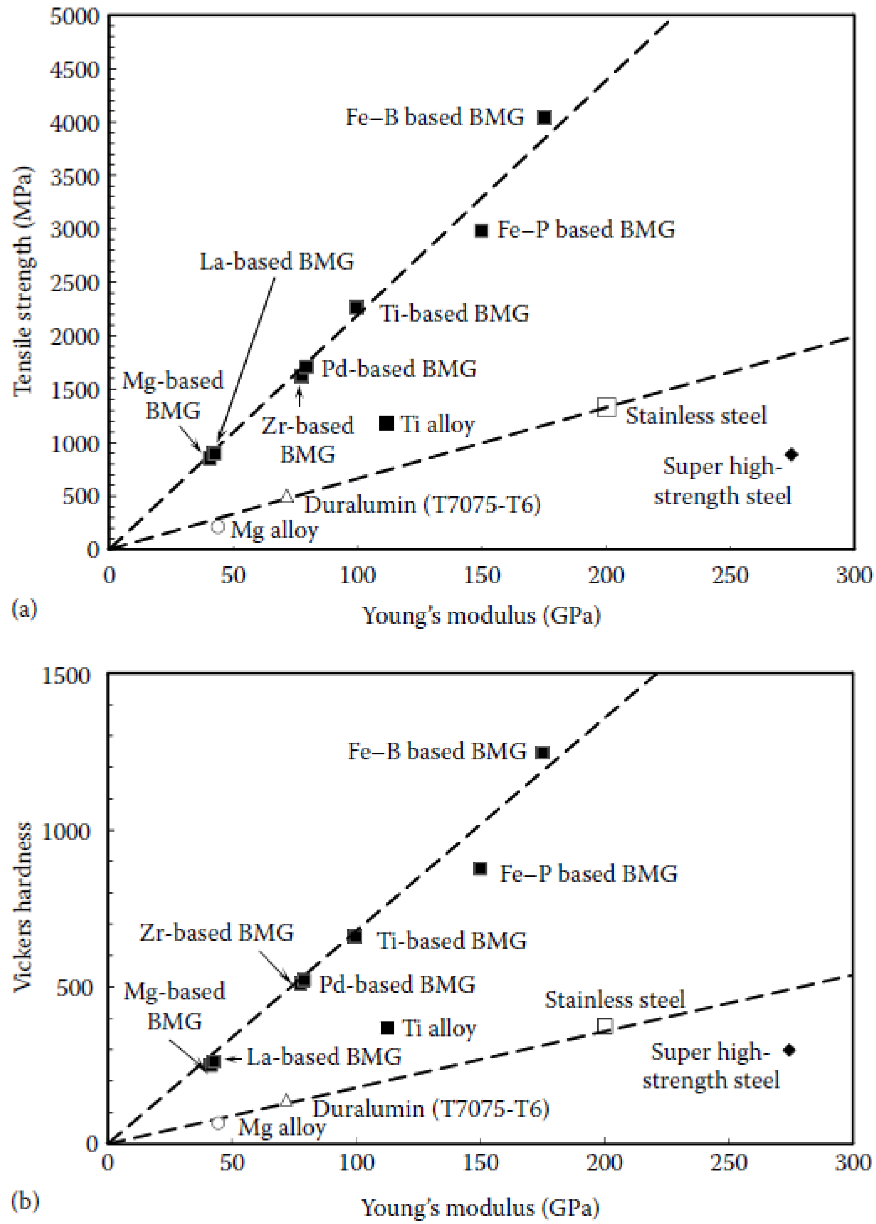

FIGURE 8.13
Relationship between (a) tensile strength and Young's modulus and (b) Vickers hardness and Young's modulus for some typical BMGs. The data for crystalline alloys are also shown for comparison. (Reprinted from Inoue, A., *Acta Mater.*, 48, 279, 2000. With permission.)

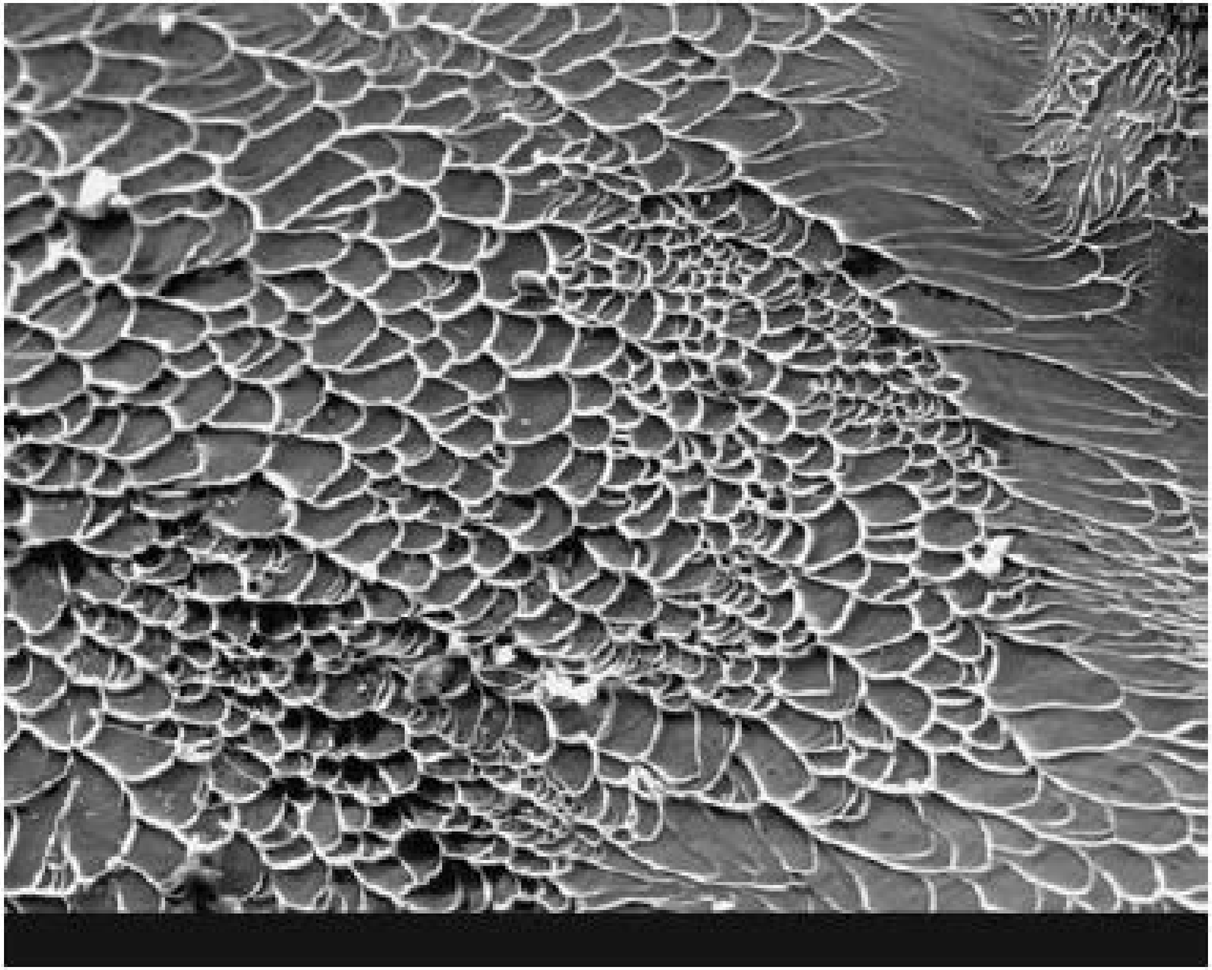

FIGURE 8.27
Scanning electron micrograph of the fractured surface of a bulk metallic glass alloy specimen. Note the vein pattern, which is typical of many metallic glasses that fracture along a shear band. Such microstructures are obtained both in tension and compression.

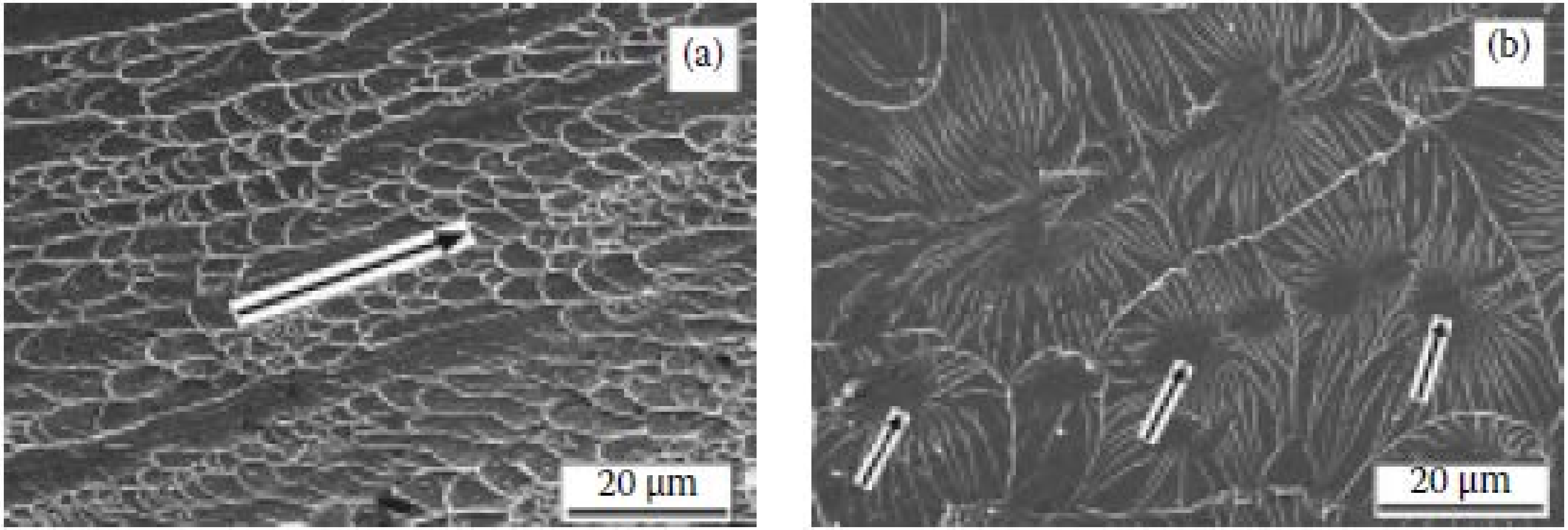

FIGURE 8.28
Comparison of the fracture surfaces of $Zr_{59}Cu_{20}Al_{10}Ni_8Ti_3$ BMG alloy that has failed under (a) compressive loading and (b) tensile loading. Notice that the specimen that has failed under compressive loading exhibits vein-like pattern while the specimen that had failed in tension shows round cores with vein-like features radiating outward from their centers. The arrow in (a) shows the shear direction, while the arrows in (b) indicate the location of the round cores. (Reprinted from Zhang, Z.F. et al., *Acta Mater.*, 51, 1167, 2003. With permission.)

What governs plasticity in metallic glasses?

Plastic deformation in metallic glasses

Plastic deformation in metallic glass

- *N*o dislocation / *N*o slip plane
- Inhomogeneously localized plastic flow in the shear band

interrupt the localization of stress and deformation

- Prevent propagation of single shear band ➡ BMG matrix composites
- Multiple shear band formation

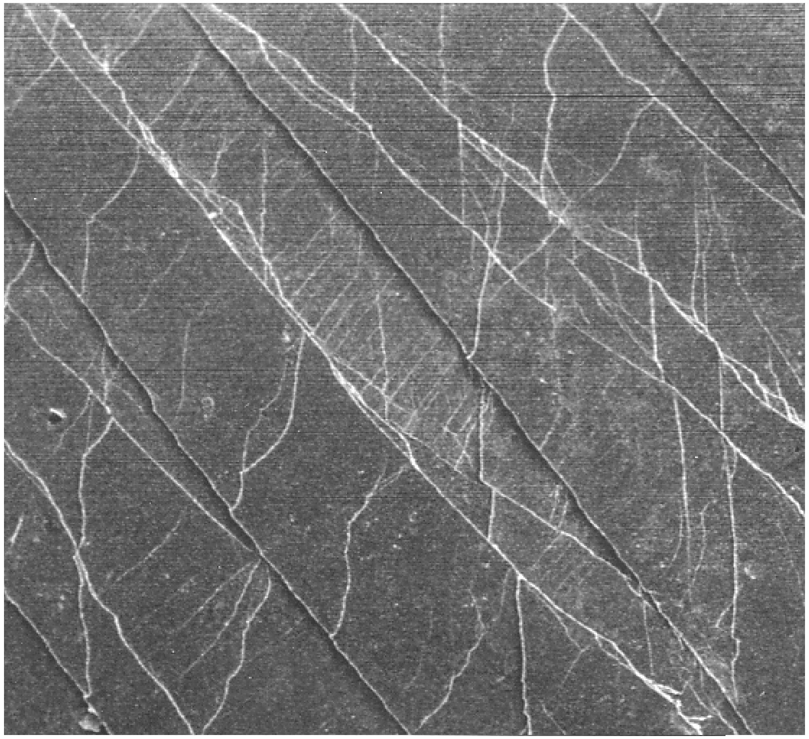

Ex-situ BMG matrix composites

1) Casting : hard/ductile particle

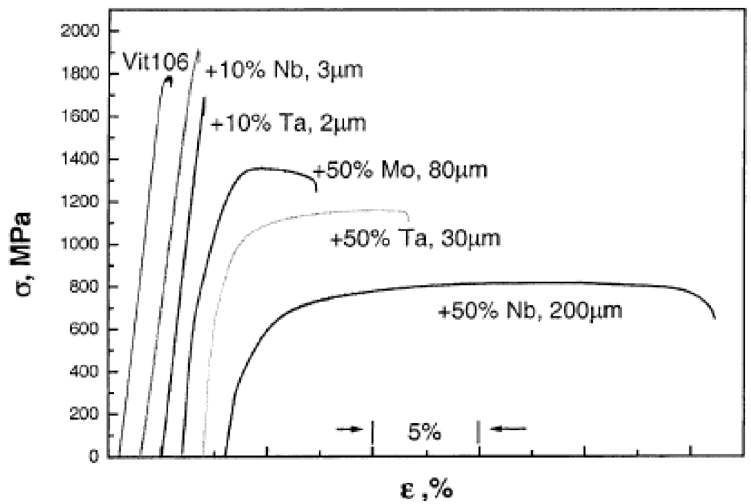

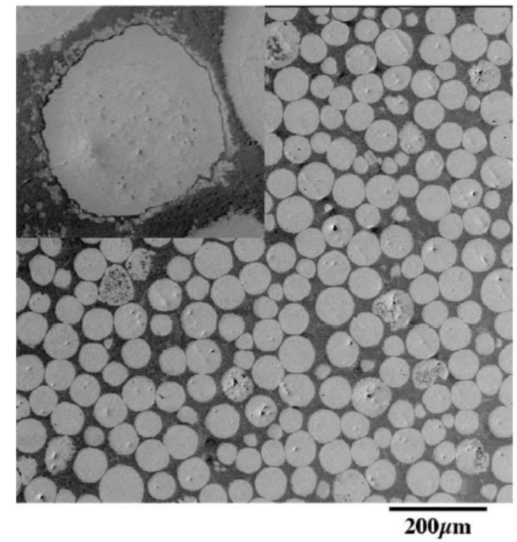

(Johnson et al., Acta Mater.,1999)

2) Extrusion : ductile powder

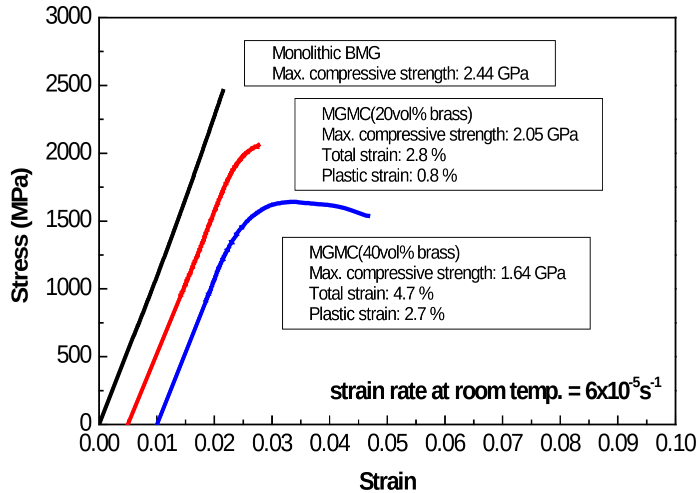

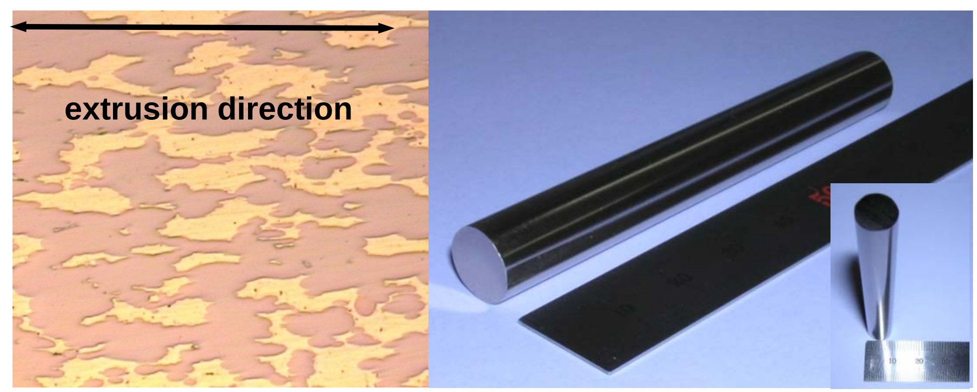

(Kim et al., J. Non-cryst. Solids, 2002)

In-situ BMG matrix composites

1) Solidification : formation of primary ductile phase

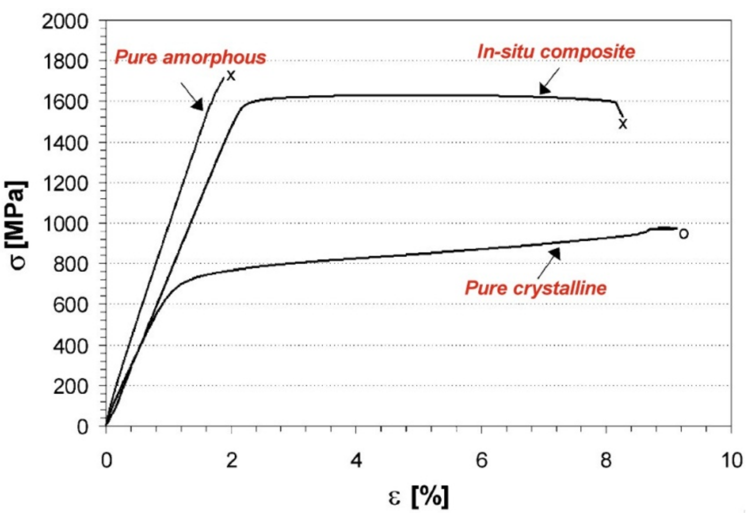

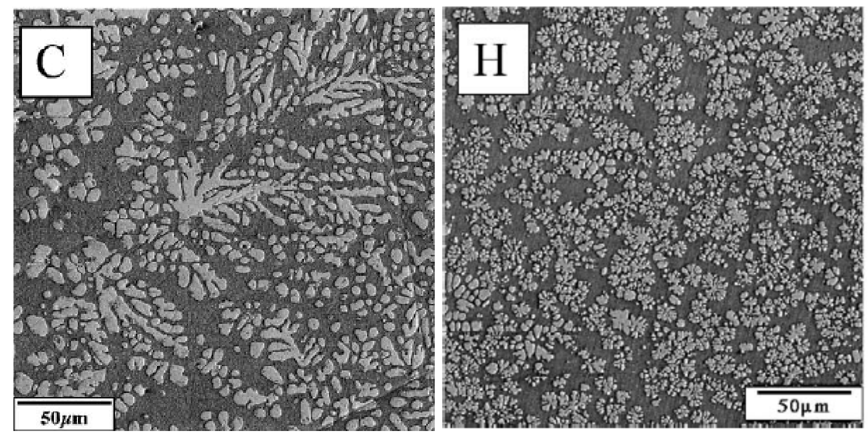

(Johnson et al., Acta Mater., 2001)

2) Solidification : precipitation of ductile phase

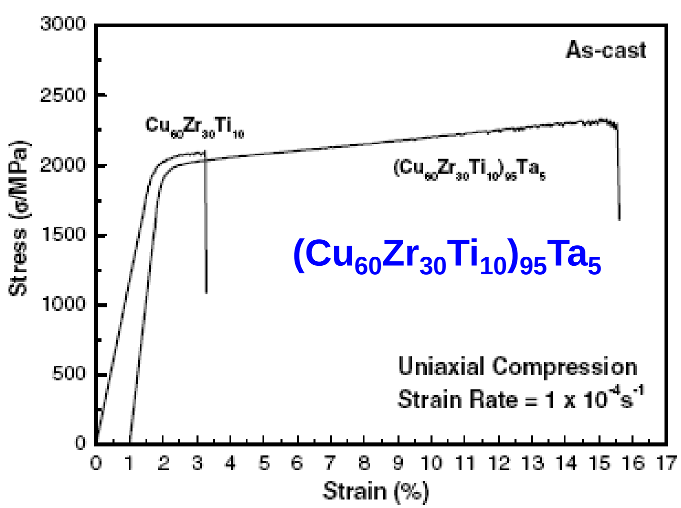

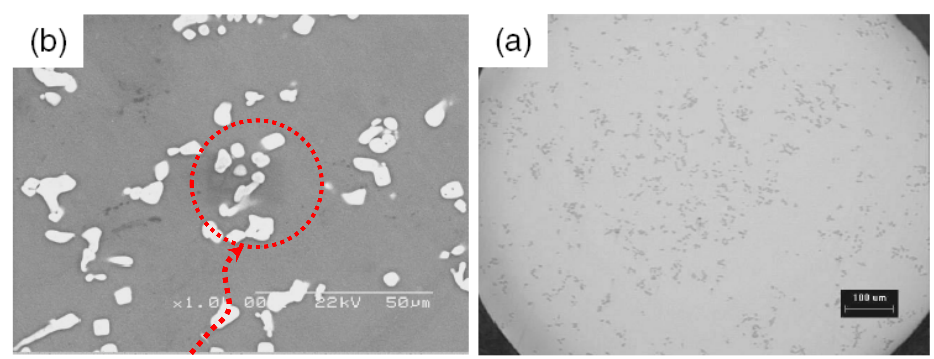

Ta rich particle

(Johnson et al., Acta Mater., 2001)

Size of heterogeneity

Shear bands are ~20 nm in width

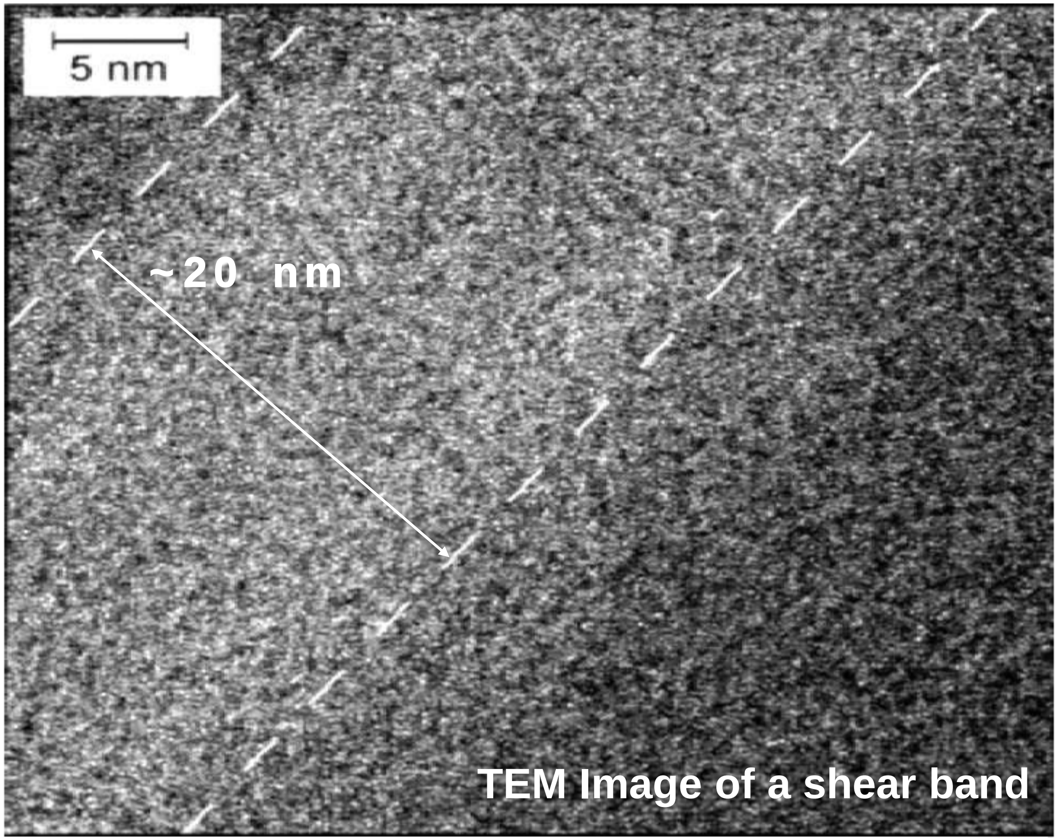

- **Prevent propagation of single shear band**

➡ **Micro- or nanometer scale heterogeneity**

Size of heterogeneity

- Elementary flow event in an metallic glasses

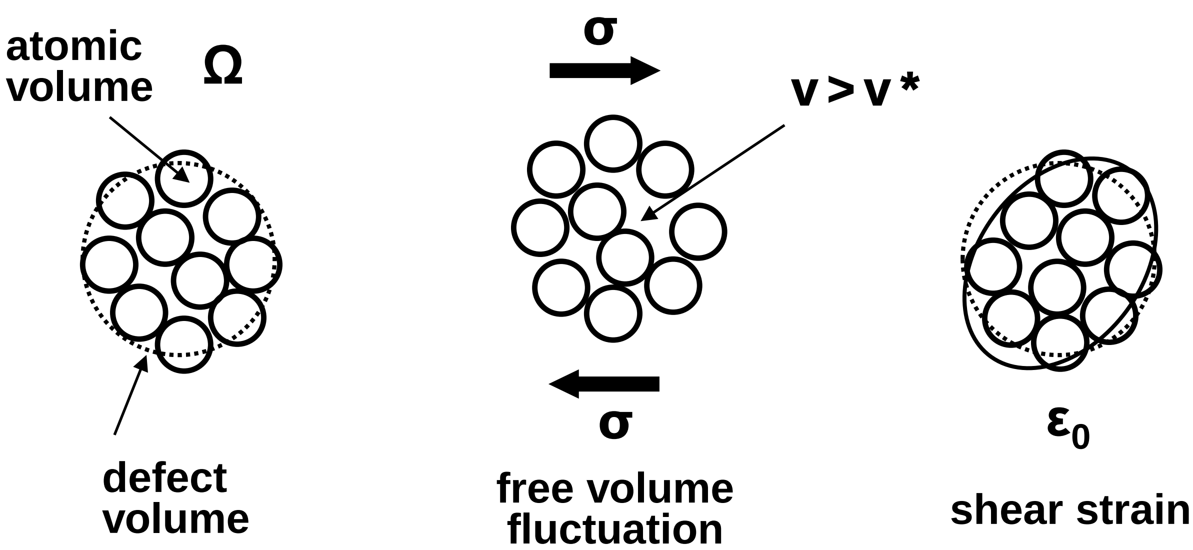

Probability $\exp(A\frac{v^*}{v_f})$

average free volume

Flow governed by localized defect (~10 atoms) and creates defects

atomic scale heterogeneity

$$\eta = \eta_0 \exp\left\{A\frac{V_0}{V_f}\right\}$$

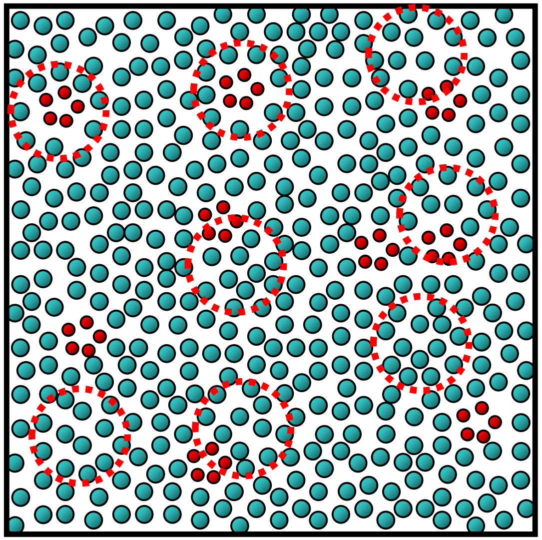

Plastic deformation in metallic glasses

- Flow governed by localized defect (~10 atoms)
- Flow creates defects

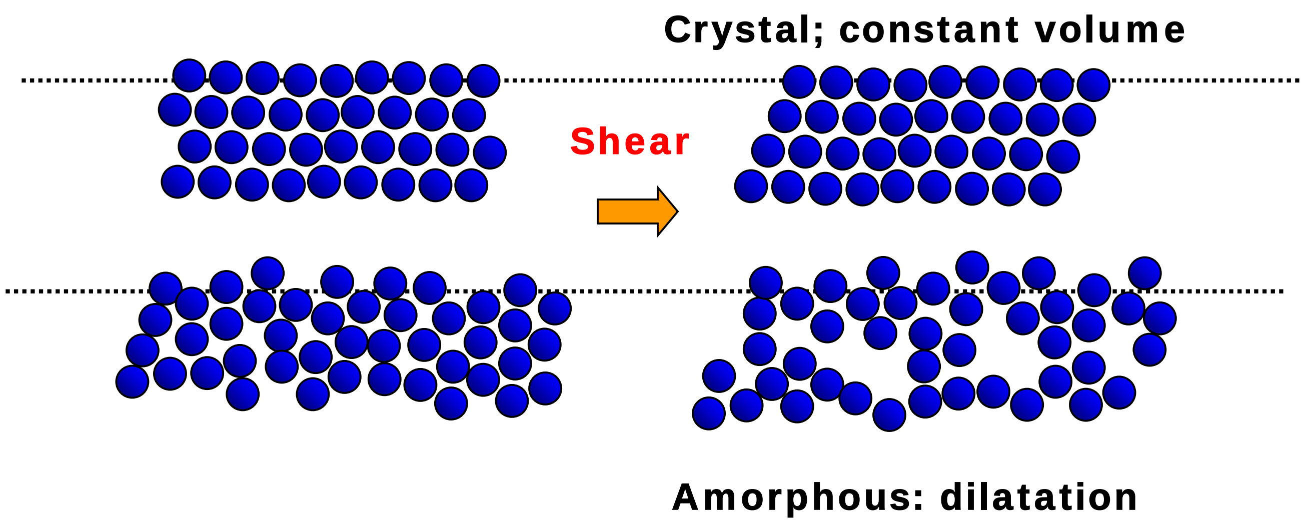

- Shear bands form by accumulation of defects

Understanding how shear bands form and propagate in metallic glasses

Fragility

- Fragility ~ extensively use to figure out liquid dynamics and glass properties corresponding to "frozen" liquid state

< Classification of glass >

Strong network glass **: Arrhenius behavior**

$$\eta = \eta_0 \exp[\frac{E_a}{RT}]$$

Fragile network glass **: Vogel-Fulcher relation**

$$\eta = \eta_0 \exp[\frac{B}{T - T_0}]$$

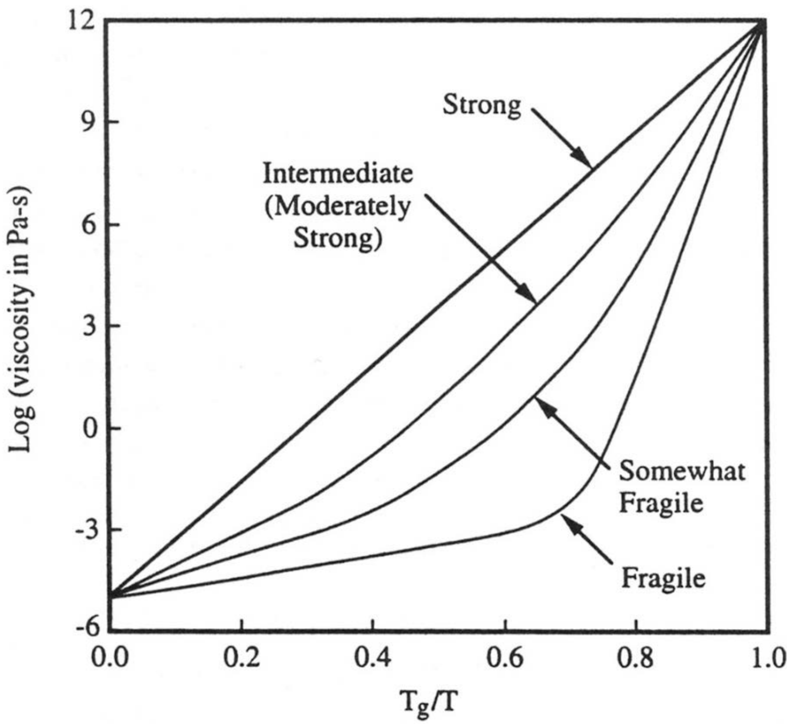

< Quantification of Fragility >

$$m = \left.\frac{d \log \eta(T)}{d(T_{g,n}/T)}\right|_{T=T_{g,n}} = \left.\frac{d \log \tau(T)}{d(T_g/T)}\right|_{T=T_g}$$

Slope of the logarithm of viscosity, η (or structural relaxation time, τ) at T_g

Correlation between fragility and plasticity

- Correlation between elastic constants and plasticity

Low G/B → *High ν* → **shear collapse**

(shear modulus / bulk modulus) ***(poisson's ratio)*** ***(multiple shear band)***

Jan Schroers et al, , Phys. Rev. Lett. 93, 255506 (2004).

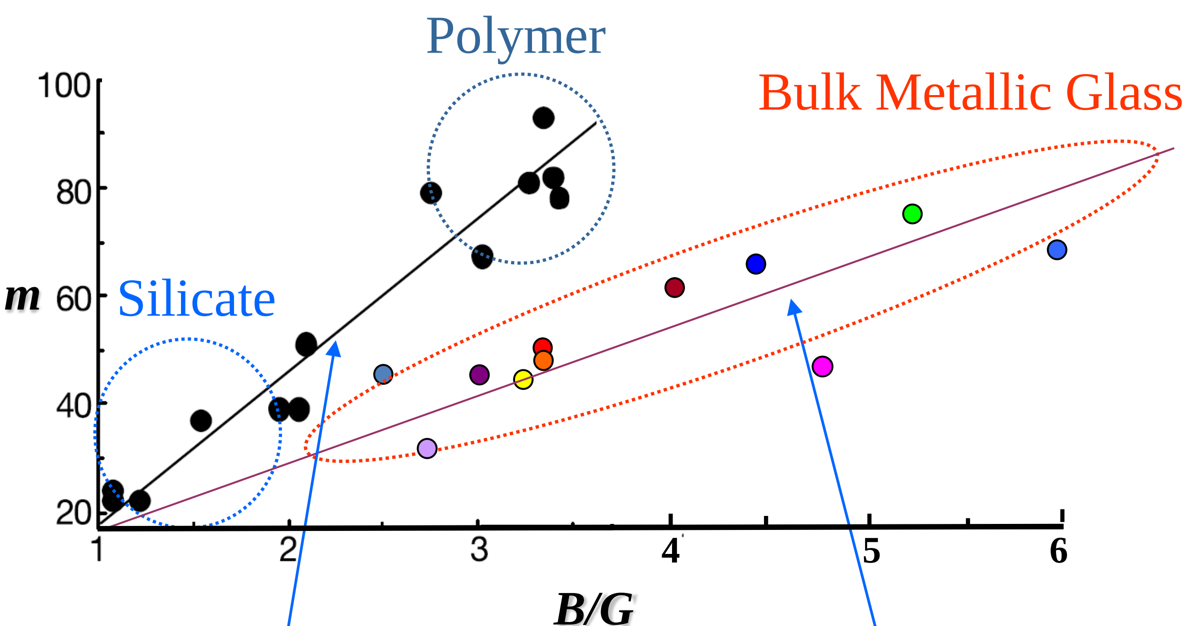

$$m - 17 = 29(B/G - 1) \qquad m - 17 = 14(B/G - 1)$$

*** J. Mater. Res. 23, 523 (2008)**

Correlation between fragility and plasticity

Low G/B
High ν → *High m* (*fragility index*) → **Large Plasticity** (*multiple shear band*)

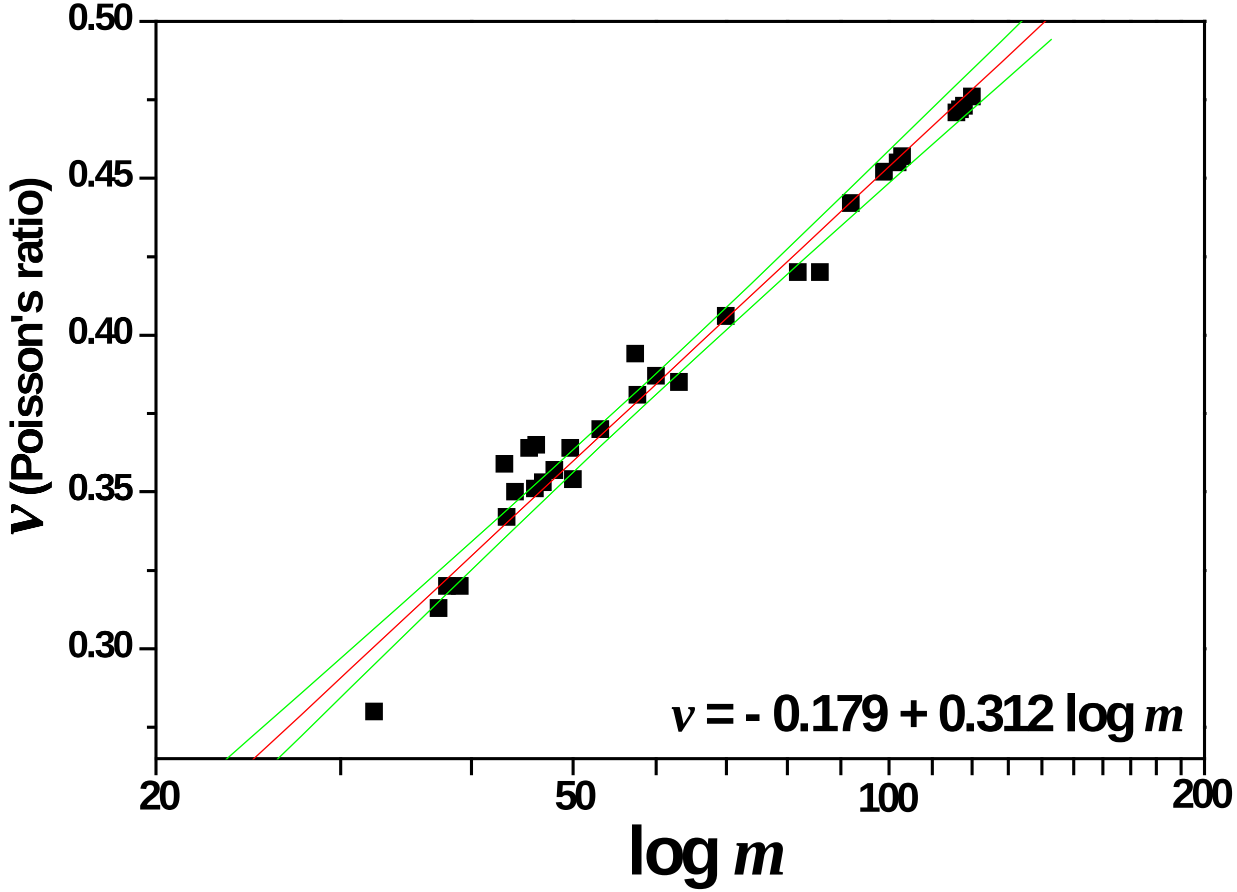

* Appl. Phys. Lett., 91, 031907.

Enhancement plasticity in BMGs with atomic scale heterogeneity

a) Effect of quenched-in quasicrystal nuclei

Effect of quenched-in quasicrystal nuclei

2 mm rod

(a) $Zr_{63}Ti_5Nb_2Cu_{15.8}Ni_{6.3}Al_{7.9}$

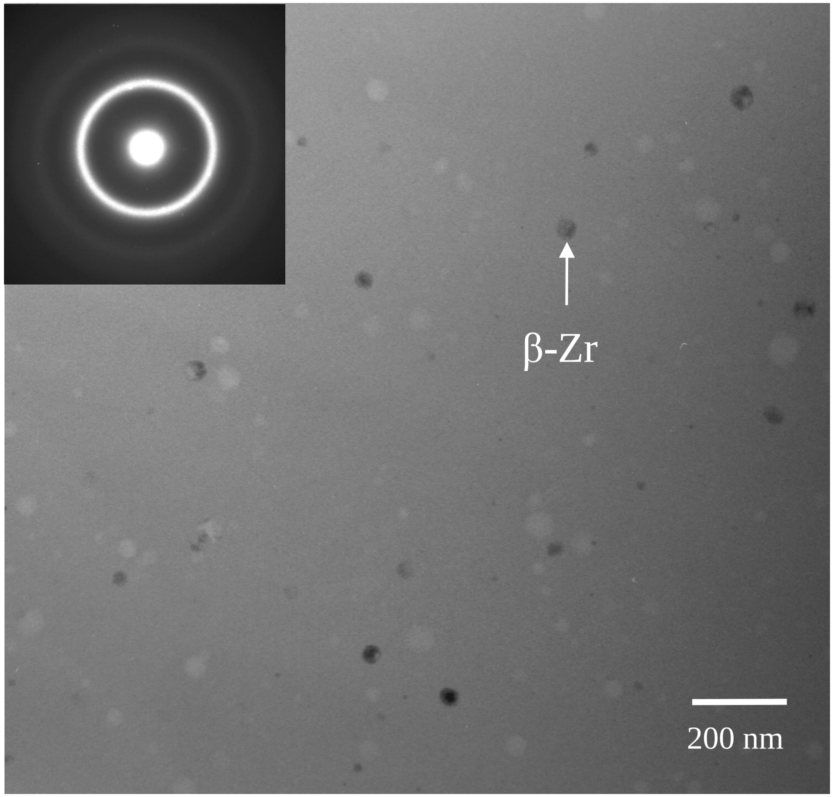

β-Zr particle (~70 nm) in amorphous matrix

(b) $Zr_{57}Ti_8Nb_{2.5}Cu_{13.9}Ni_{11.1}Al_{7.5}$

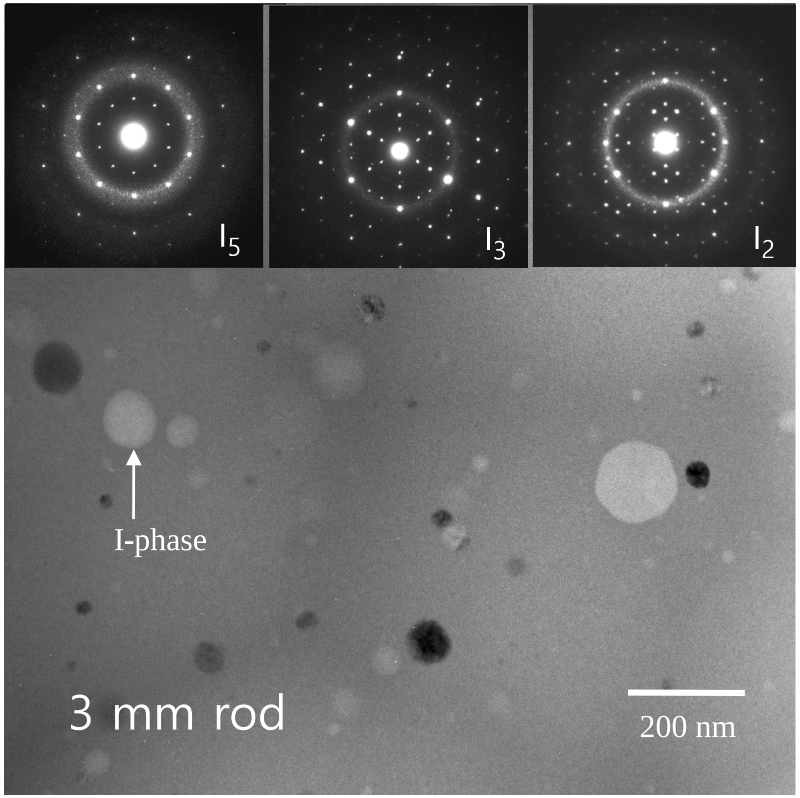

I-phase particle in amorphous matrix

Effect of quenched-in quasicrystal nuclei

- Compression test

* unpublished (2008)

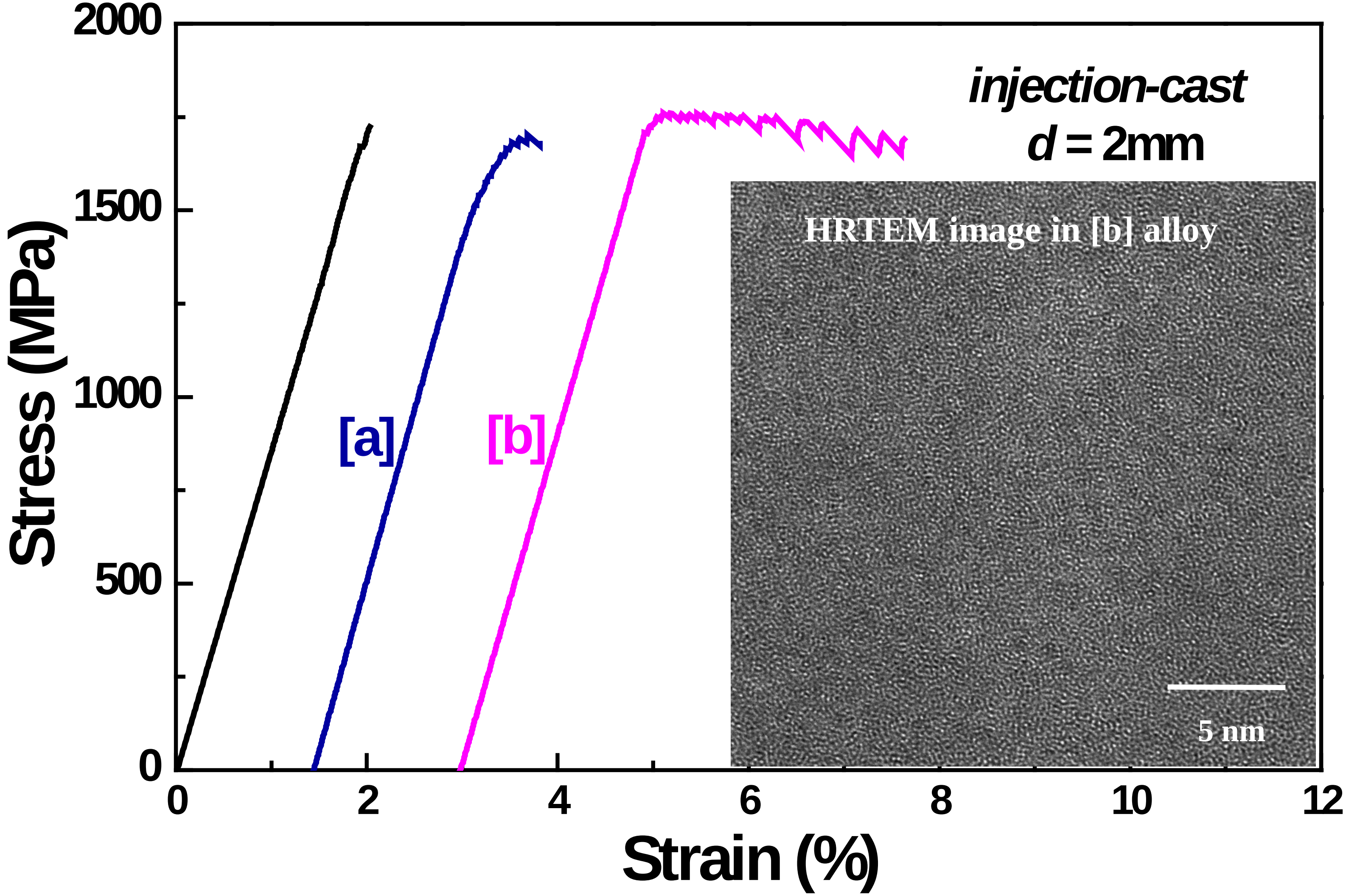

Enhancement plasticity in BMGs with atomic scale heterogeneity

a) Effect of element having positive enthalpy of mixing among constituent elements

Improvement of plasticity in monolithic BMGs

* **Enhancement of plasticity in monolithic BMGs**

→ No clear explanations so far.

* **Reports for enhancement of plasticity in monolithic BMGs**

	Compressive plastic strain, ε_p (%)
$Zr_{59}Ta_5Cu_{18}Ni_8Al_{10}$ [1]	~ 6.1
$Zr_{57}Ti_5Cu_{20}Ni_8Al_{10}$	~ 1.1
$Ni_{59}Zr_{16}Nb_7Ti_{13}Si_3Sn_2$ [2]	~ 6.2
$Ni_{59}Zr_{20}Ti_{16}Si_2Sn_3$	~ 2.1
$Cu_{47}Ti_{33}Zr_7Nb_4Ni_8Si_1$ [3]	~ 4.1
$Cu_{47}Ti_{33}Zr_{11}Ni_8Si_1$	~ 1.5
$Cu_{43}Ag_7Zr_{43}Al_7$ [4]	~ 4.1
$Cu_{50}Zr_{43}Al_7$	~ 1.5

1 *Xing et al., Phys. Rev. B (2001)*

2 *Lee et al., Intermetalics (2004), BMG III*

3 *Park et al., J. Non-cryst. Sol. (2005)*

4 *Sung et al., Met. Mater. –Int (2004) and Oh et al., Scripta Mater. (2005)*

(Ta-Zr: +13KJ/mol, Nb-Zr: +17KJ/mol, Nb-Ti: +9KJ/mol,Cu-Ag: +5 KJ/mol)

- Previous results on the effect of micro-alloying on plasticity

: **Effect of elements having positive heat of mixing**

Alloy design

*** Substitution of Zr with Y in Cu-Zr-Al system**

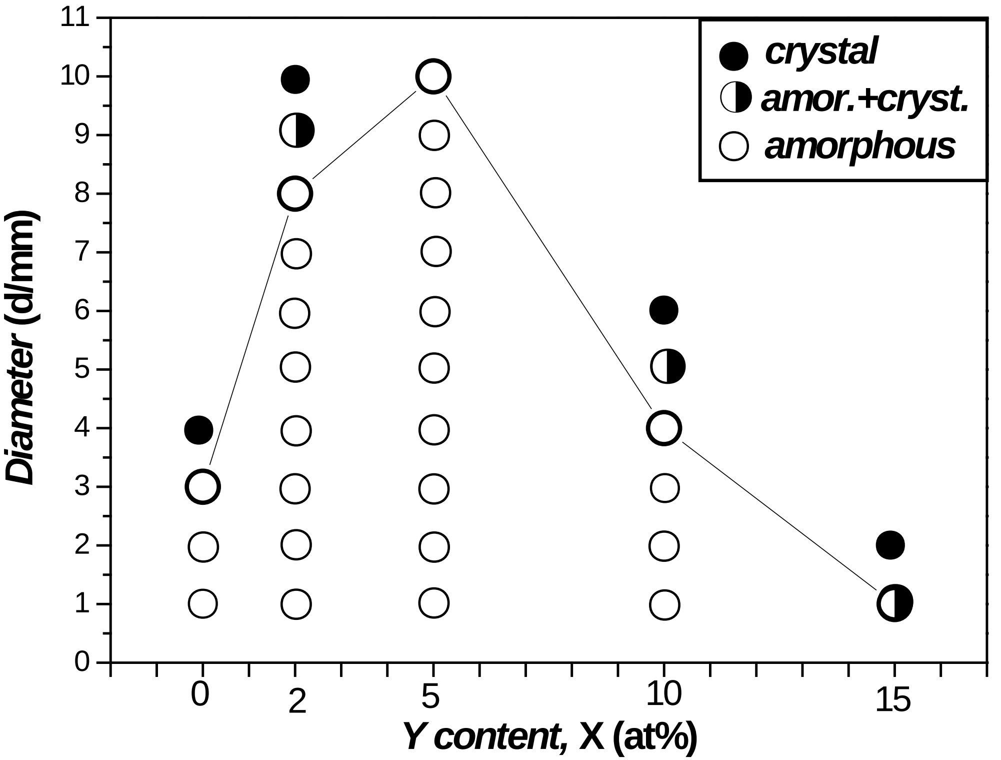

D. Xu, G. Duan and W.L. Johnson, Phys. Rev. Lett. 92, 245504 (2004)

$Cu_{46}Zr_{47-x}Al_7Y_x$

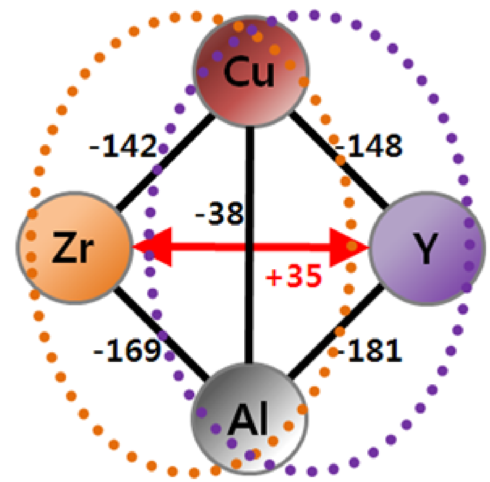

Possibility of two phase !!!

→ Cu-Zr-Al , Cu-Y-Al

Indirect evidence of inhomogeneity
= Phase separation

*** Acta Materialia, 54, 2597 (2006)**

Thermal analysis : DSC results

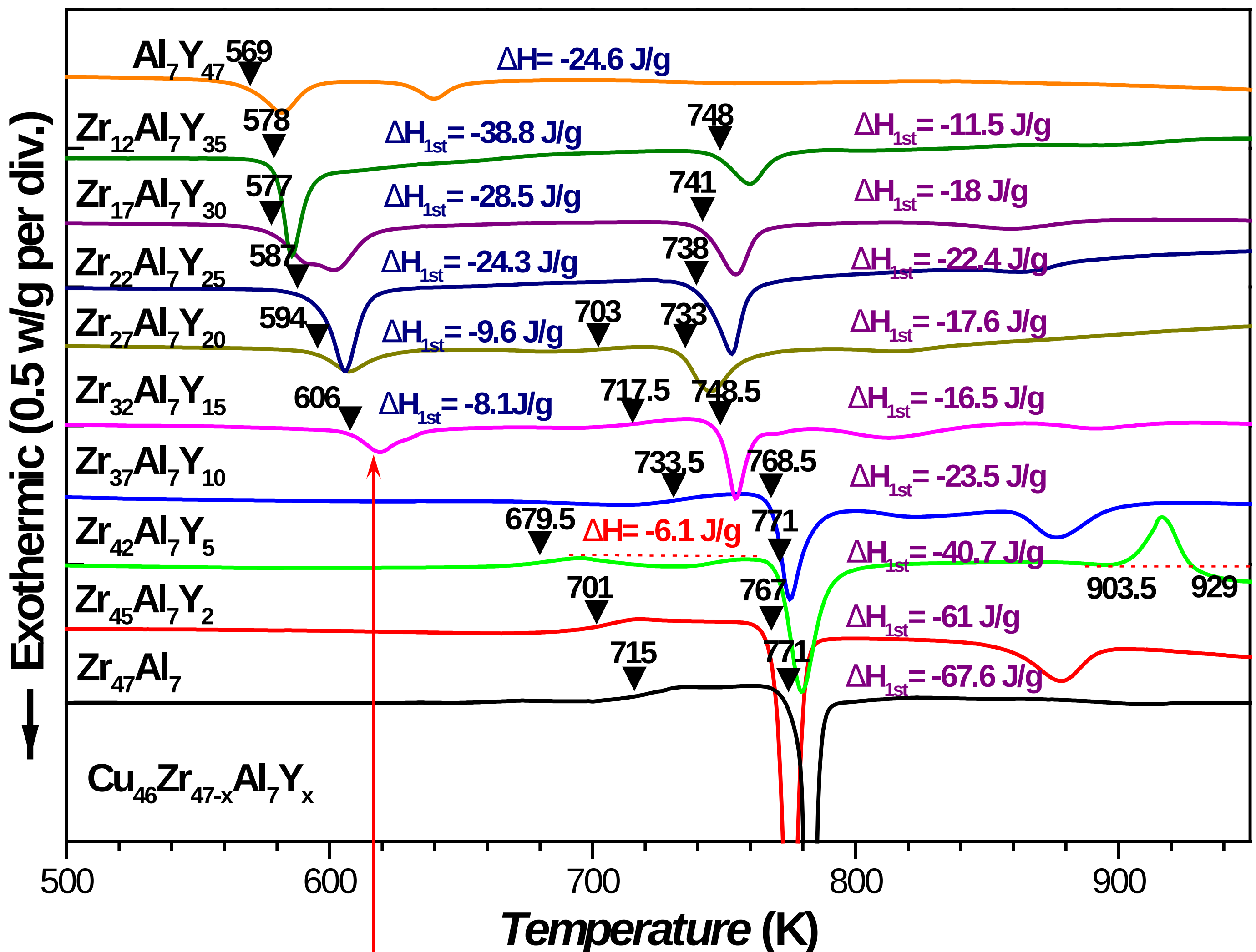

Exothermic peak which exhibit that Y rich amorphous phase crystallize

Structural analyses : TEM results

As-melt-spun

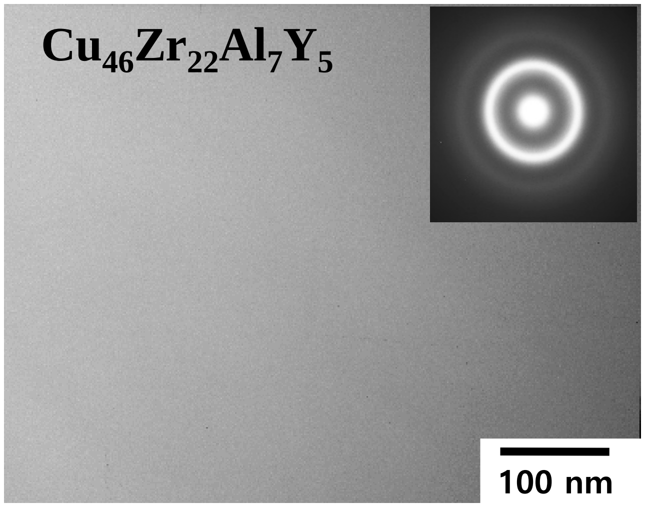

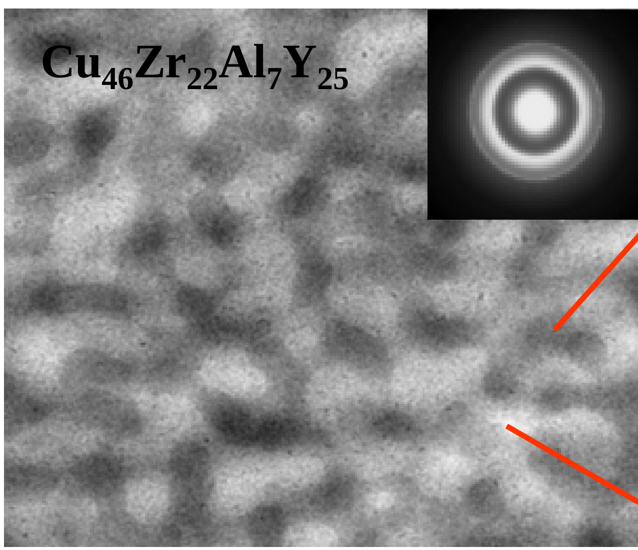

- With increasing Y content, Compositional inhomogeniety → Phase separation

$Cu_{53.4}Zr_{31.8}Y_{8.3}Al_{6.5}$ (CuZr-rich)

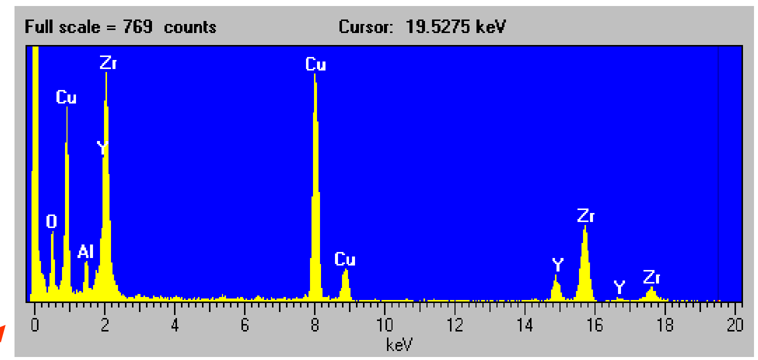

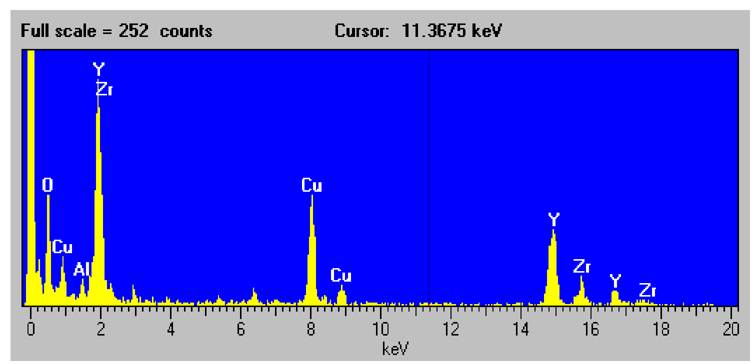

$Cu_{35.7}Zr_{12.8}Y_{44.3}Al_{7.2}$ (CuY-rich)

Compression test in Cu-Zr-Al-Y alloy system

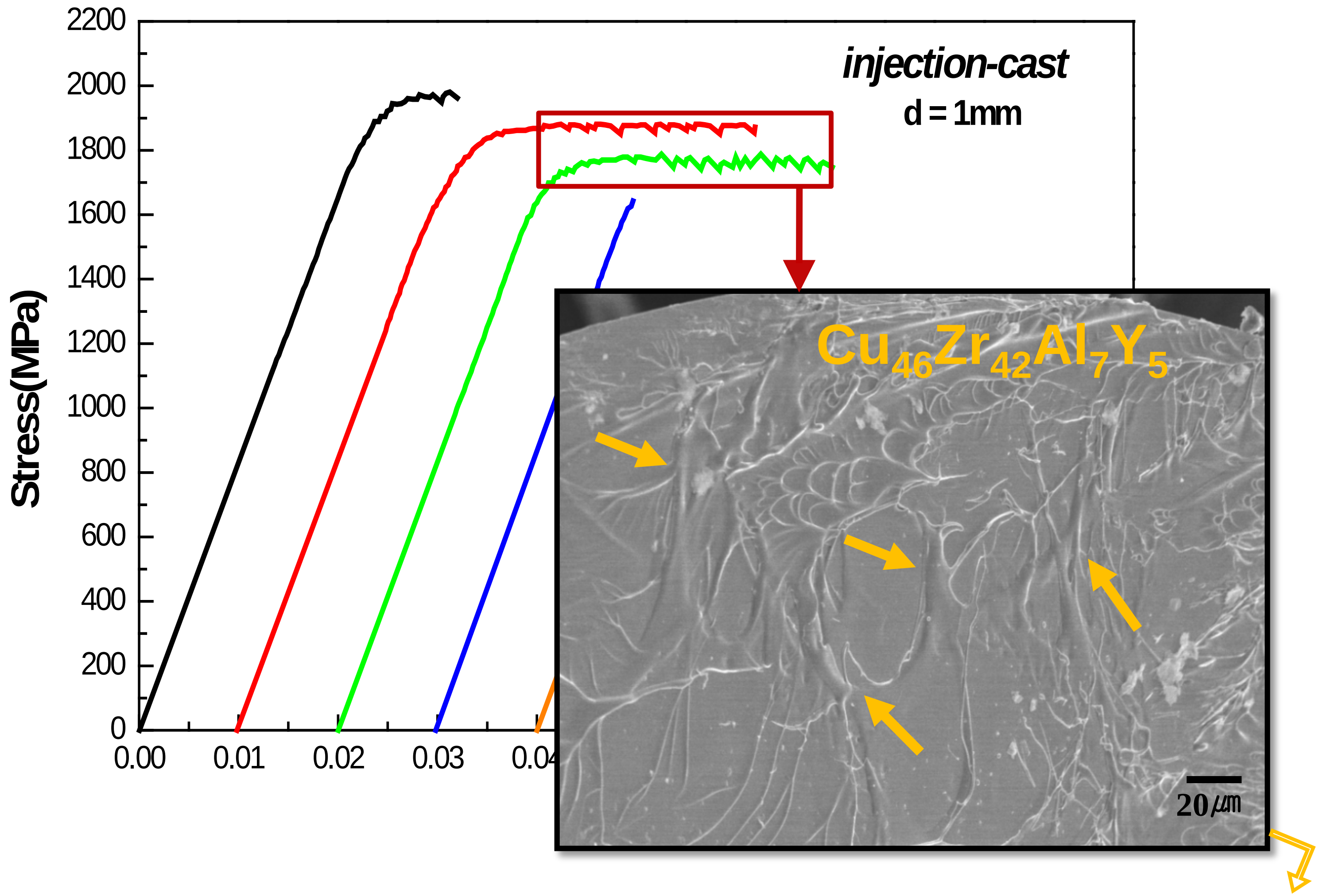

▶ A larger amount of strain along the shear band led to localized melting before fracture

Measurement of viscosity using TMA

<Supercooled liquid region>

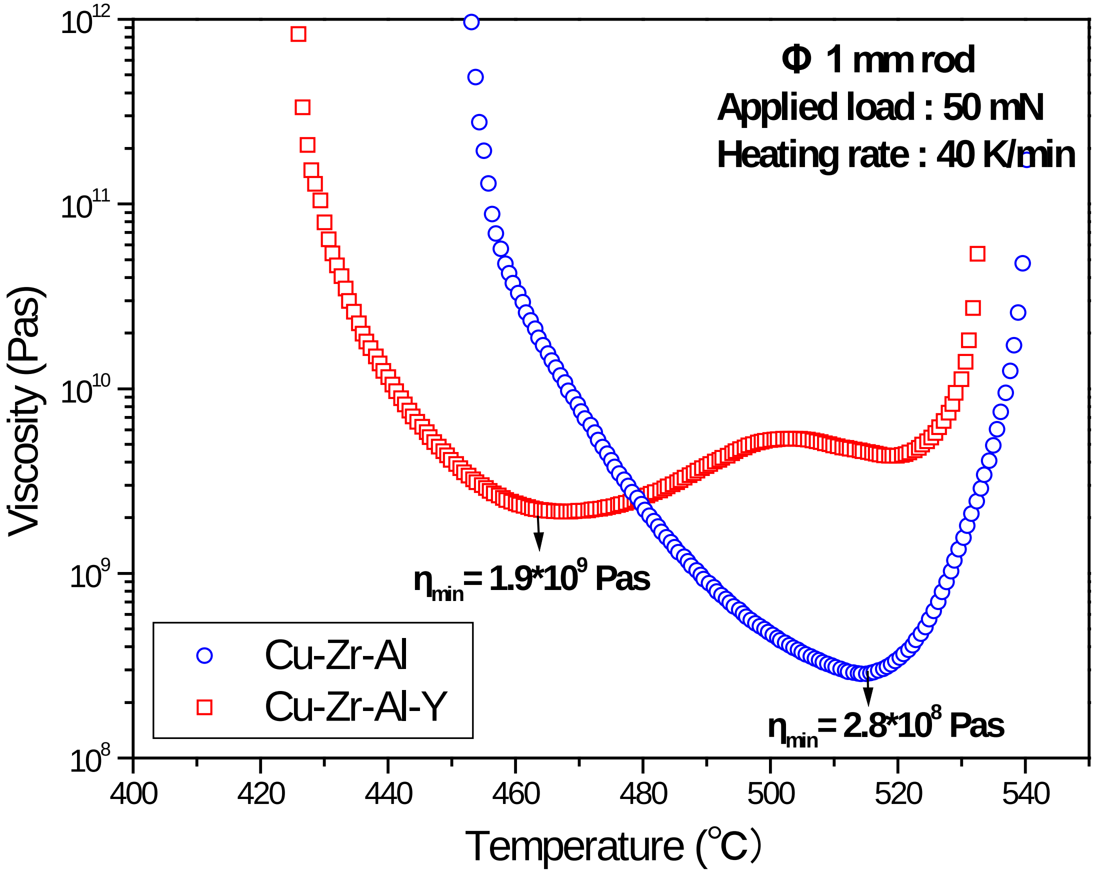

<1st Crystallization behavior>

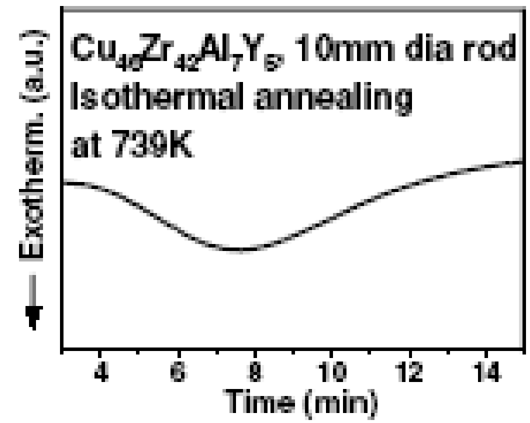

: nucleation and growth

$Cu_{46}Zr_{47}Al_7$ < **$Cu_{46}Zr_{42}Al_7Y_5$**

η_{min} = 2.8*10^8 pas

η_{min} = 1.9*10^9 pas

Relatively easy crystallization

Structural analyses: HRTEM

$Cu_{46}Zr_{42}Al_7Y_5$

As-melt-spun | **Heated up to 480℃**

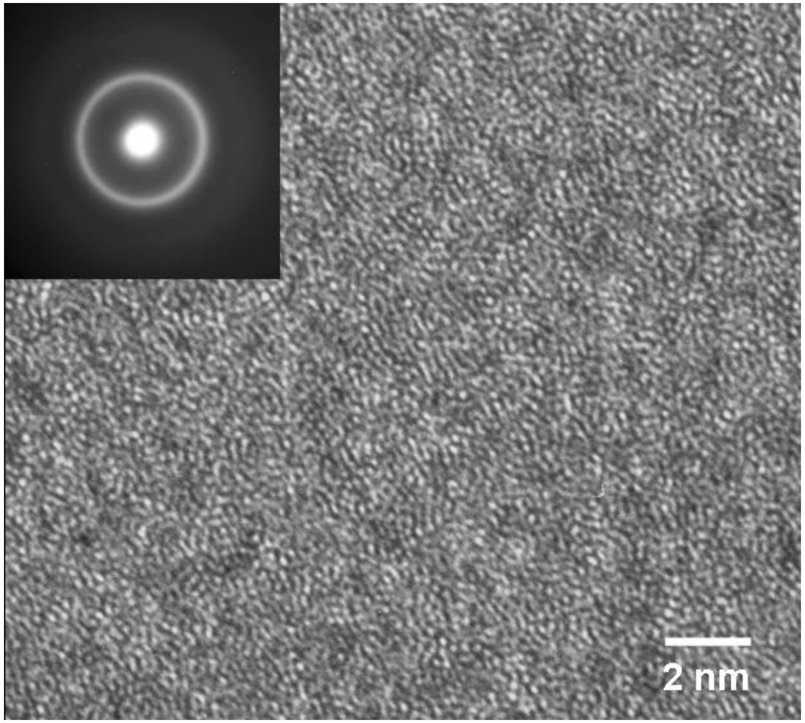

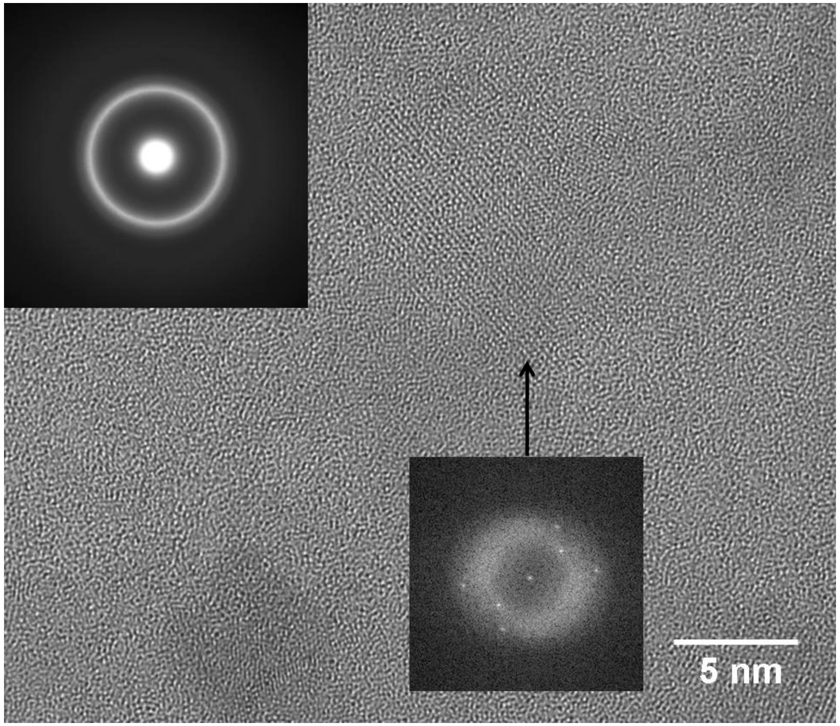

: nanocrystallization of Y rich amorphous phase due to relatively lower GFA

* Acta Materialia, 54, 2597 (2006)

In-situ WAXS analysis of $Cu_{46}Zr_{42}Al_7Y_5$ during heating

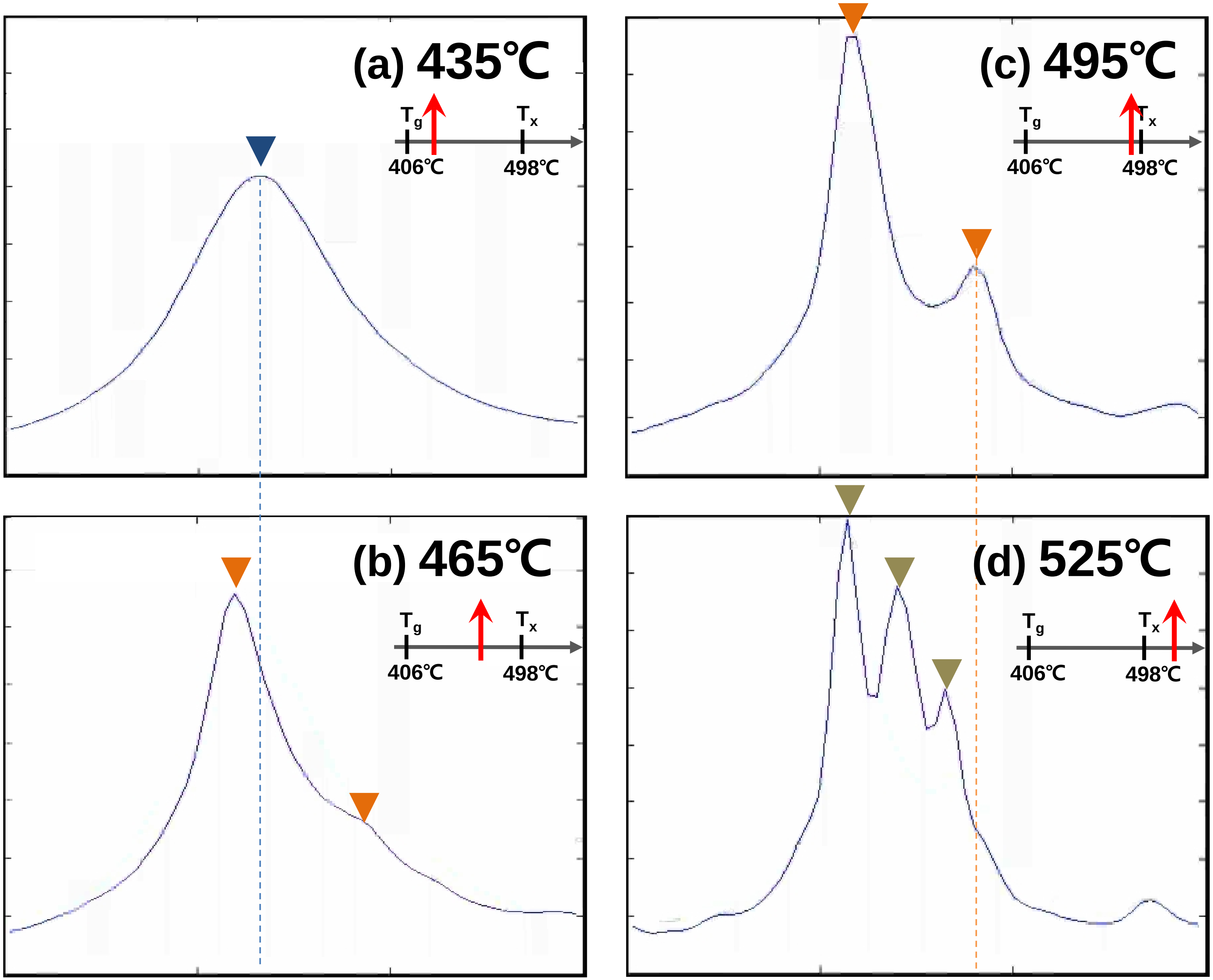

Obtained from Argon National Lab.

Visualization of Atoms by FIM

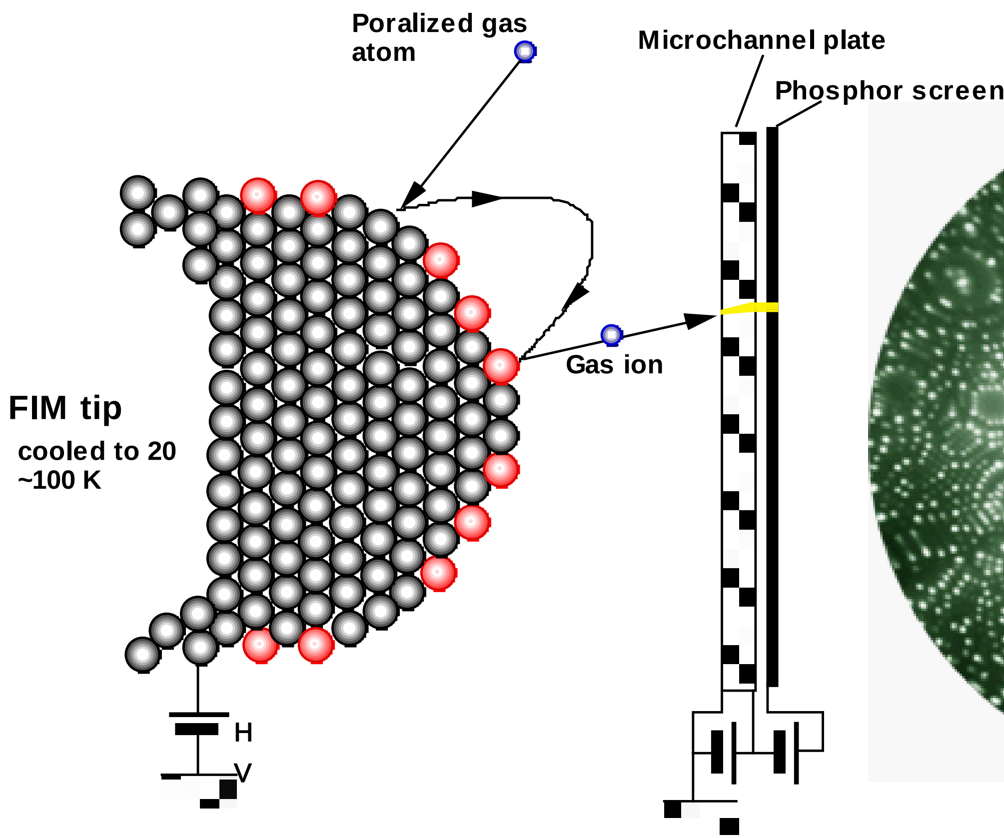

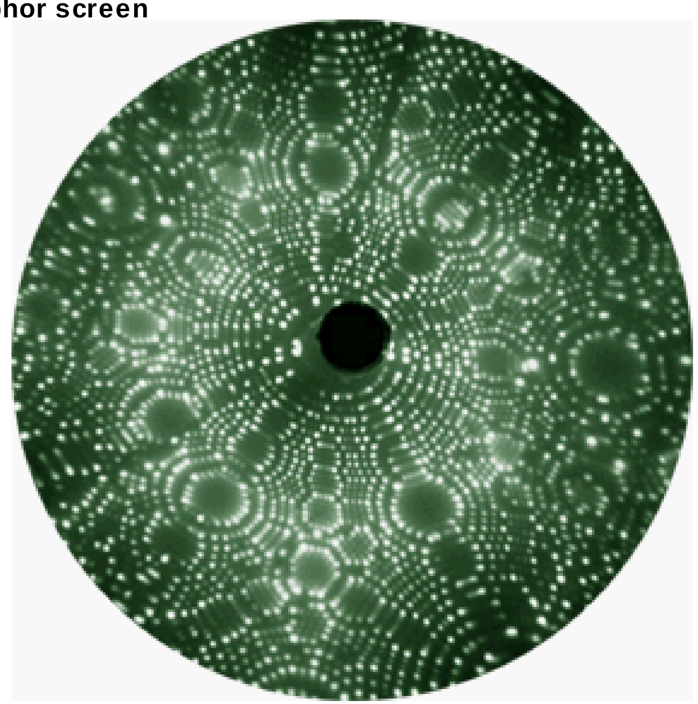

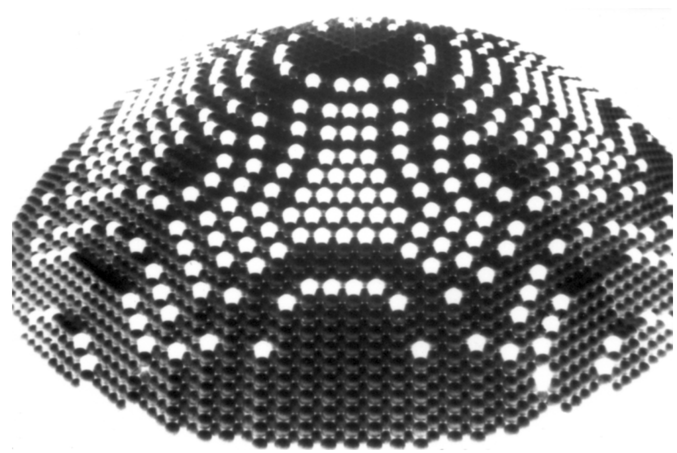

Analysis of atoms by 3DAP

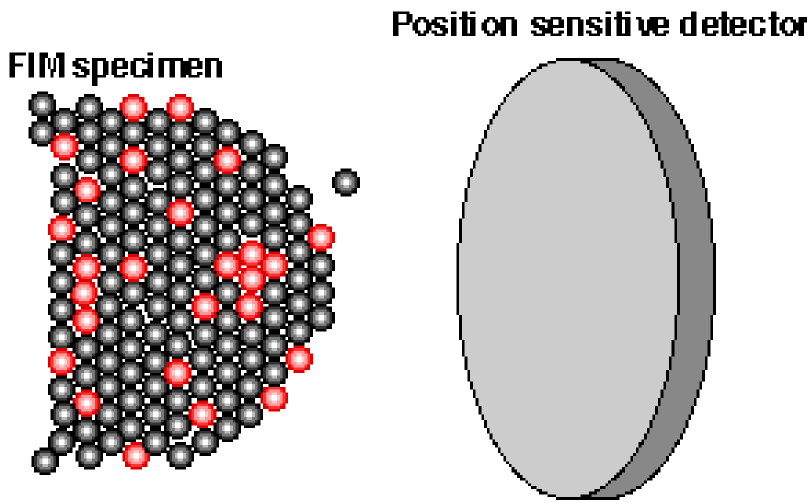

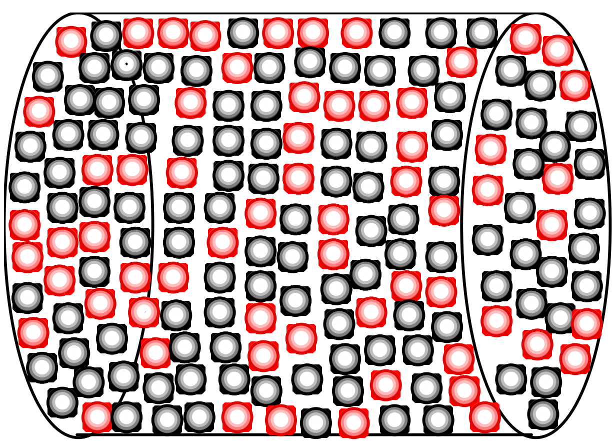

η’ precipitates in Al-Zn-Mg alloy

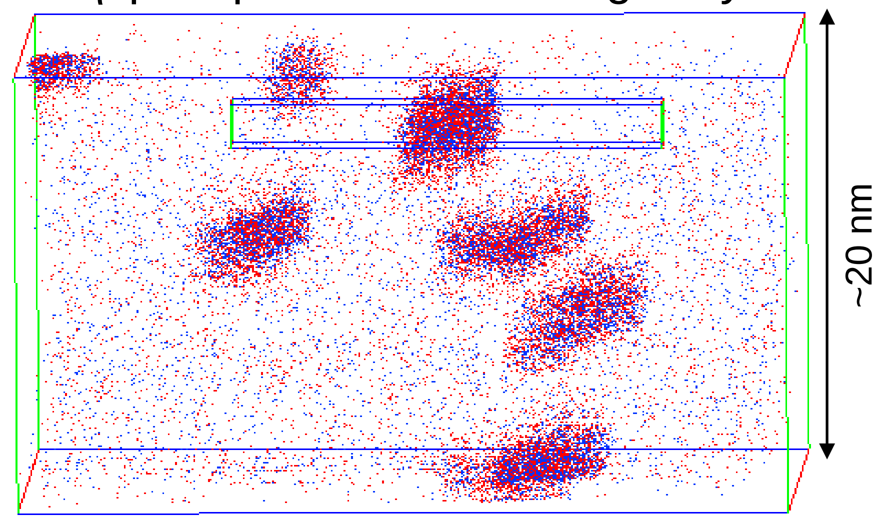

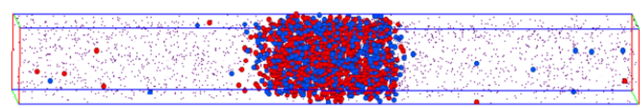

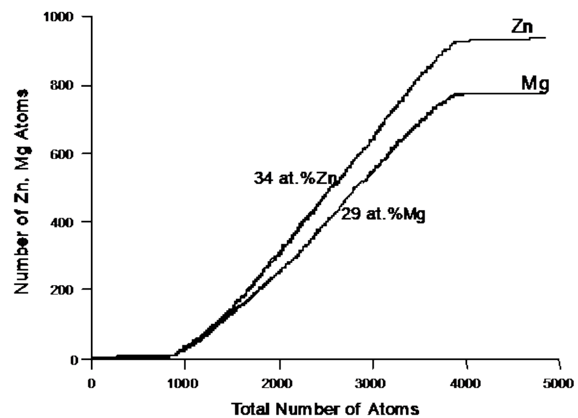

Energy-compensating reflectron lens

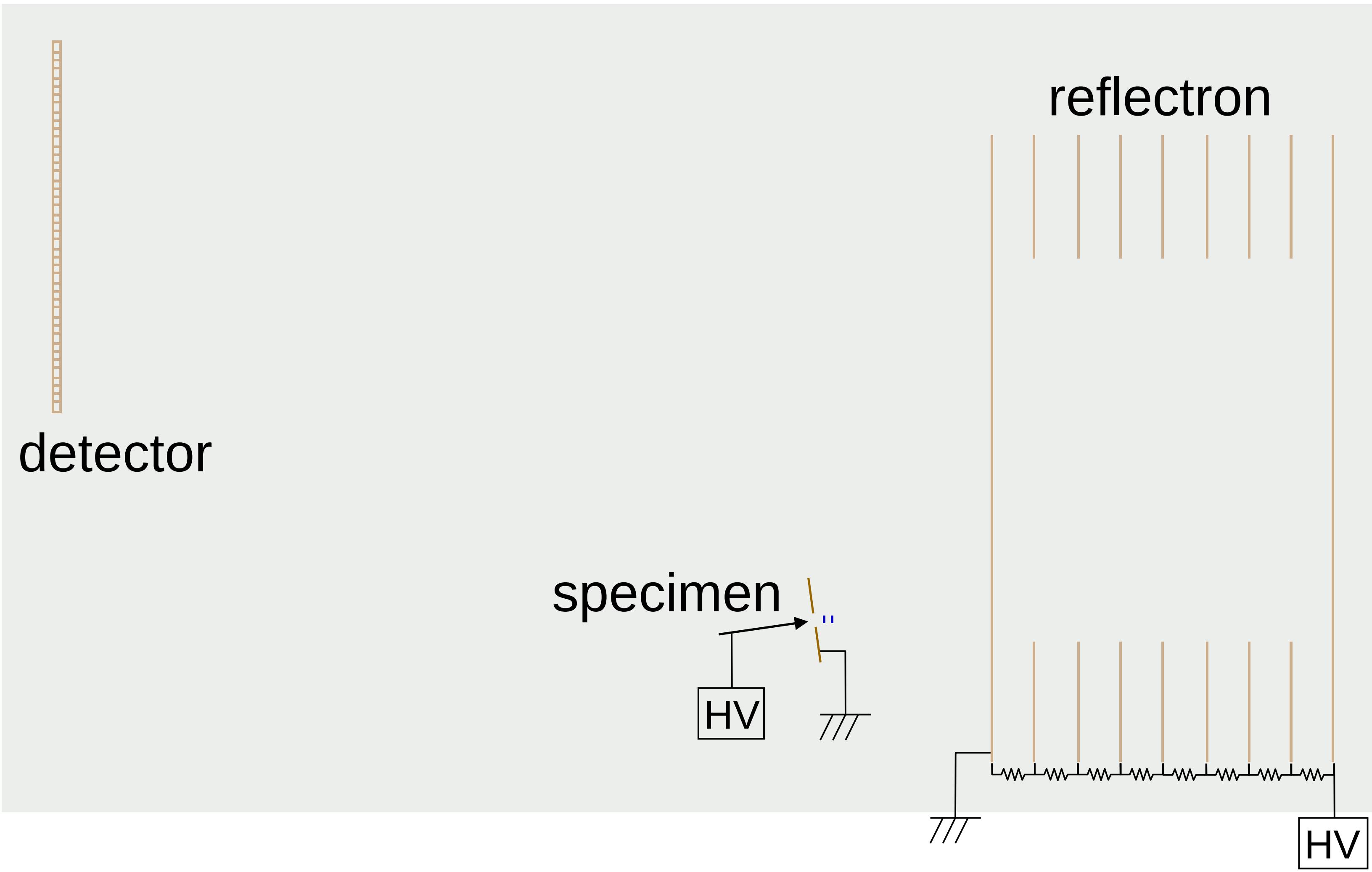

NIMS 3DAP

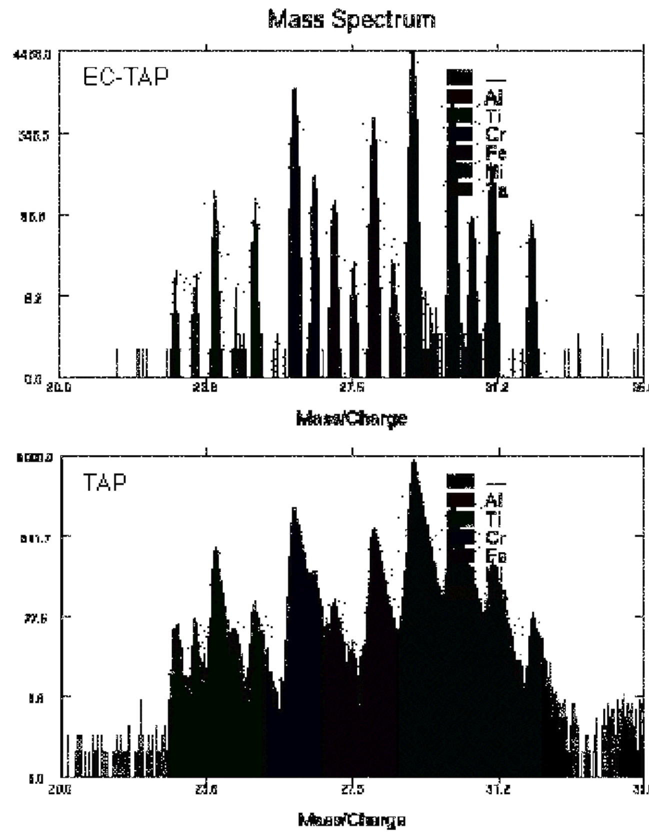
Mass Spectrum
EC-TAP
Al
Ti
Cr
Fe
Ni
Ta
Mass/Charge
TAP
Al
Ti
Cr
Fe
Mass/Charge

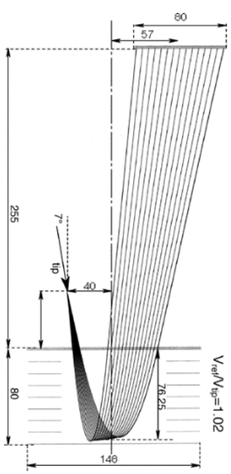
60
57
255
7°
tip
40
80
76.25
146
V_{ref}/V_{tip}=1.02

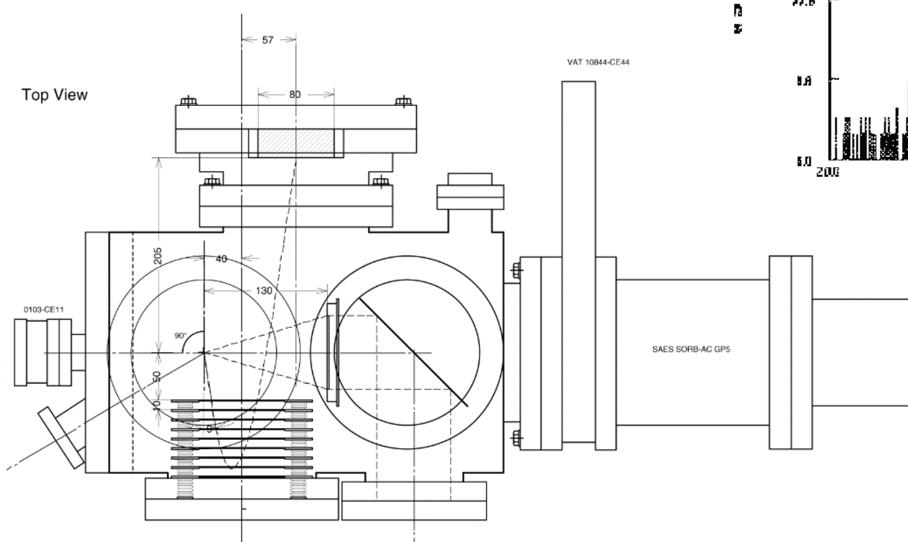
Top View
57
80
VAT 10844-CE44
0103-CE11
205
40
130
90°
50
10
SAES SORB-AC GP5
181

Complementary structural analysis

Local Chemical Composition

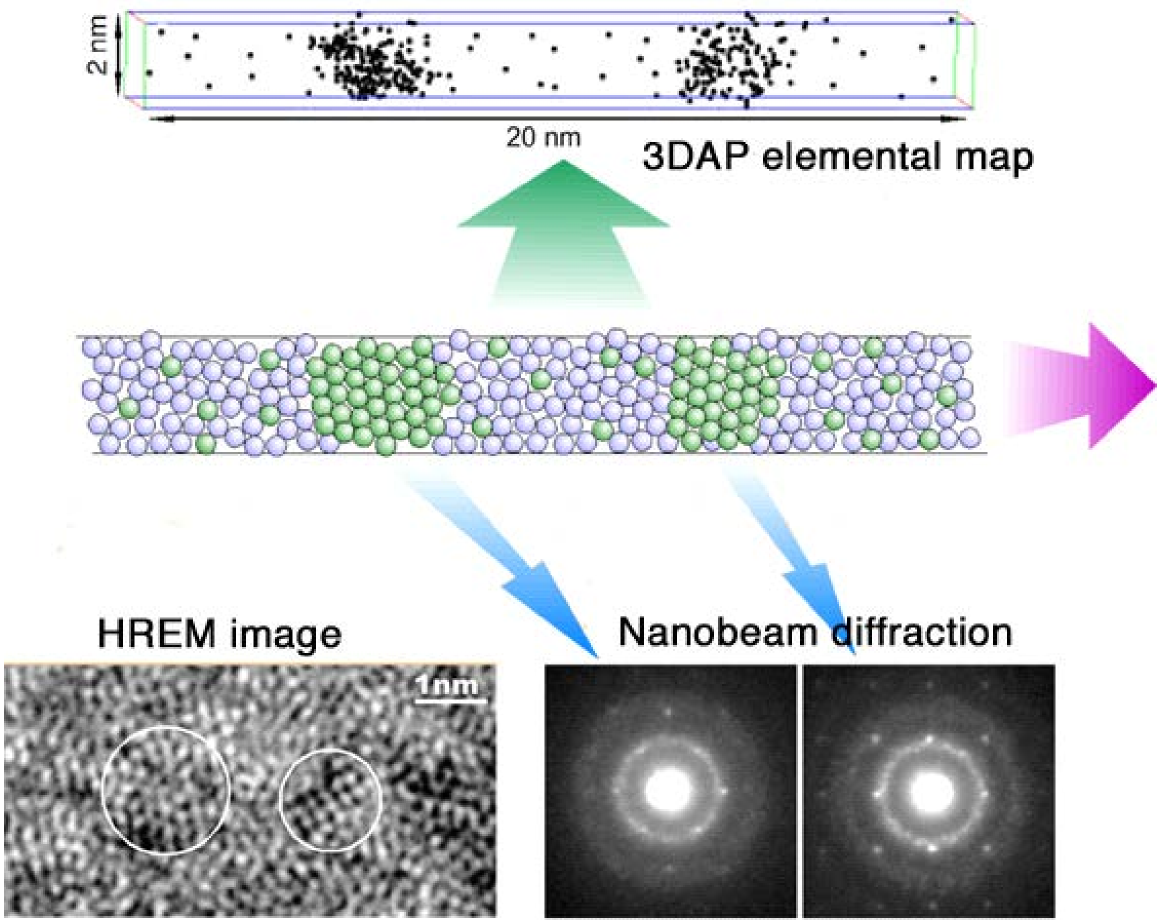

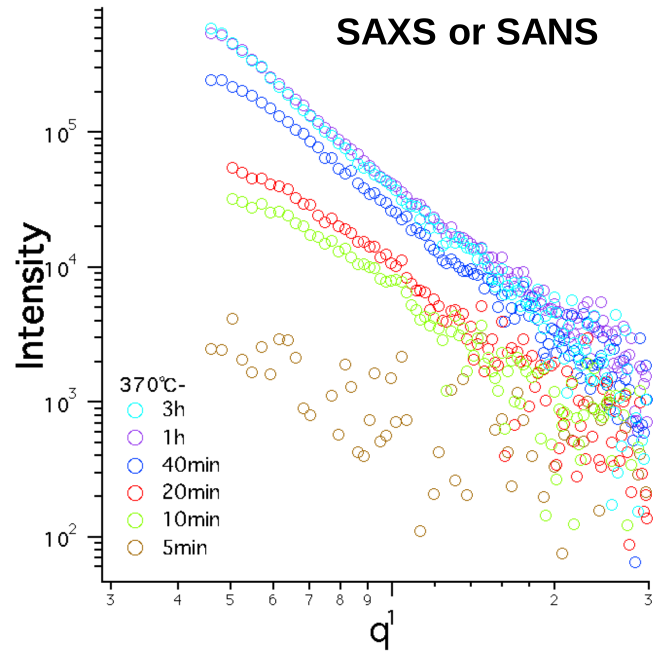

Local Structure

Average Scale

APT results of $Cu_{46}Zr_{47-x}Al_7Y_x$ (x = 0, 5, 10, 15) ribbons

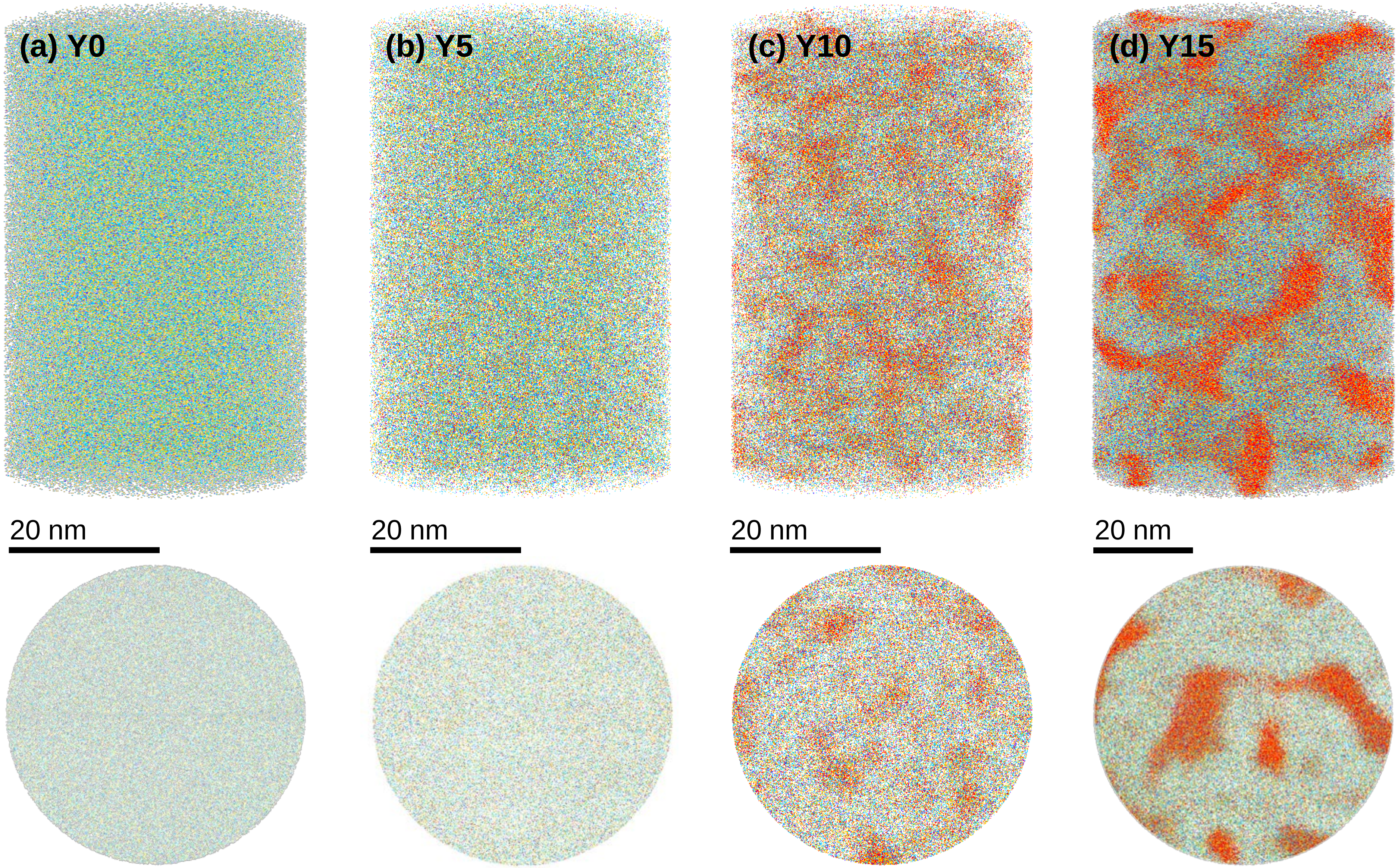

APT reconstructions showing the distribution of the alloy metallic elements (Cu-Yellow; Zr-blue; Al-purple; Y-red). The upper images are three-dimensional views for cylindrical regions, and the lower images are 2 nm-thick virtual slices of the respective reconstructions.

Statistical binomial frequency distribution analysis

The quality of the binomial fit was quantified using p-value and μ parameters, as listed in the inset tables.

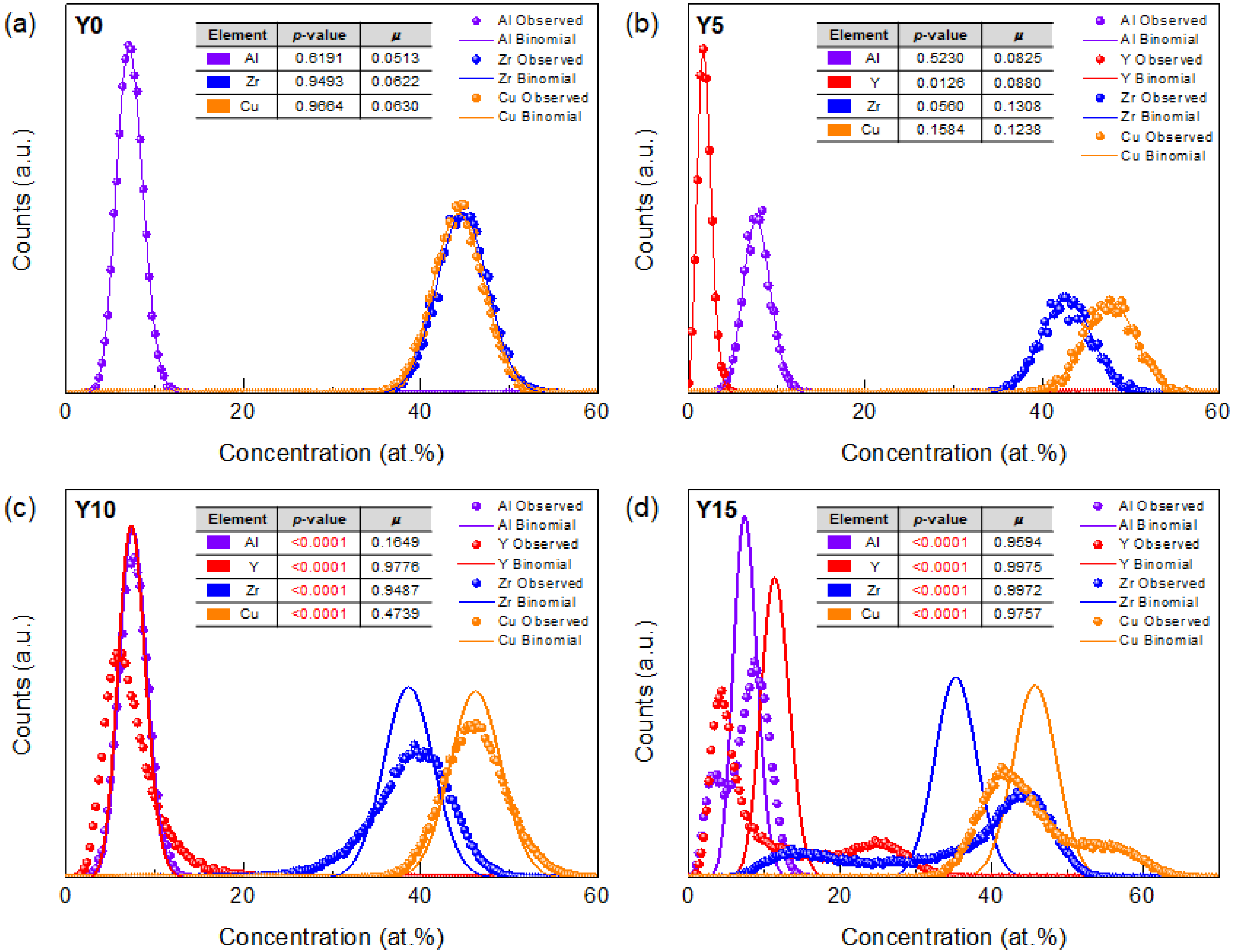

Proxigrams with respect to interfaces btw Zr- and Y-rich region

calculated with a bin size of 0.3 nm

Compositional heterogeneity with nanoscale network

Phase separation with interconnected structure

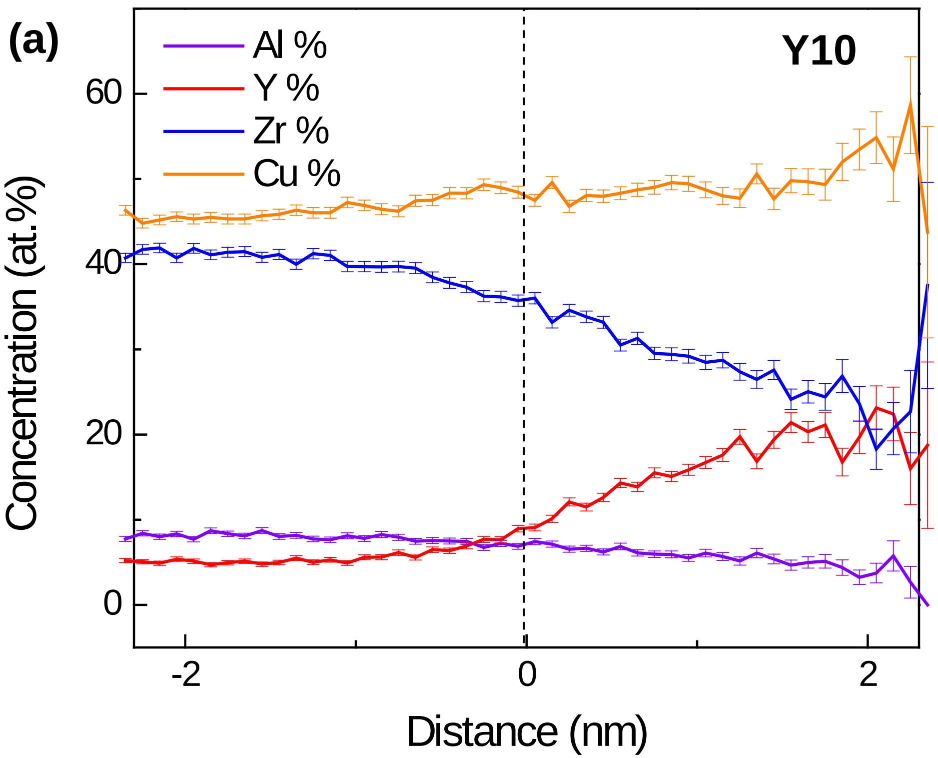

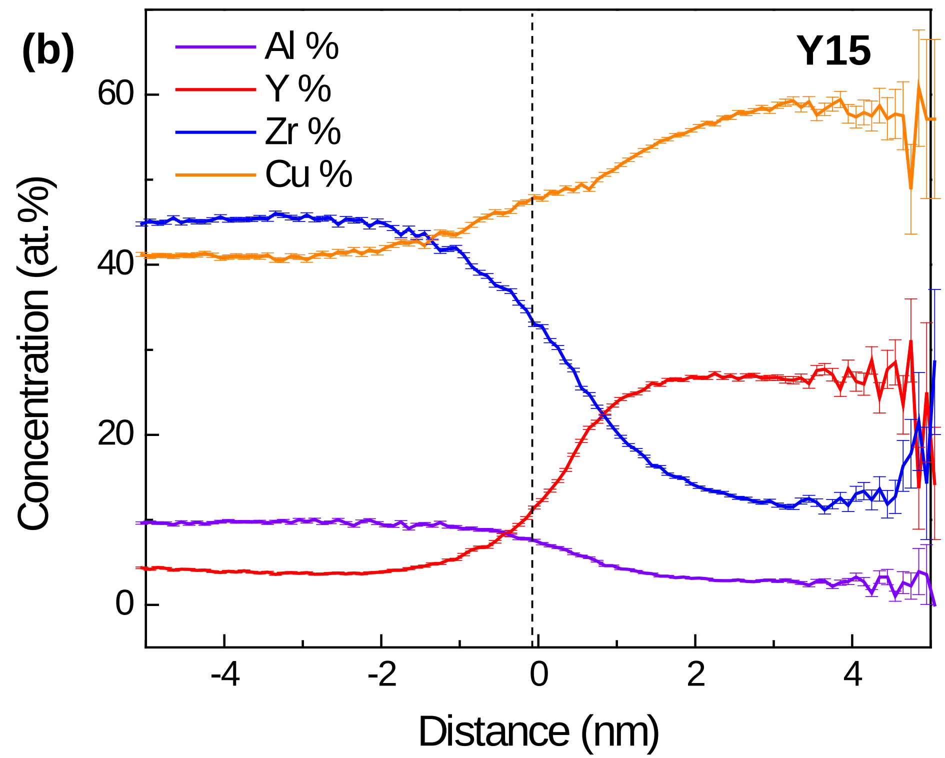

The interfaces (distance=0) in (a) and (b) are estimated from the frequency distribution analysis results to be the positions with Y composition of 10 at. % and 16 at.%, respectively.

APT results of $Cu_{46}Zr_{37}Al_7Y_{10}$ vs $Cu_{46}Zr_{32}Al_7Y_{15}$ ribbons

Compositional heterogeneity with nanoscale network

Y10

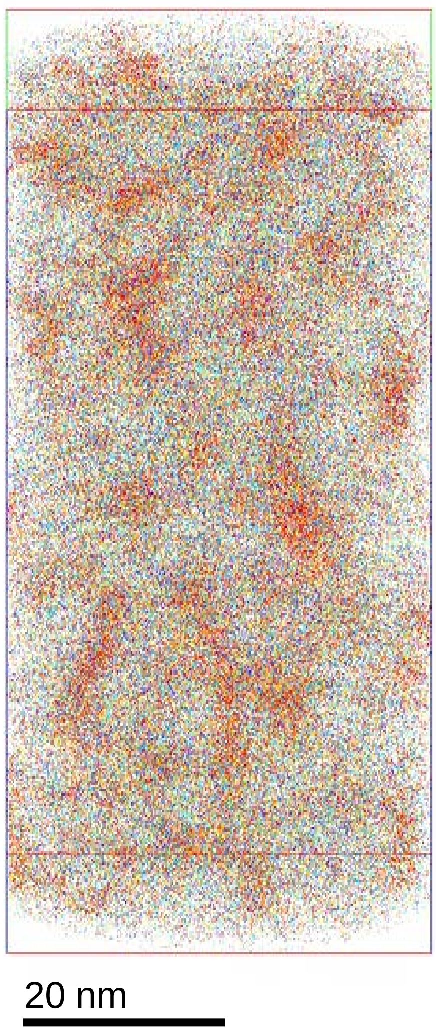

Phase separation with interconnected structure

Y15

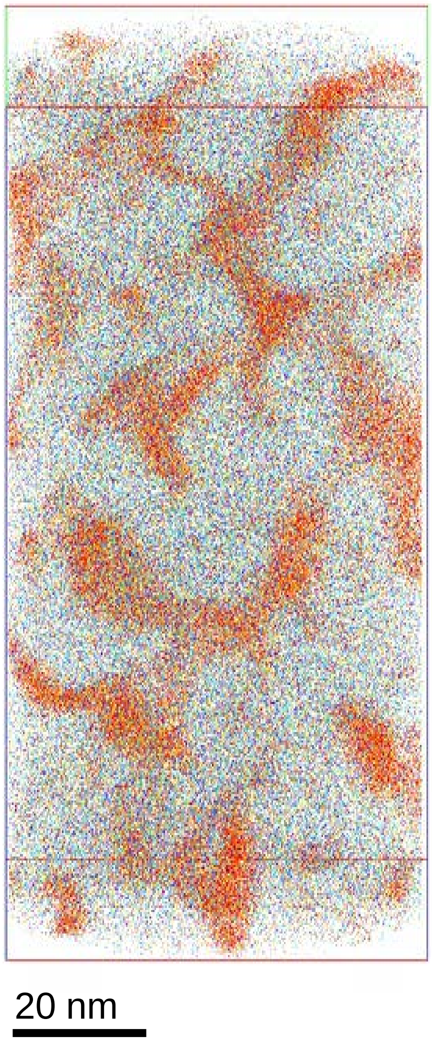

Effect of element having positive enthalpy of mixing

- **Abnormal behavior of supercooled liquid region**

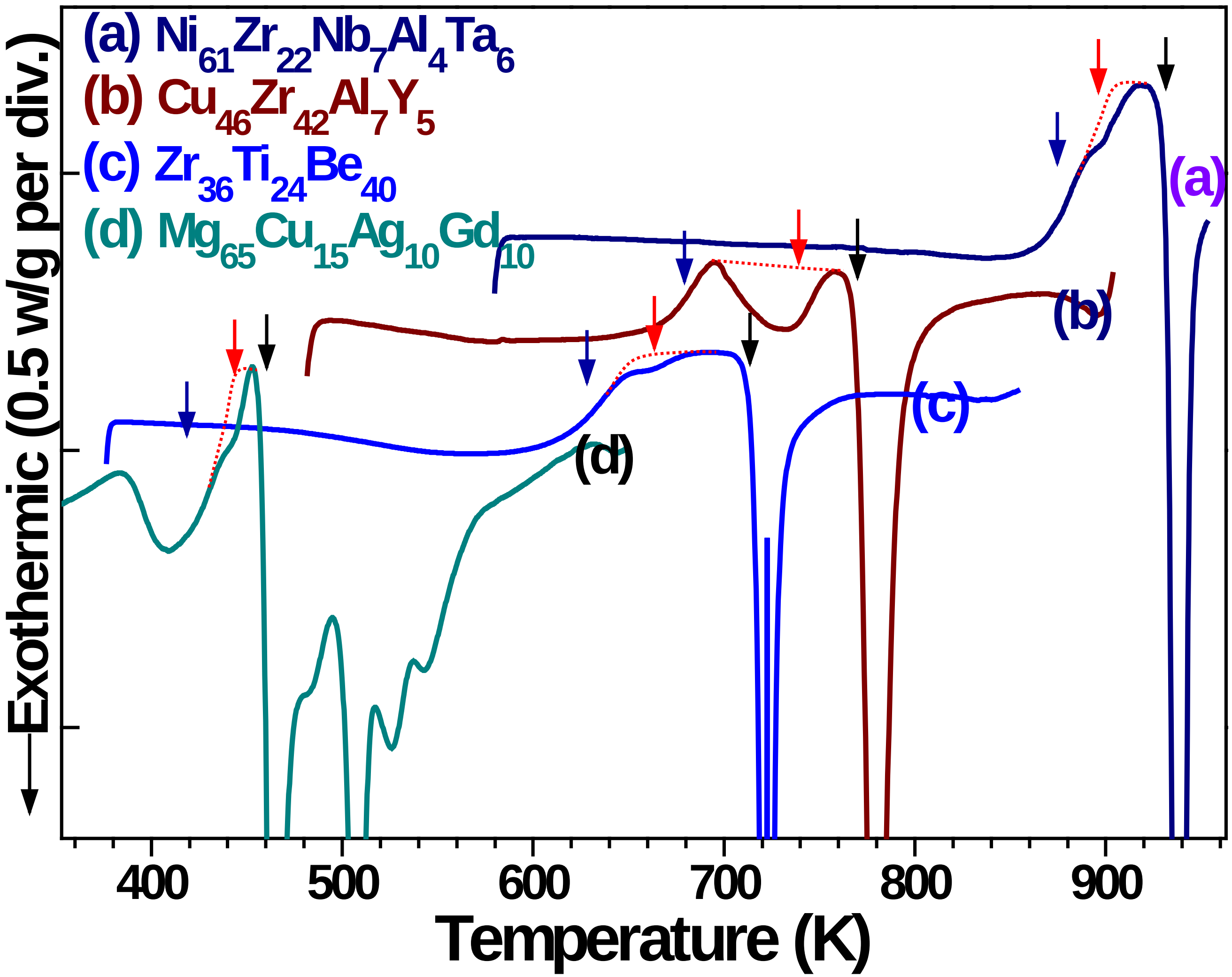

Effect of element having positive enthalpy of mixing

- **Atom probe concentration depth profiles in $Ni_{61}Zr_{22}Nb_7Al_4Ta_6$**

(a) As-cast **(b) H876** **(c) H897**

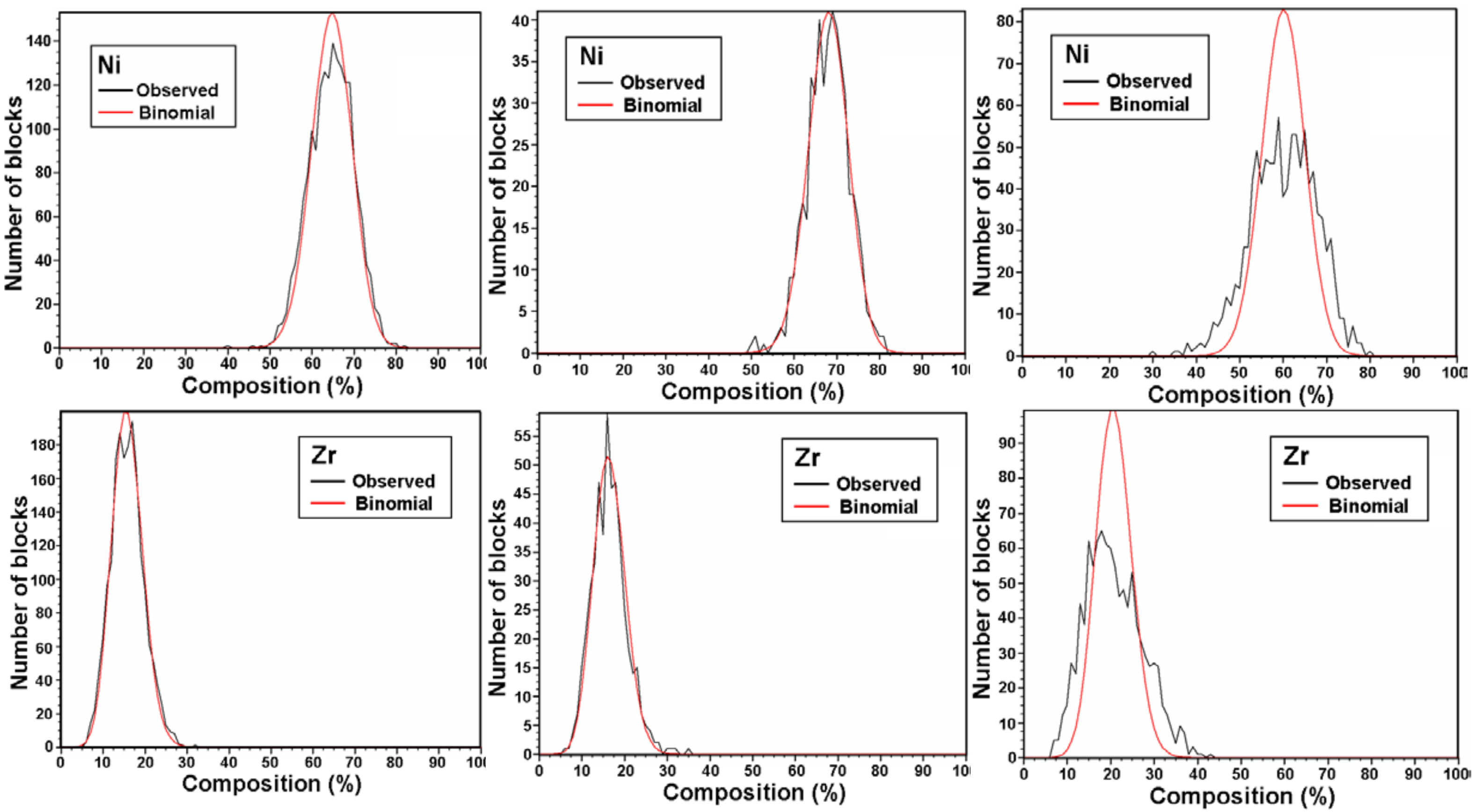

easy crystallization

Effect of element having positive enthalpy of mixing

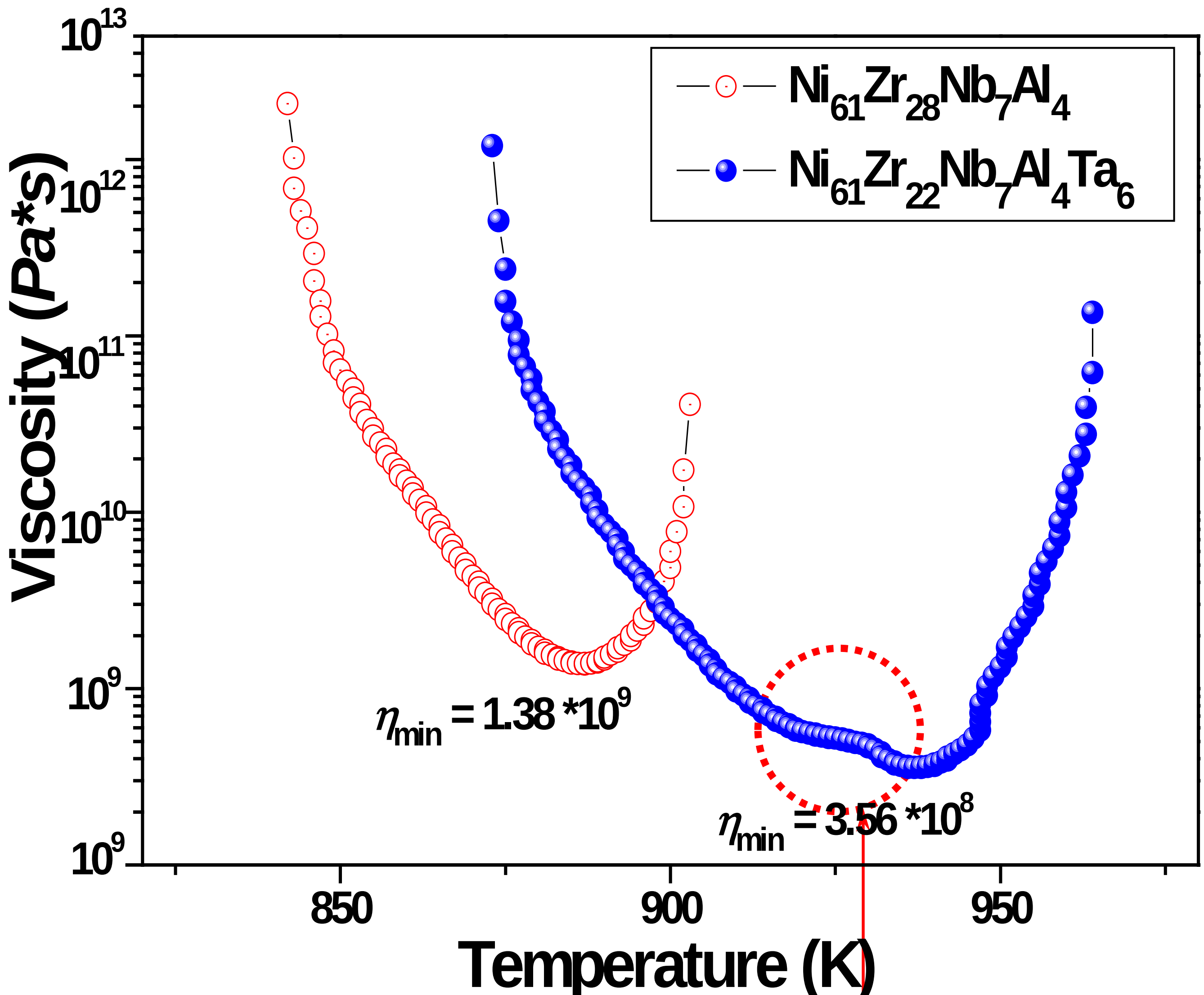

Ordering in supercooled liquid region

Enhancement plasticity in BMGs with atomic scale heterogeneity

b) Effect of element having significantly different enthalpy of mixing among constituent elements

Effect of element having large different enthalpy of mixing

- **Cu-Zr-Be ternary alloy system**

* Acta Materialia, 56 3120 (2008)

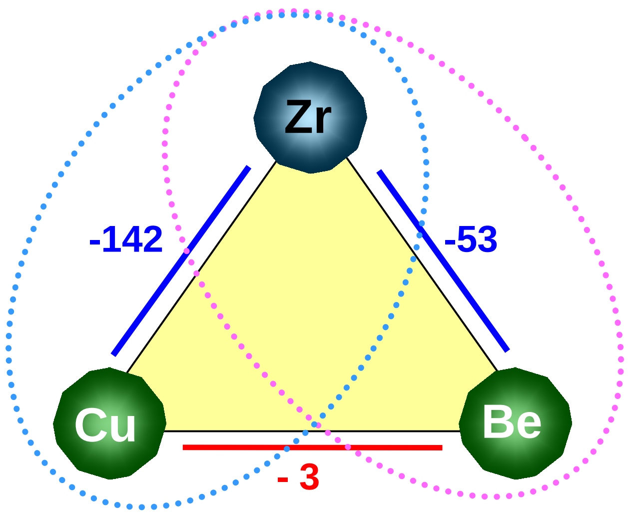

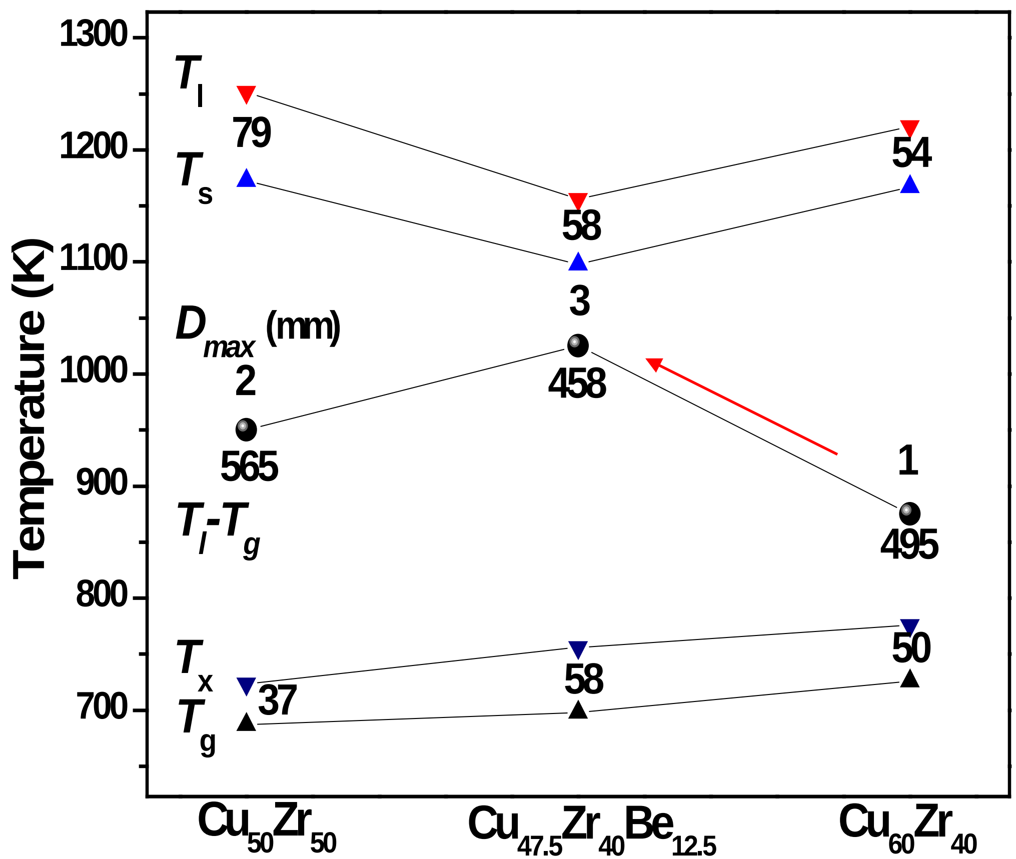

Effect of element having large different enthalpy of mixing

- Compression test

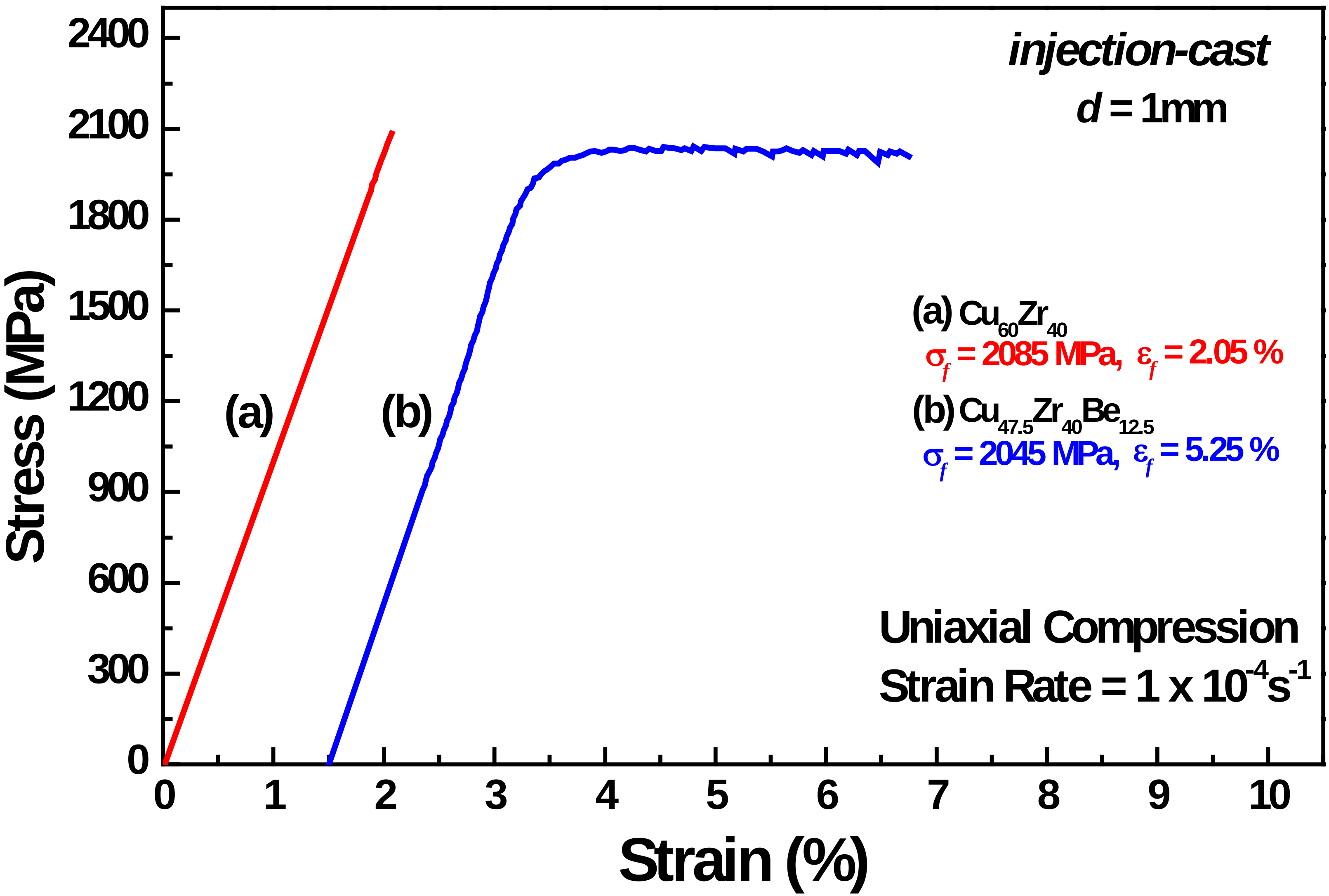

Effect of element having large different enthalpy of mixing

- **3DAP-FIM results**

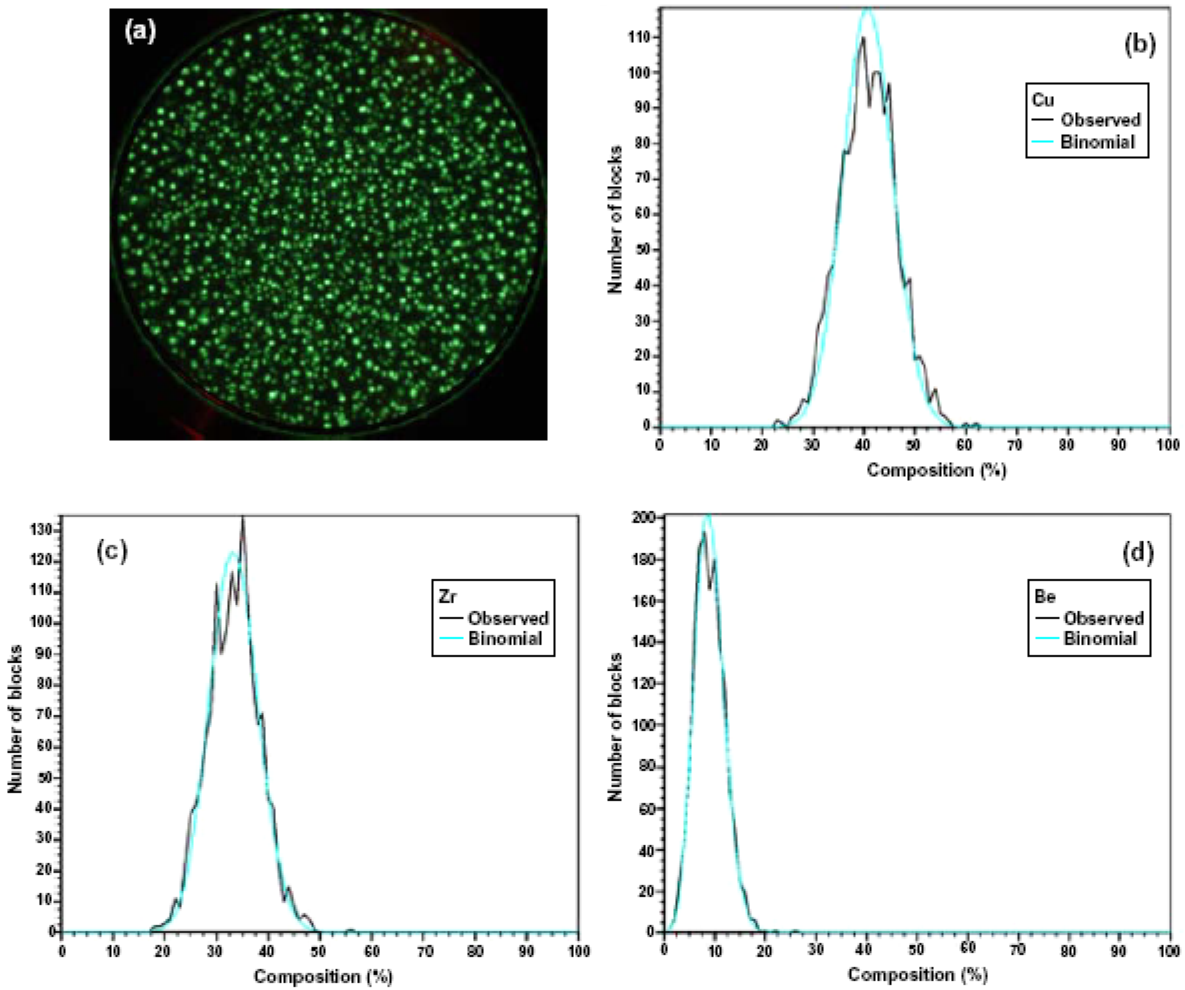

(a) FIM image and (b)-(d) composition depth profile of the as-spun $Cu_{47.5}Zr_{40}Be_{12.5}$ ribbon sample

Effect of element having large different enthalpy of mixing

* Acta Materialia, 56 3120 (2008)

EXAFS analysis

	r (Å)		*N*		Total *N*	σ^2	
	Cu-Cu	Cu-Zr	Cu-Cu	Cu-Zr		Cu-Cu	Cu-Zr
$Cu_{60}Zr_{40}$	2.49	2.69	3.0	3.7	6.7	0.0116	0.0233
$Cu_{47.5}Zr_{40}Be_{12.5}$	2.51	2.70	2.5	4.8	7.3	0.0107	0.0227
	Zr-Zr	Zr-Cu	Zr-Zr	Zr-Cu		Zr-Zr	Zr-Cu
$Cu_{60}Zr_{40}$	3.10	2.68	6.9	4.4	11.3	0.0263	0.0124
$Cu_{47.5}Zr_{40}Be_{12.5}$	3.12	2.69	6.2	3.5	9.7	0.0257	0.0130

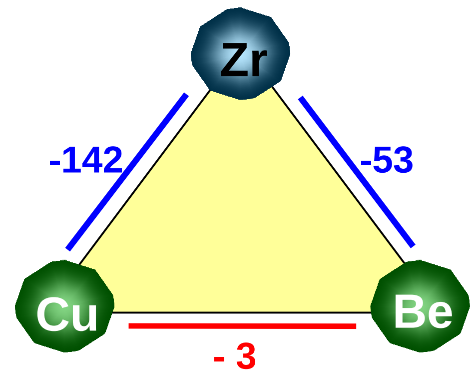

Atoimic diameter in Å: Cu-Cu = 2.56, Cu-Zr = 2.88, Zr-Zr = 3.20.

Cargill-Spaepen short-range order parameters, η

	Z_{AB}	$<Z>$	Z^*_{AB}	Z^{**}_{AB}	η
$Cu_{60}Zr_{40}$	3.7	8.540	3.416	3.546	0.043
$Cu_{47.5}Zr_{40}Be_{12.5}$	4.8	7.348	2.939	3.855	0.245

Cargill-Spaepen SRO parameter

$$\eta = Z_{AB} / Z^{**}_{AB} - 1$$

$$Z^{**}_{AB} = x_B Z_B Z_A / < Z >$$

$\eta > 0$

chemical ordering between AB nearest-neighbor pairs

Enhancement plasticity in BMGs with atomic scale heterogeneity

c) Effect of atomic scale heterogeneity on SB nucleation

Effect of alloy composition on SB nucleation

*Ni-Nb-Zr ternary alloy system

$Ni_{60}Nb_{40}$ and $Ni_{60}Nb_{20}Zr_{20}$ alloys

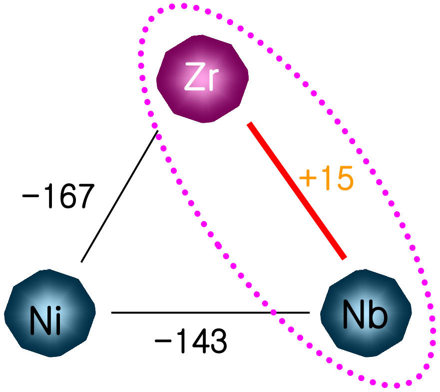

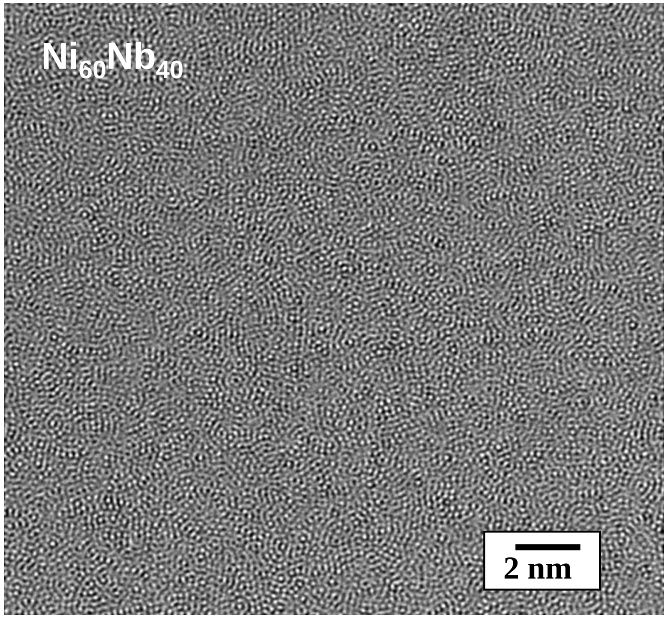

Zr addition

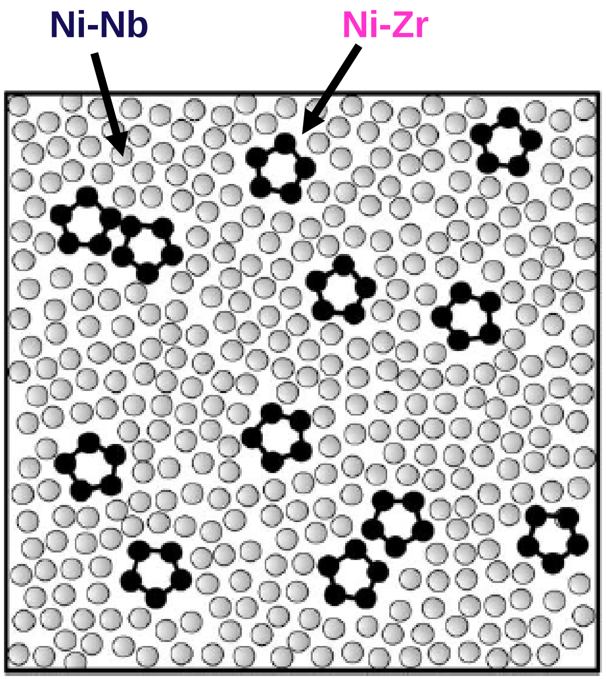

Compositional inhomogeniety

(conformed by EXAFS)

Experimental equipment

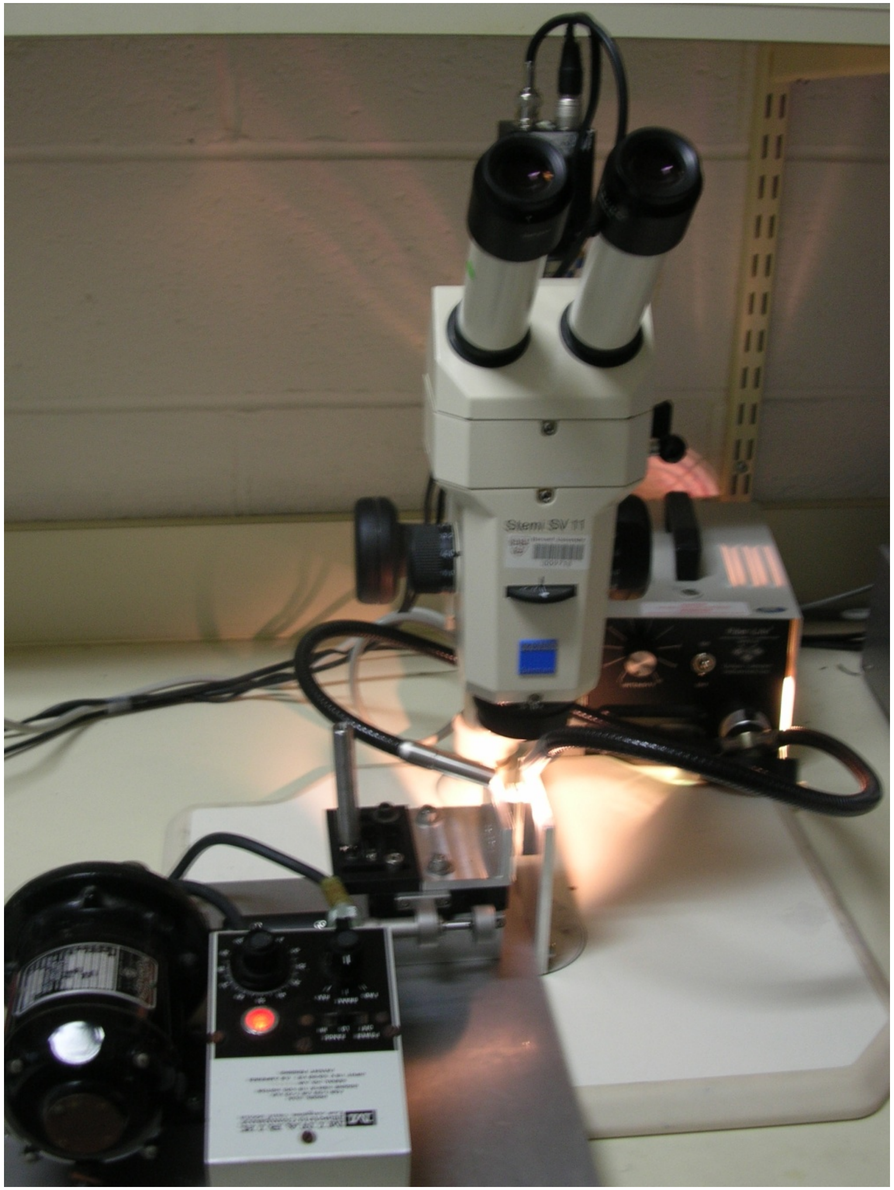

Normal camera
25 frames per sec
Interval : 0.04 sec

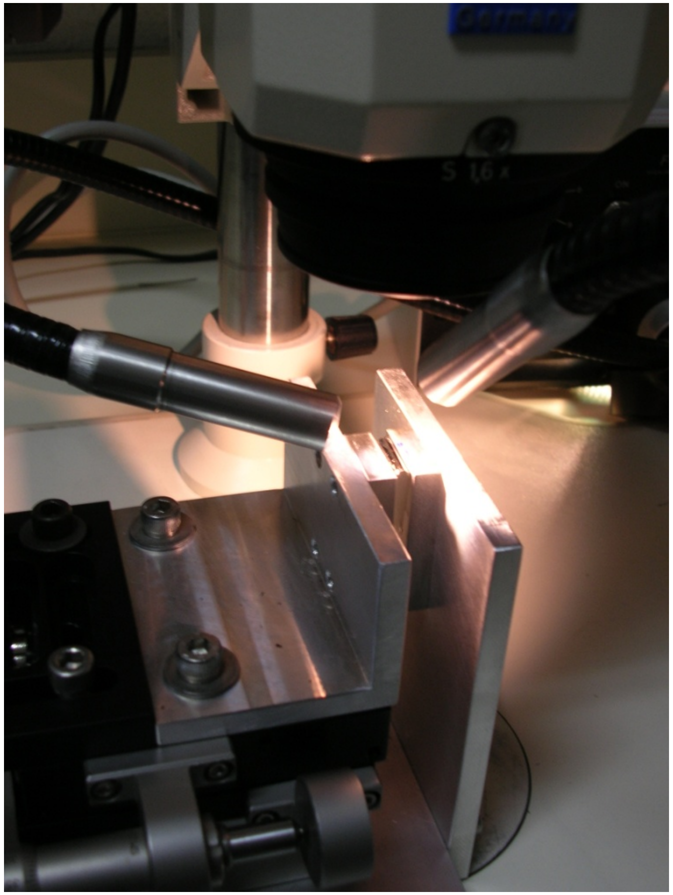

Effect of local favored structure on SB nucleation

- $Ni_{60}Nb_{40}$: fully amorphous phase

S=0.016 mm/sec

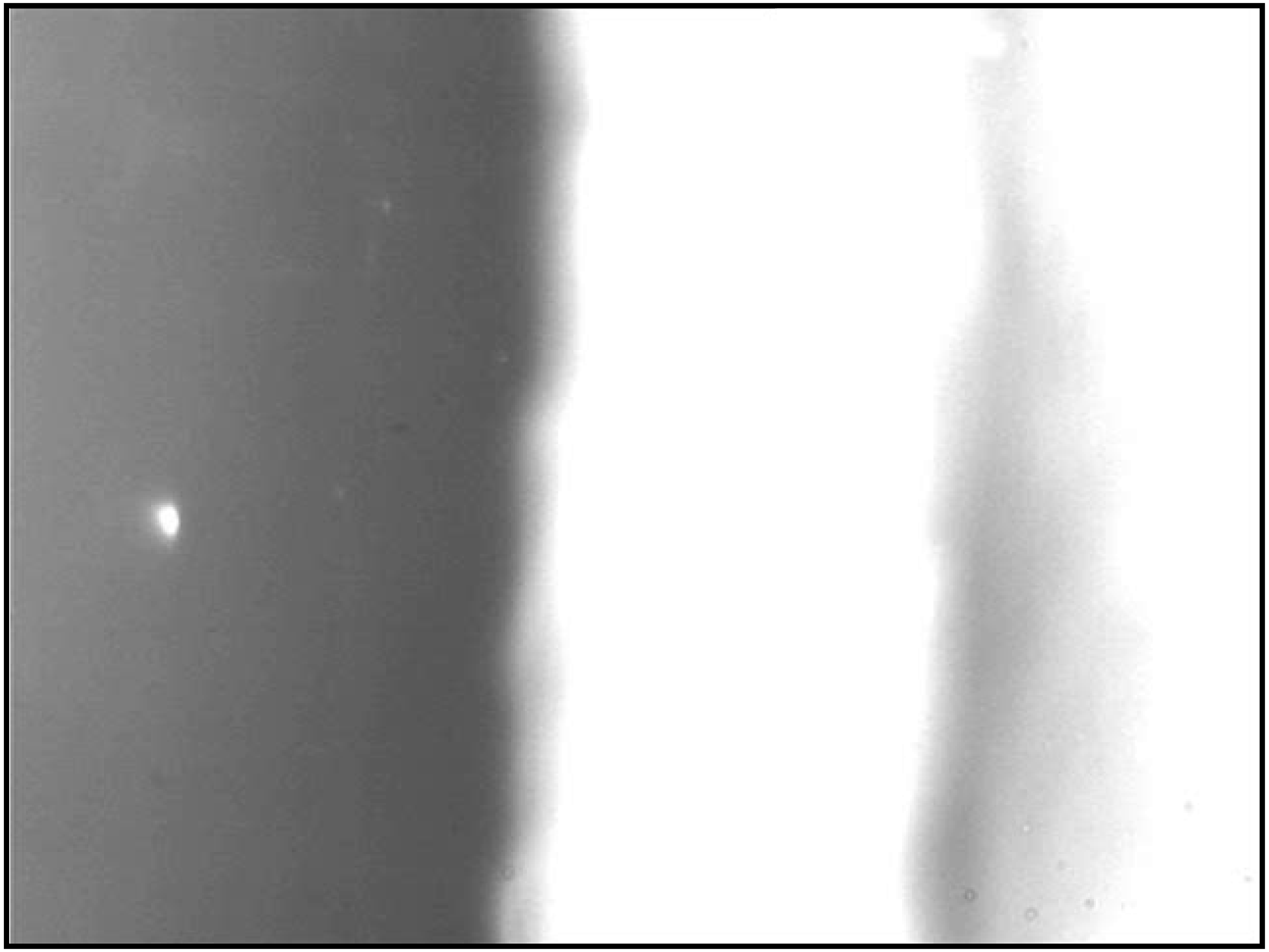

100 µm

Effect of local favored structure on SB nucleation

- $Ni_{60}Nb_{20}Zr_{20}$: amorphous phase with local favored structure

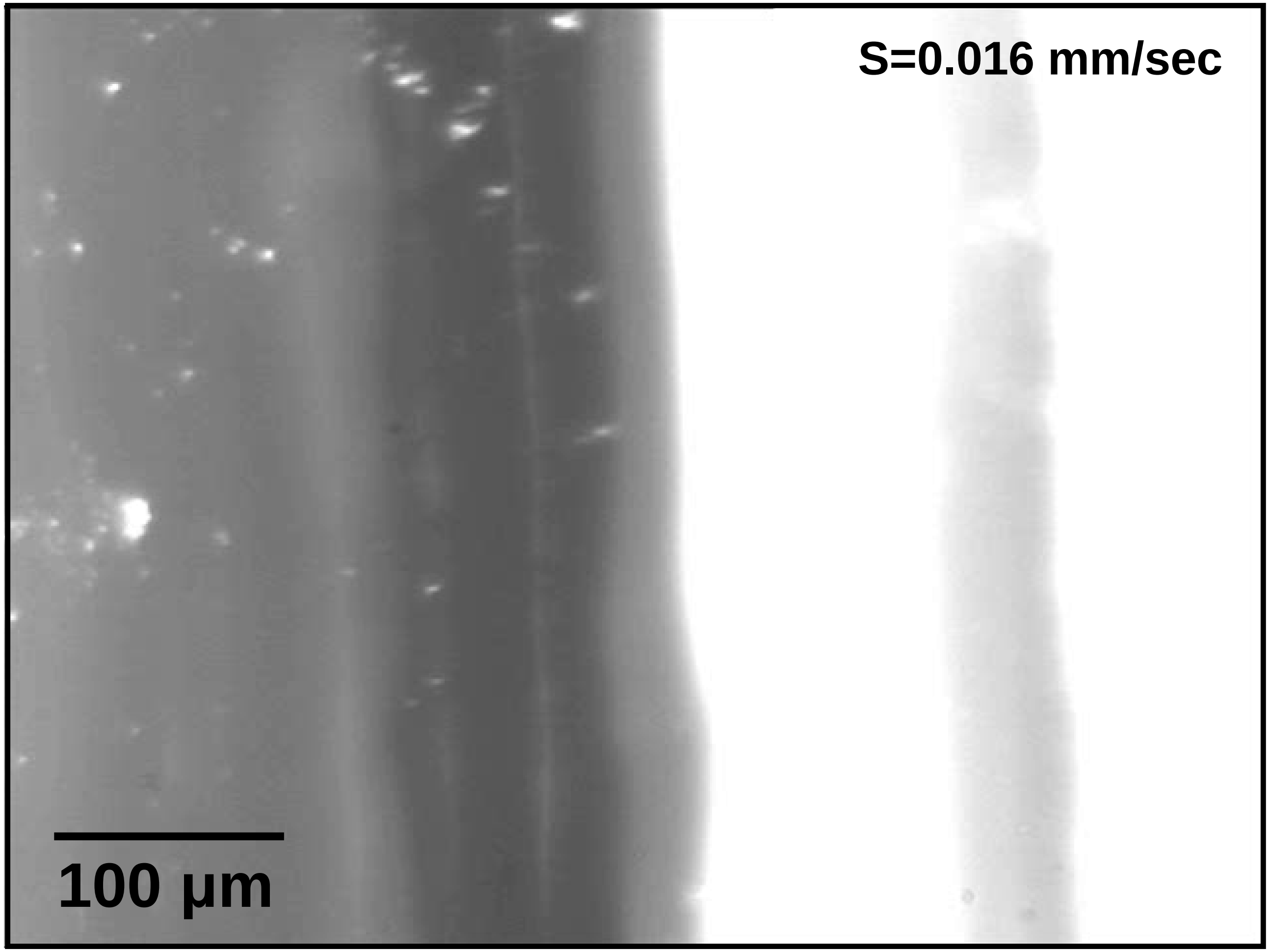

- **Increased nucleation sites of shear bands**

  ; evaluate the local heterogeneity in amorphous phase

Tailoring of structural inheterogeneity

- **Alloy design** + **Process control**

atomic scale inhomogeneity generation **Solidification under appropriate conditions**

Enhanced plasticity in $Ni_{60}Nb_{32}Zr_8$, $Ni_{60}Nb_{30}Zr_{10}$ BMGs (σ_{max} : 3.2 GPa, ε_p : 2.5 %)

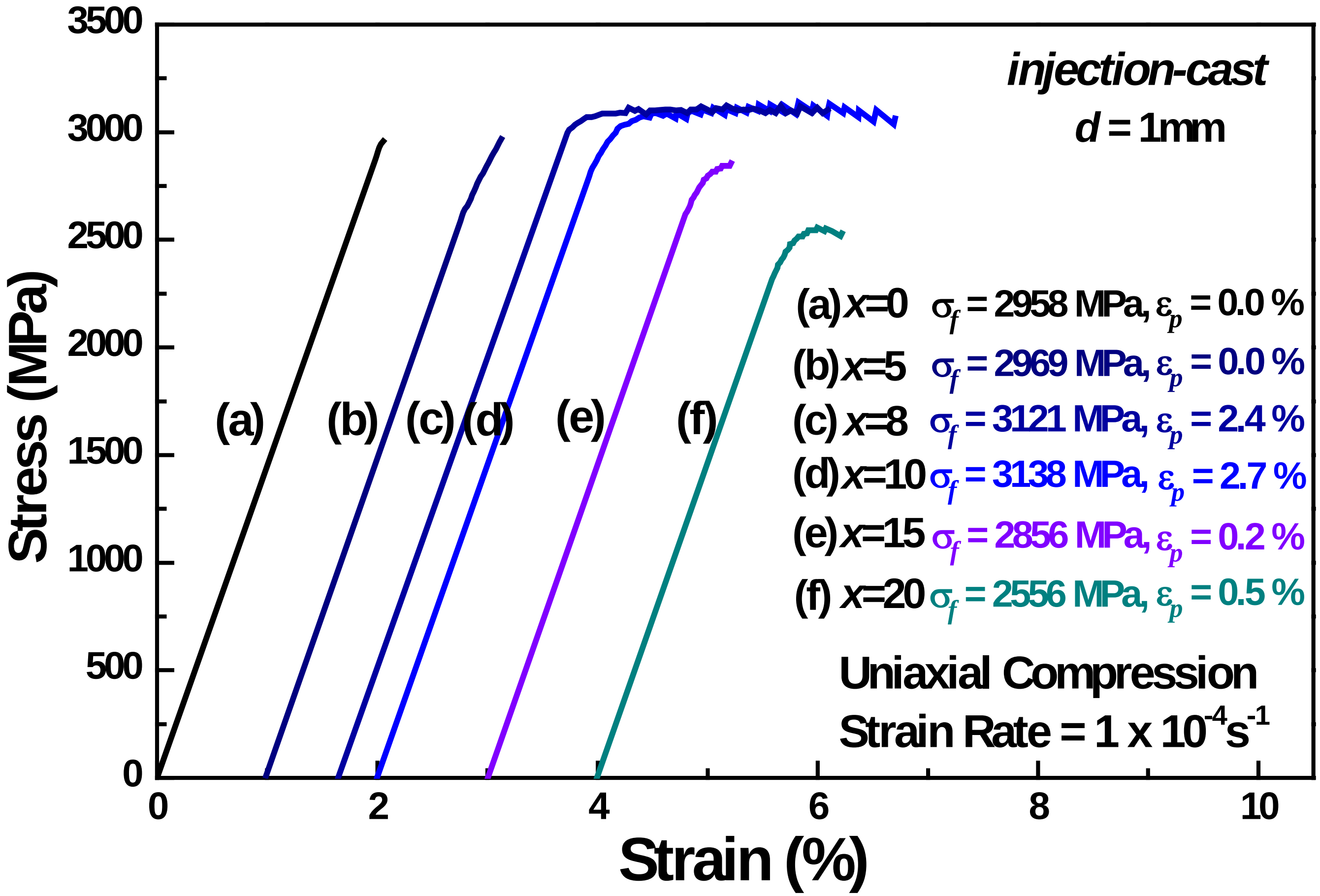

Comparison of Work-hardenability depending on 2nd Phases

S.C.

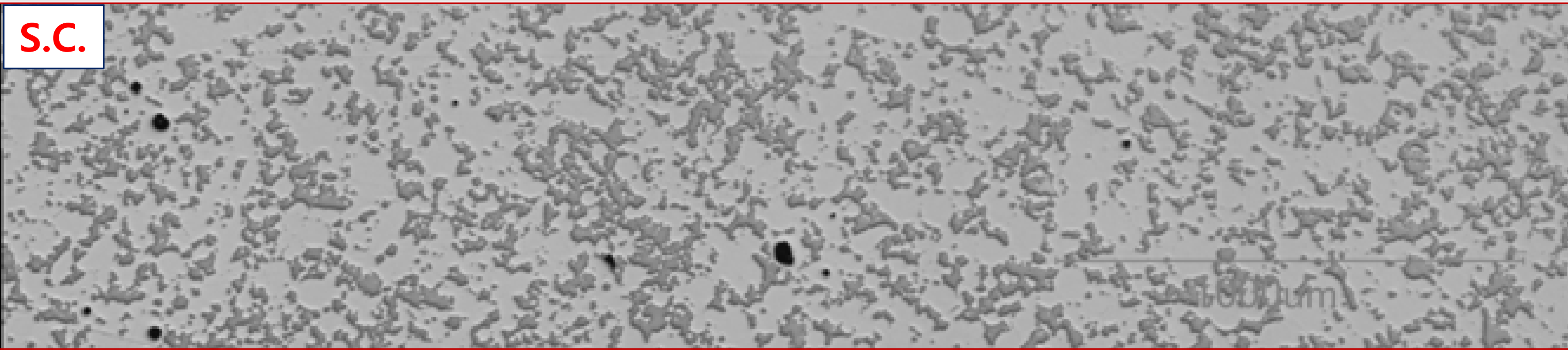

H.C.

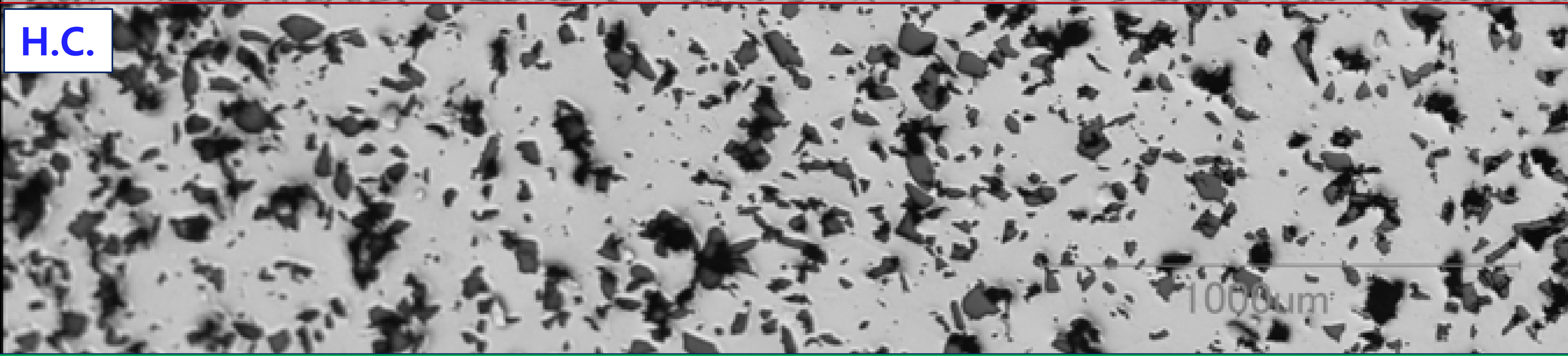

SMA

Comparison of Work-hardenability depending on 2nd Phases

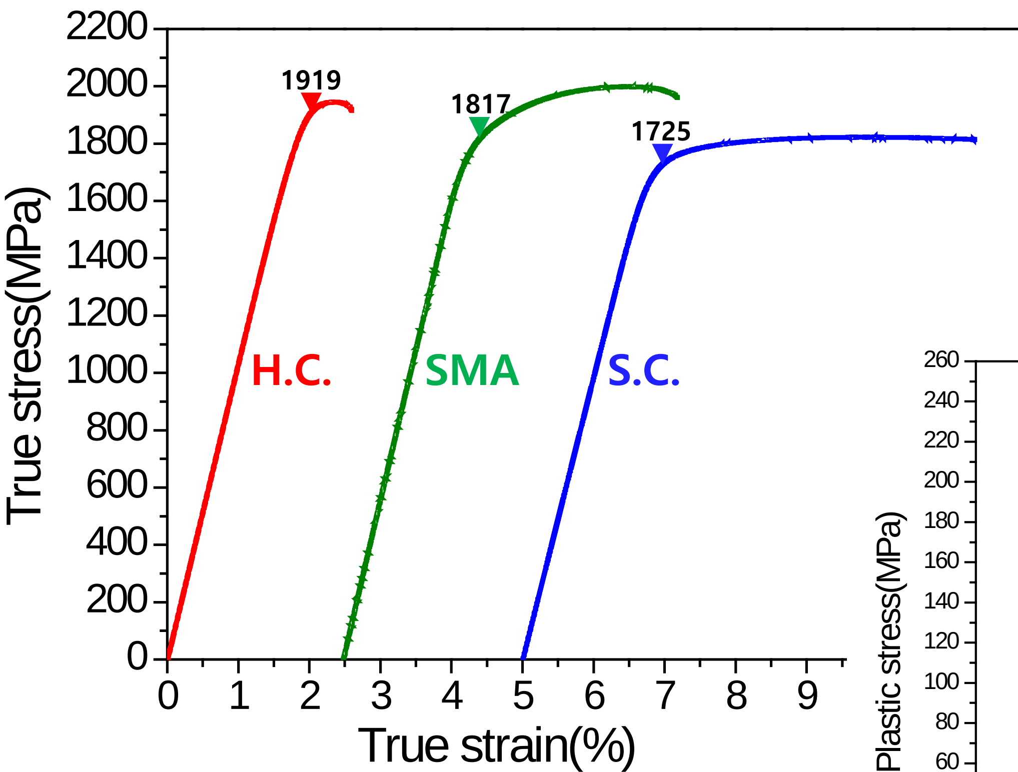

$$\sigma_p = \sigma - \sigma_y$$

$$\varepsilon_p = \varepsilon - \varepsilon_y - \frac{\sigma_p}{E}$$

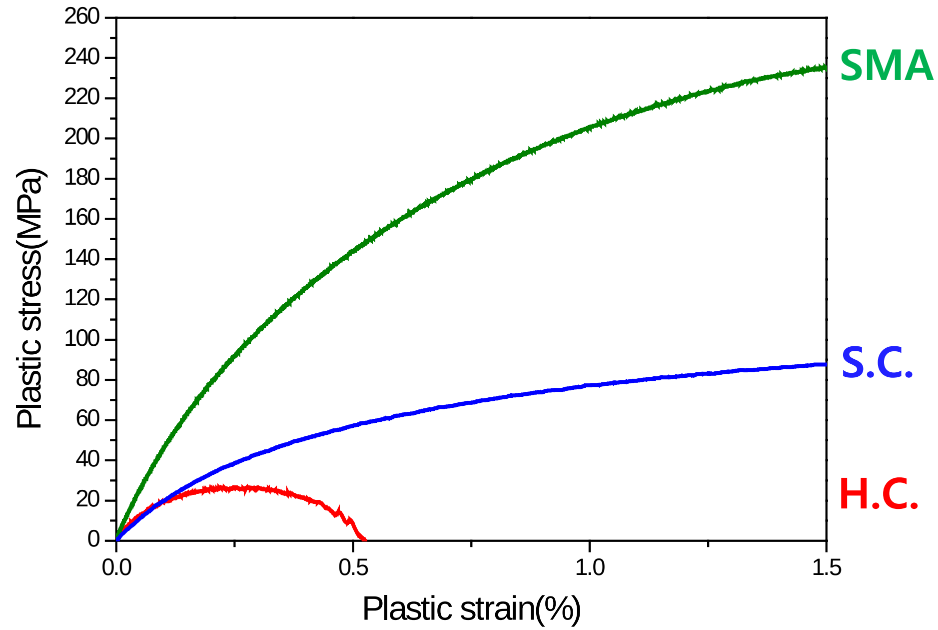

- **SMA : Strain hardening**
- **H.C., S.C. : Strain softening**

Higher strain hardening of SMA, then larger work hardenability of BMGMCs

Strain hardening(2nd) ➡ Work hardening

(SMA > S.C. > H.C.) (SMA > S.C. > H.C.)

Investigation of deformation of BMGC with "soft" phases

*** BMGCs with soft crystalline 2nd phases**

(a)

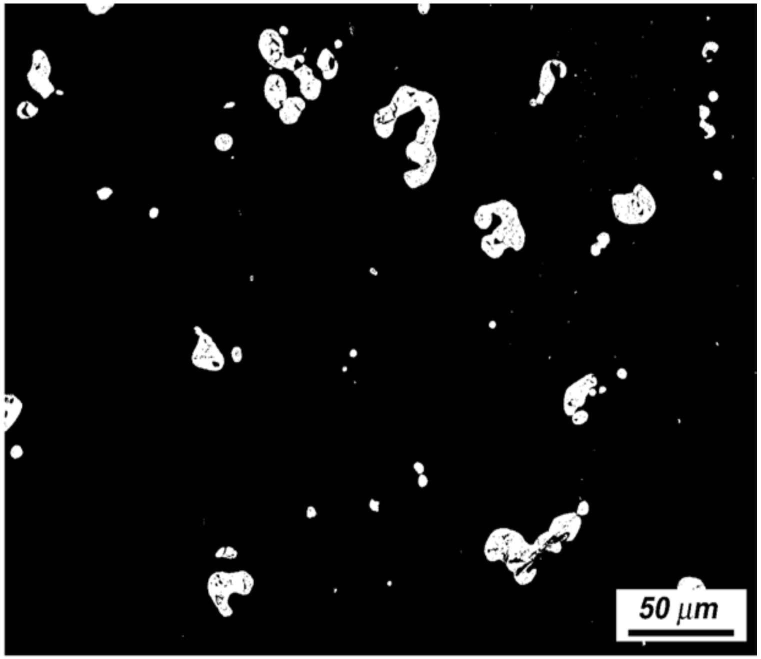

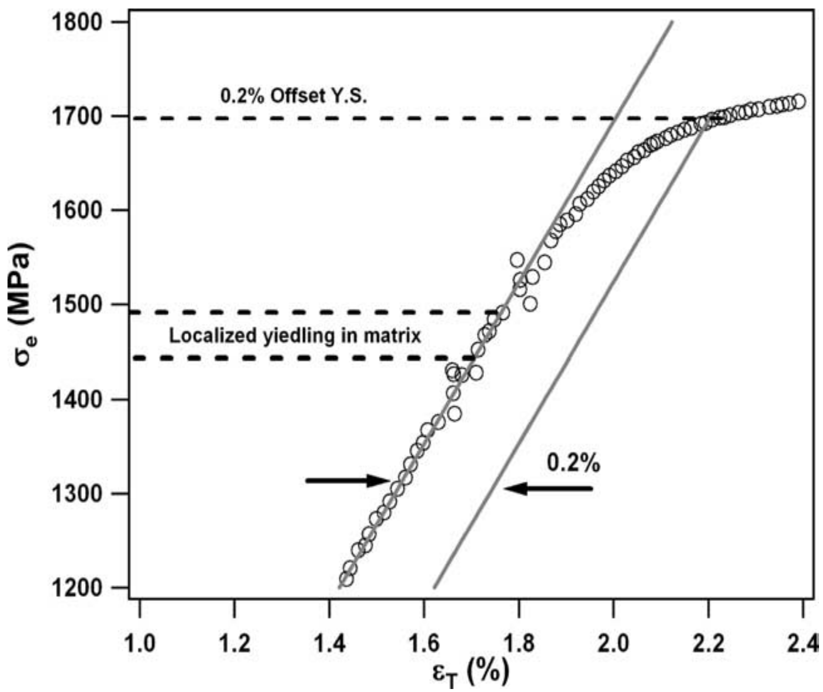

- **Zr based metallic glass + 8% Ta**
- **Compression test with in-situ X-ray synchrotron diffraction**

(Beamline 1-ID beamline of the Advanced Photon Source at Argonne National Laboratory)

Investigation of deformation of BMGC with "soft" phases

* BMGCs with soft crystalline 2nd phases

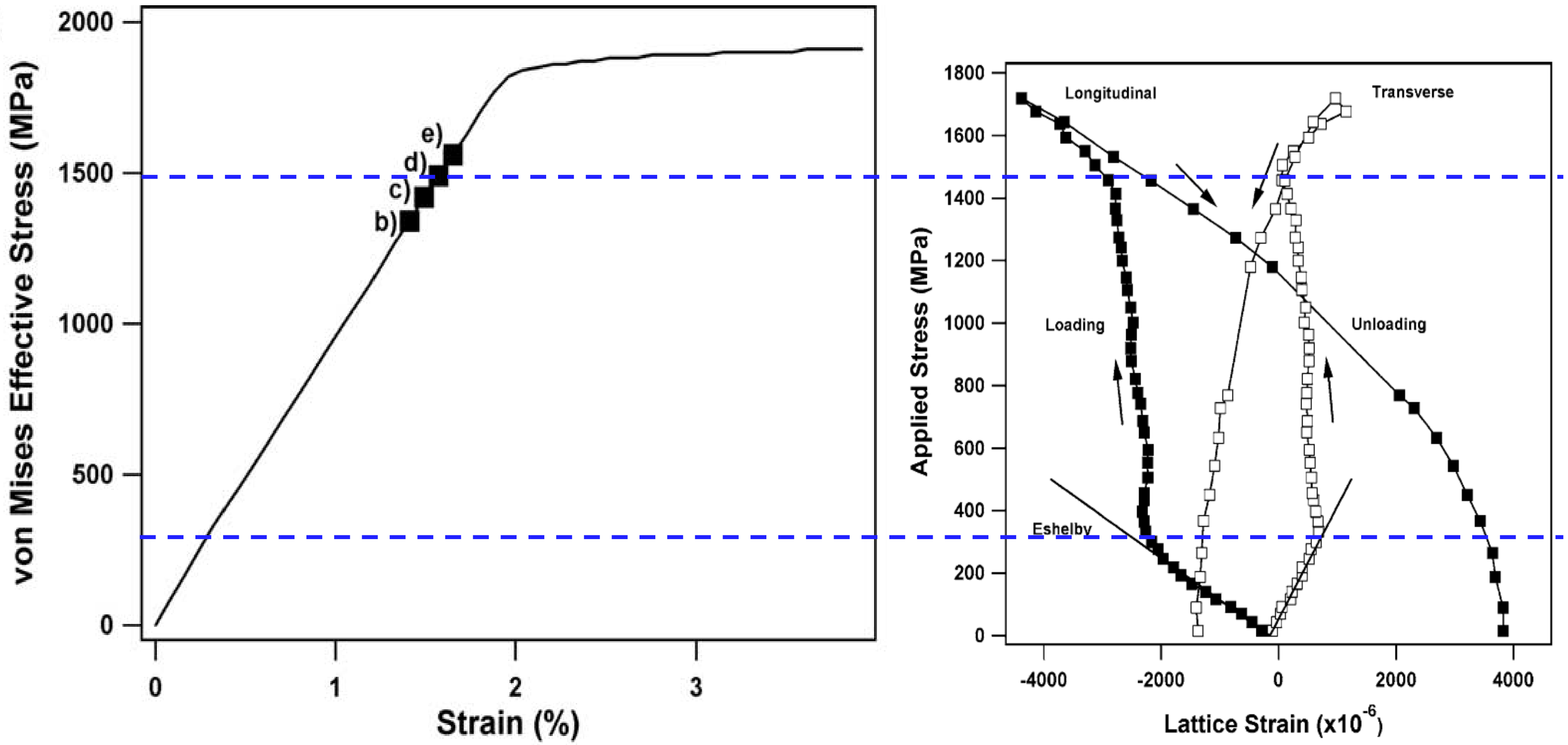

- At approximately 325 MPa applied stress, the particles yield, which are constrained by amorphous matrix causing plastic misfit stress near the particles.
- At an applied stress of 1450 MPa (just below yield stress), the lattice stress–strain curve changes slope again for both the longitudinal and transverse directions, indicating an increase in the fraction of the load being transferred to Ta particles.

Investigation of deformation of BMGC with "soft" phases

* BMGCs with soft crystalline 2nd phases

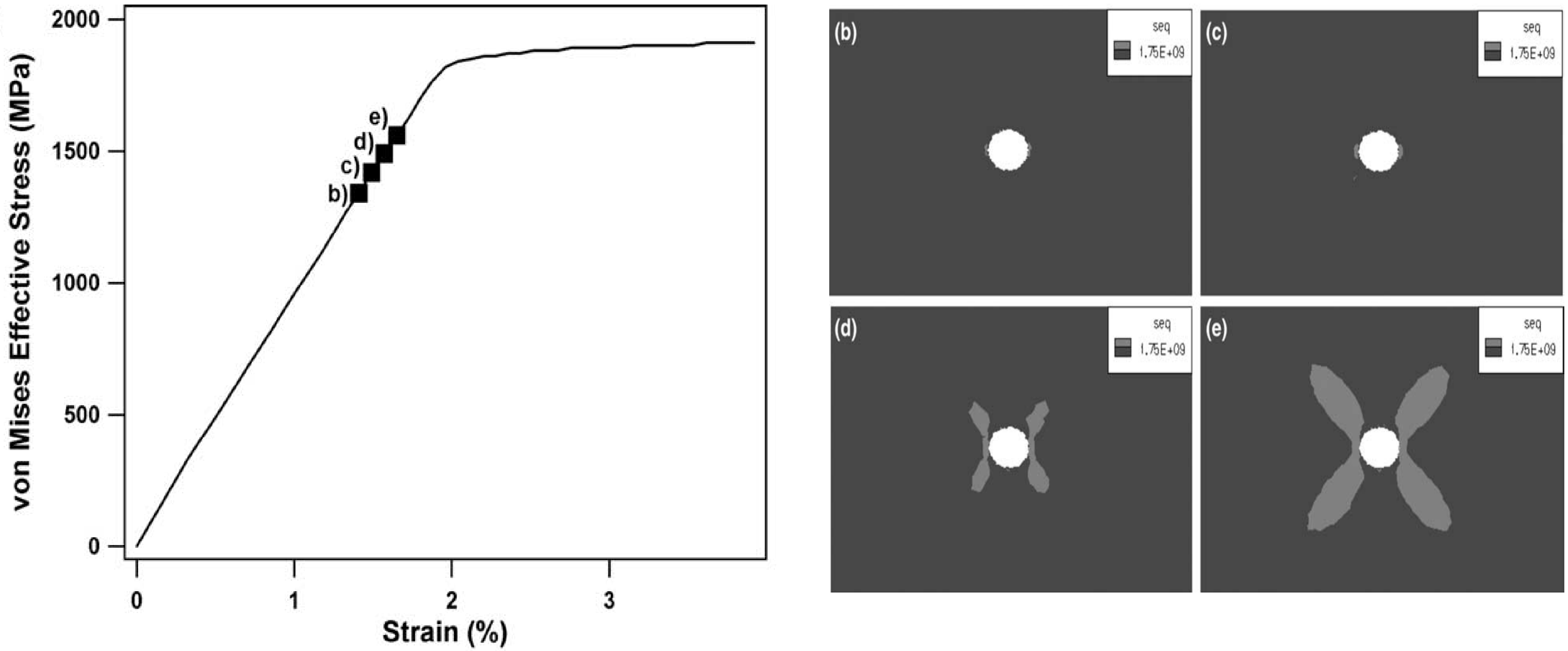

- Plastic misfit strain creates a significant stress concentration around the particles.
- Shear bands initiates near the particles due to the localized stress concentration.
- If a shear band initiates at the particle and propagates away, it will quickly encounter a region where the yield criterion is not satisfied and the shear stress is insufficient to sustain shear band propagation.

Principle of multiple shear band initiations & blocking shear bands propagation

Investigation of deformation of BMGC with "hard" phases

* BMGCs with hard ceramic 2nd phase

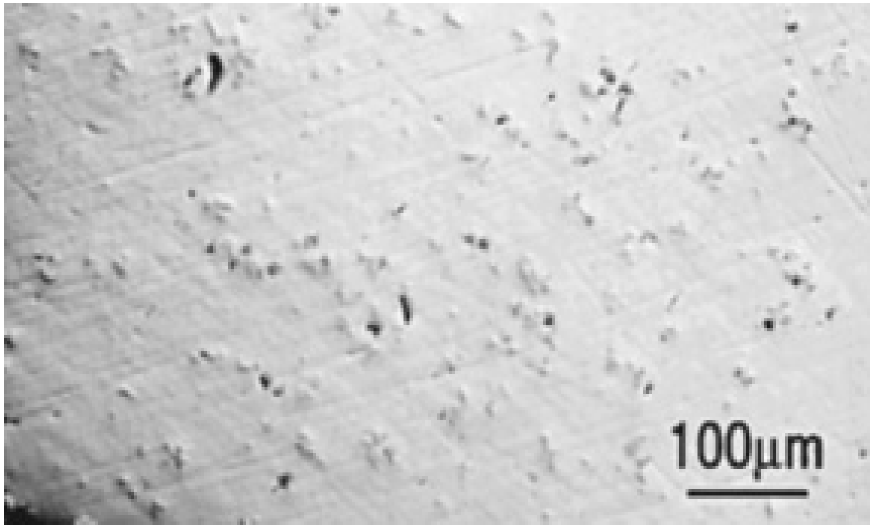

- Residual strain were measured by neutron diffraction.
- Each phase strain in the ZrC-BMG during compressive loading was estimated from the residual strains in each specimen according to following equations:

$$\varepsilon_A = \frac{\sigma_{appl.}}{E} + \varepsilon_{res\_A} \quad \varepsilon_R = \varepsilon_{res\_R} - \frac{\nu\sigma_{appl.}}{E}.$$

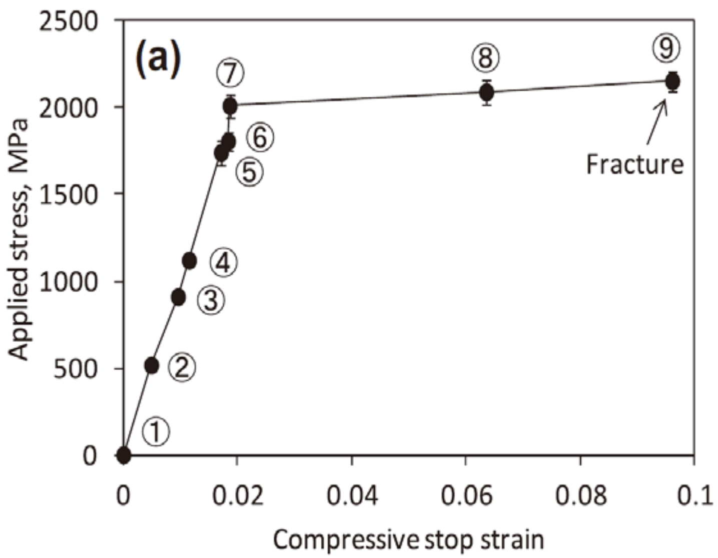

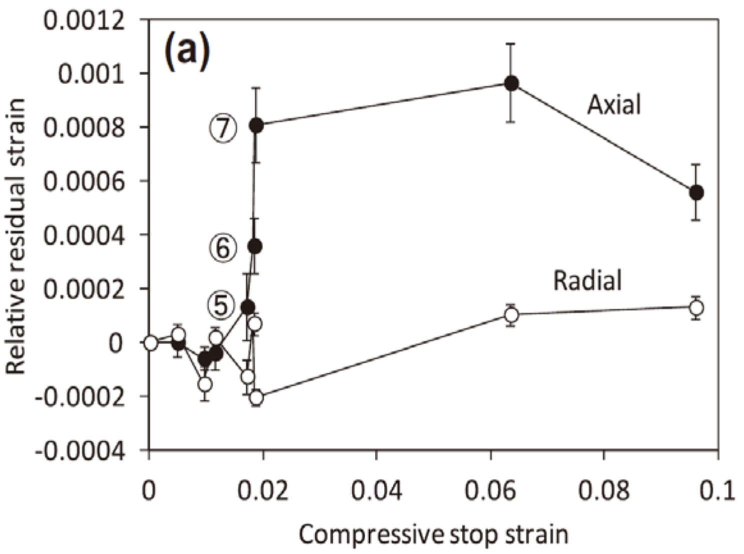

Investigation of deformation of BMGC with "hard" phases

* BMGCs with hard ceramic 2nd phases

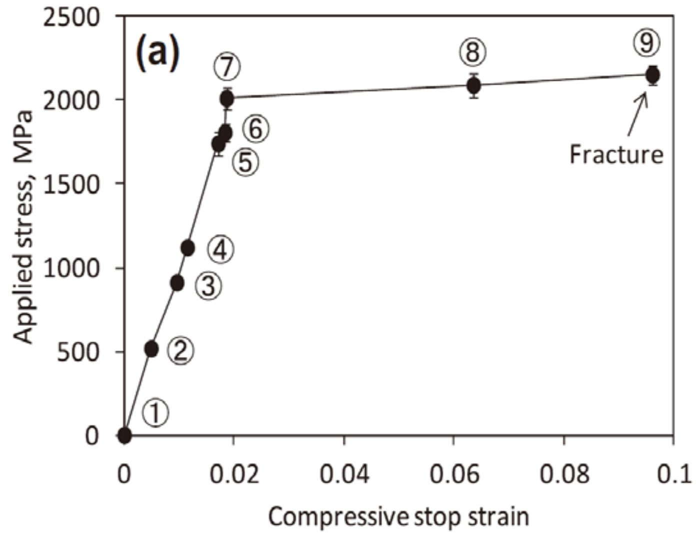

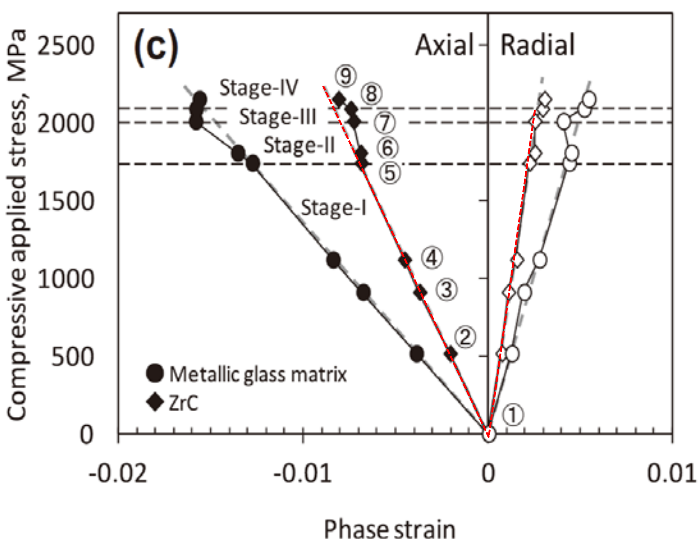

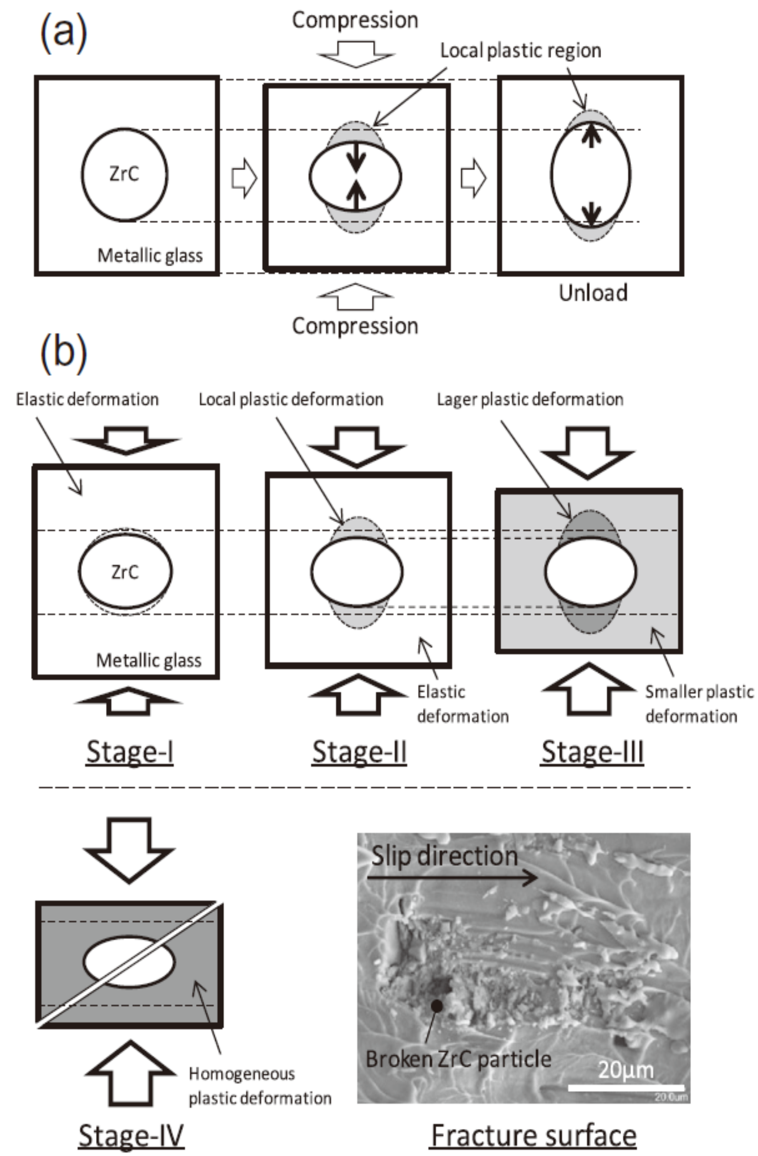

Mechanism of Work-hardening in BMGC with transformable 2nd phase

"Strain hardening of 2nd phase contributes to work hardening behavior of BMGC."

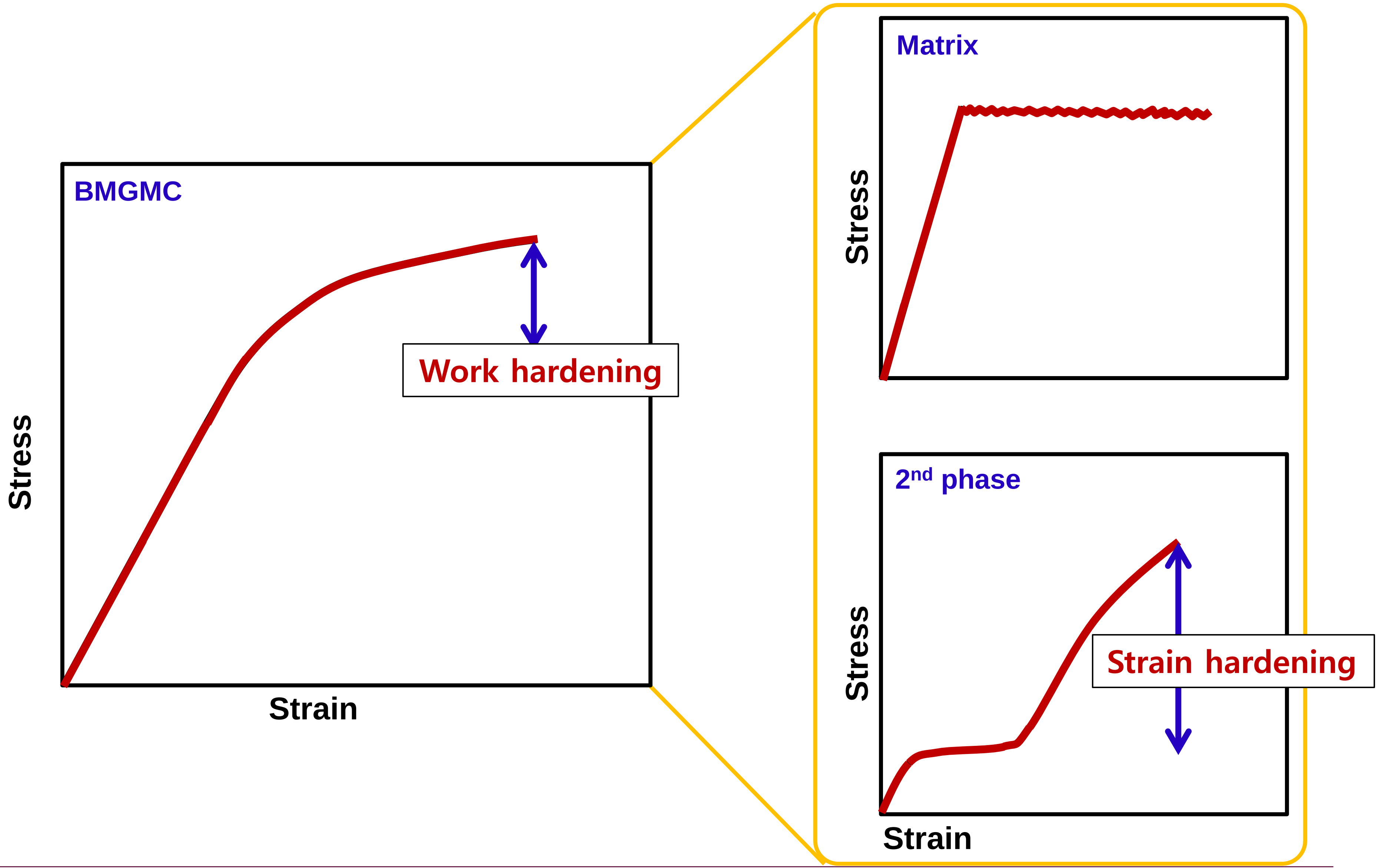

Deformation behaviors of BMGC depending on 2nd phase

< Compression >

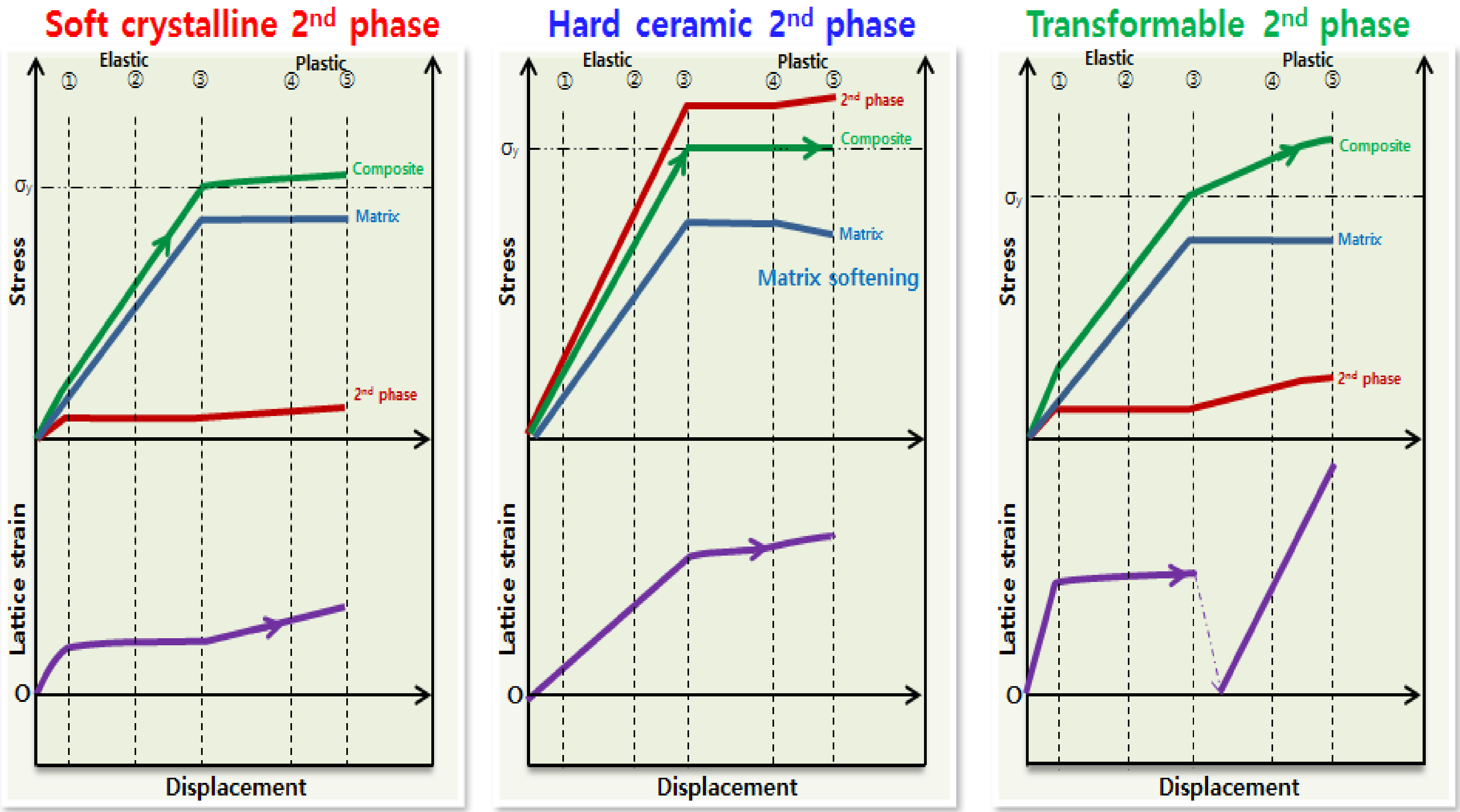

BMGMCs Strain hardening(2nd) ➡ Work hardening

(SMA > S.C. > H.C.) (SMA > S.C. > H.C.)

MATERIALS SCIENCE

10 SEPTEMBER 2010 VOL 329 SCIENCE

Shape Memory Bulk Metallic Glass Composites

Douglas C. Hofmann

Glass-forming and shape memory metals may provide a route to fabricating materials with enhanced mechanical properties.

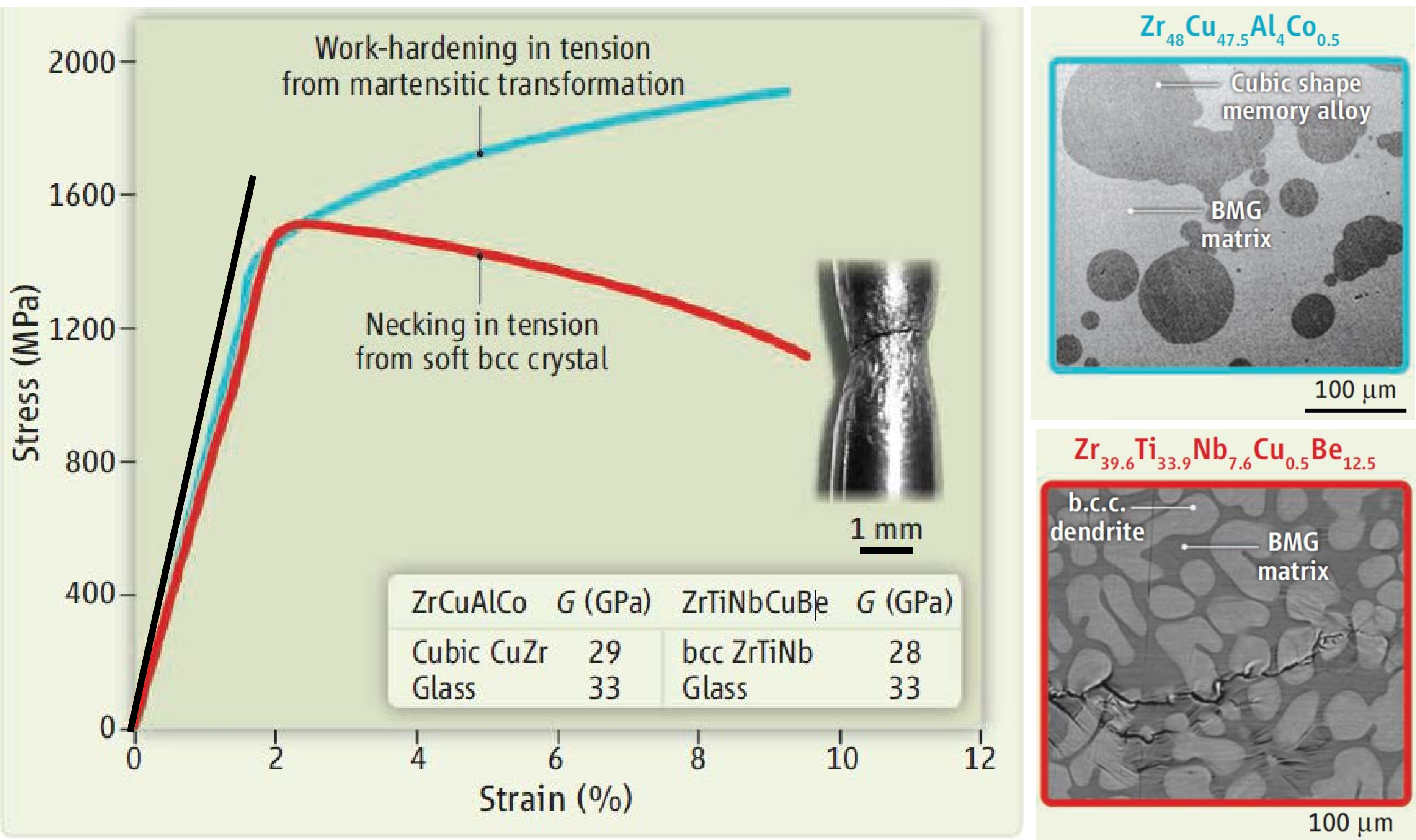

ZrCuAlCo	*G* (GPa)	ZrTiNbCuBe	*G* (GPa)
Cubic CuZr	29	bcc ZrTiNb	28
Glass	33	Glass	33

1) Work softening behavior by ductile secondary phase

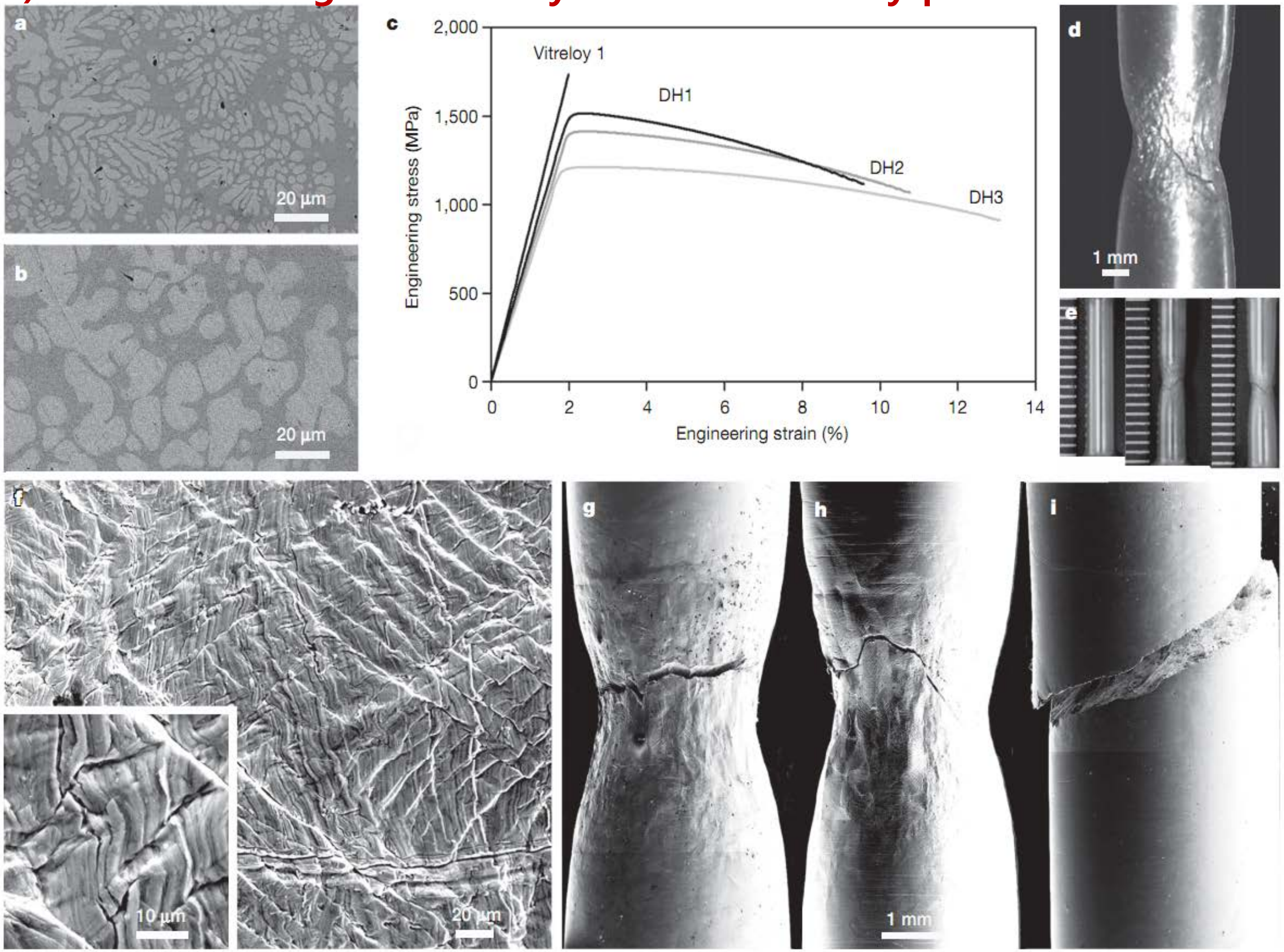

High fracture toughness: > 10 % plastic strain in tensile test

nature materials

Full text access provided to

nature.com ▸ journal home ▸ archive ▸ issue ▸ letter ▸ full text

NATURE MATERIALS | LETTER

Stress-induced phase transformation of secondary phase

Transformation-mediated ductility in CuZr-based bulk metallic glasses

S. Pauly, S. Gorantla, G. Wang, U. Kühn & J. Eckert

Affiliations | Contributions | Corresponding author

Nature Materials 9, 473–477 (2010) | doi:10.1038/nmat2767

Received 17 November 2009 | Accepted 09 April 2010 | Published online 16 May 2010

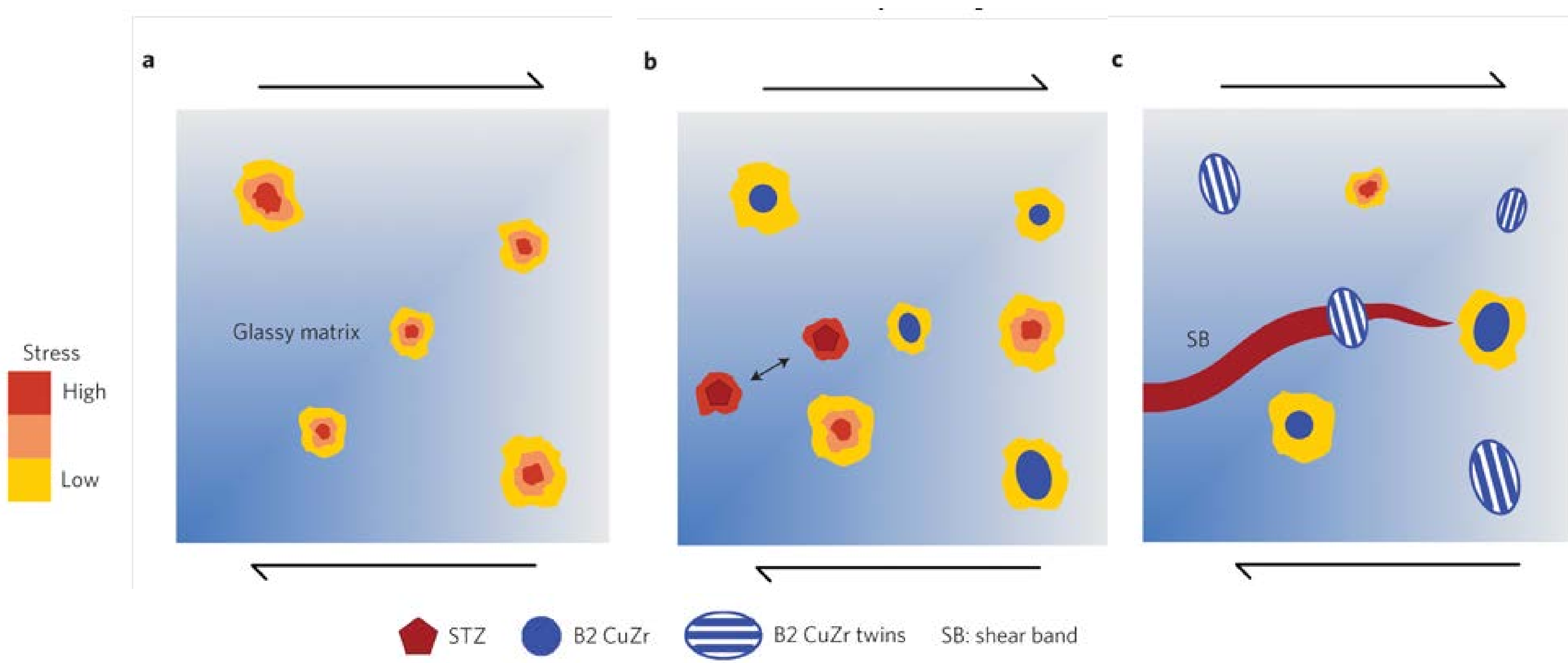

Figure 3: Microstructure of a $Cu_{47.5}Zr_{47.5}Al_5$ specimen deformed to fracture.

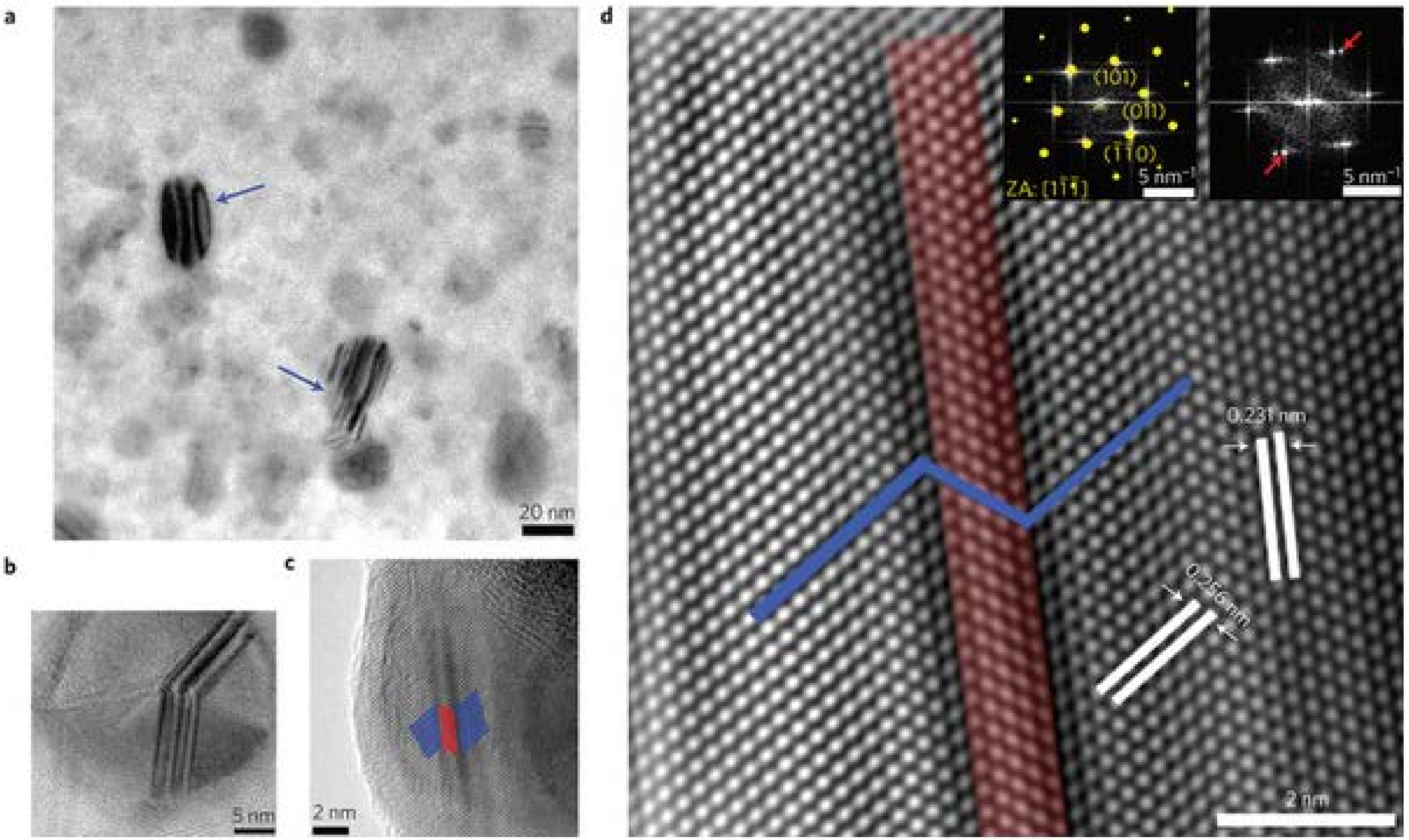

Work-hardening behavior of BMGCs in tension

www.MaterialsViews.com

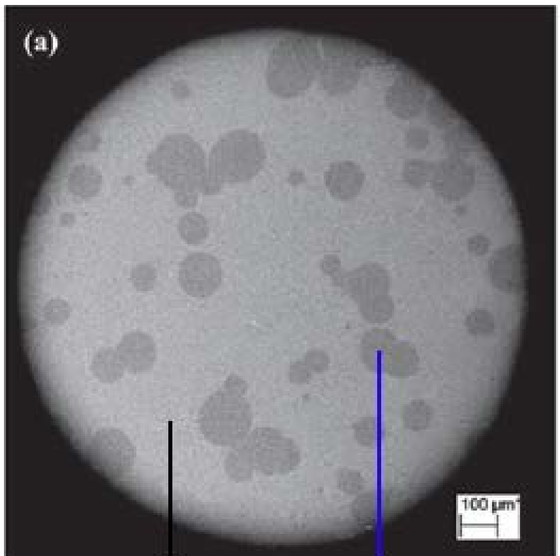

BMG matrix

CuZr B2

Transformation media

metastable phase at RT

Yuan Wu, et al. Adv. Mater. 2010, 22, 2770–2773

B2 ⟷ B19′ (temperature / stress)

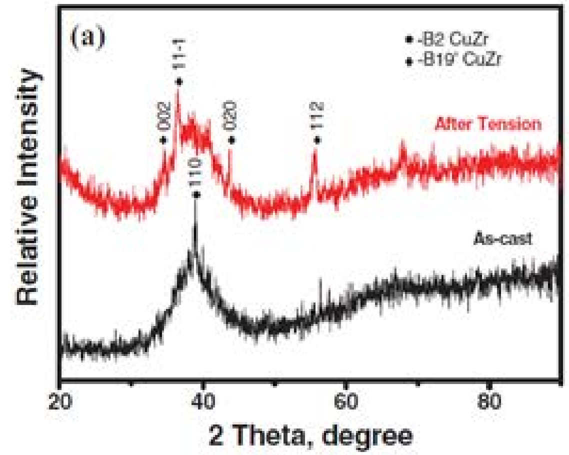

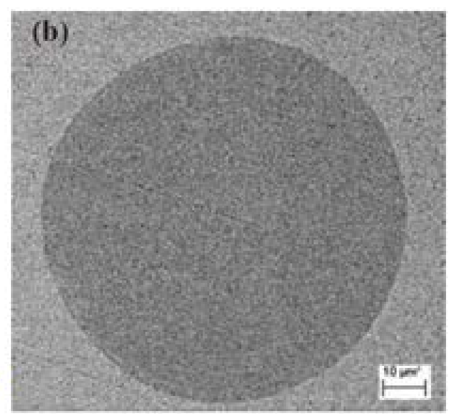

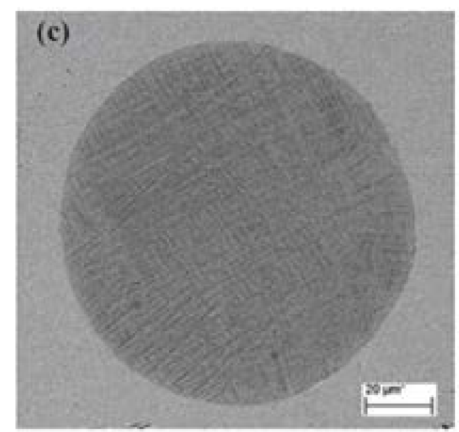

[XRD pattern & Morphology of secondary phase before / after tensile test]

Work-hardening behavior of BMGCs in tension

www.MaterialsViews.com

ADVANCED MATERIALS

www.advmat.de

COMMUNICATION

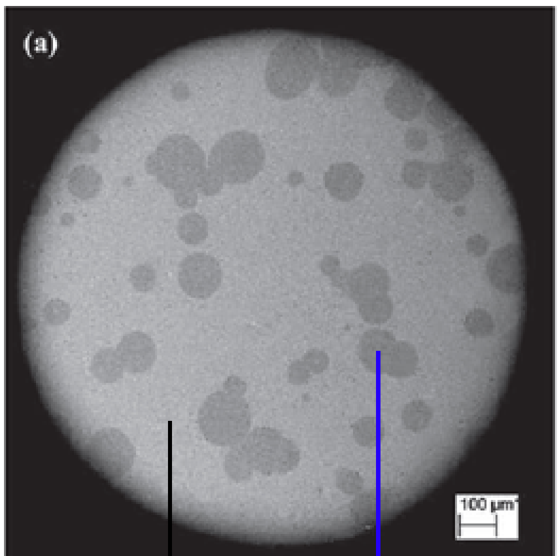

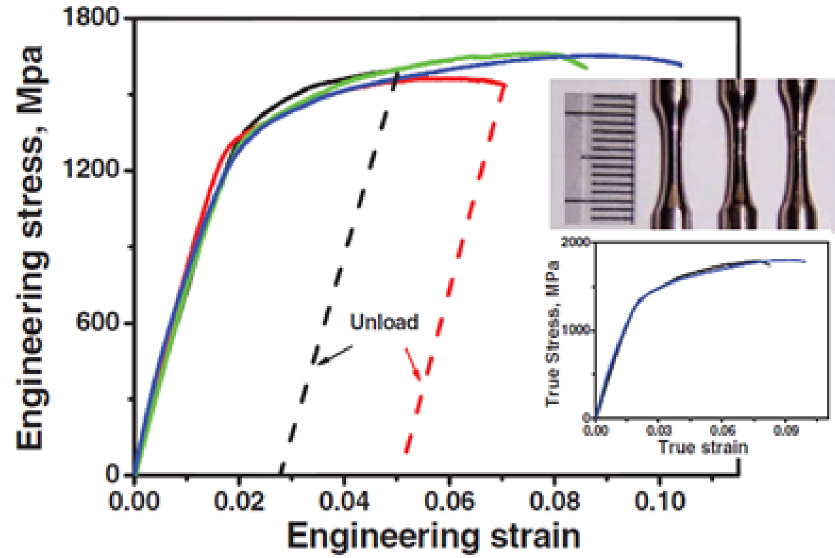

Figure 2. Engineering tensile stress–strain curves of the BMG composites. Dashed lines indicate the unloading process. Top inset shows the outer appearance of the tensile samples pre-strained at the different stages and the lower inset shows the true tensile stress–strain curves, indicating a significant strain-hardening behavior.

BMG matrix

CuZr B2

Transformation media
metastable phase at RT

Yuan Wu, et al. Adv. Mater. 2010, 22, 2770–2773

Cu-Zr-Al system

Two different deformation behaviors of BMGC depending on 2nd phase

1) **Ductile phase** $Zr_{39.6}Ti_{33.9}Nb_{7.6}Cu_{0.5}Be_{12.5}$

→ **Work softening**

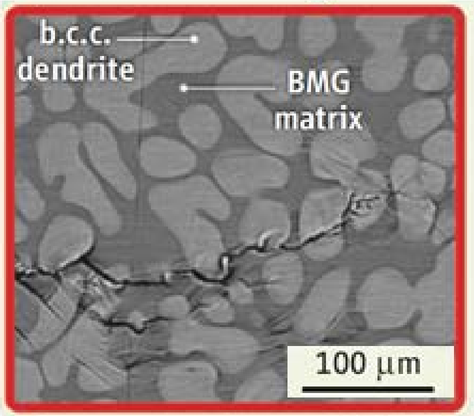

2) **Transformation media** $Zr_{48}Cu_{47.5}Al_{4}Co_{0.5}$

→ **Work hardening**

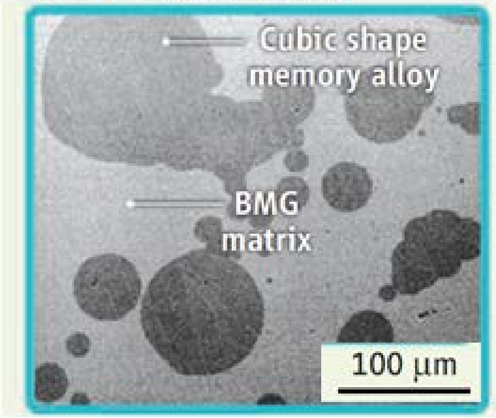

< Tension >

Douglas C. Hofmann, SCIENCE VOL 329 10 SEPTEMBER 2010

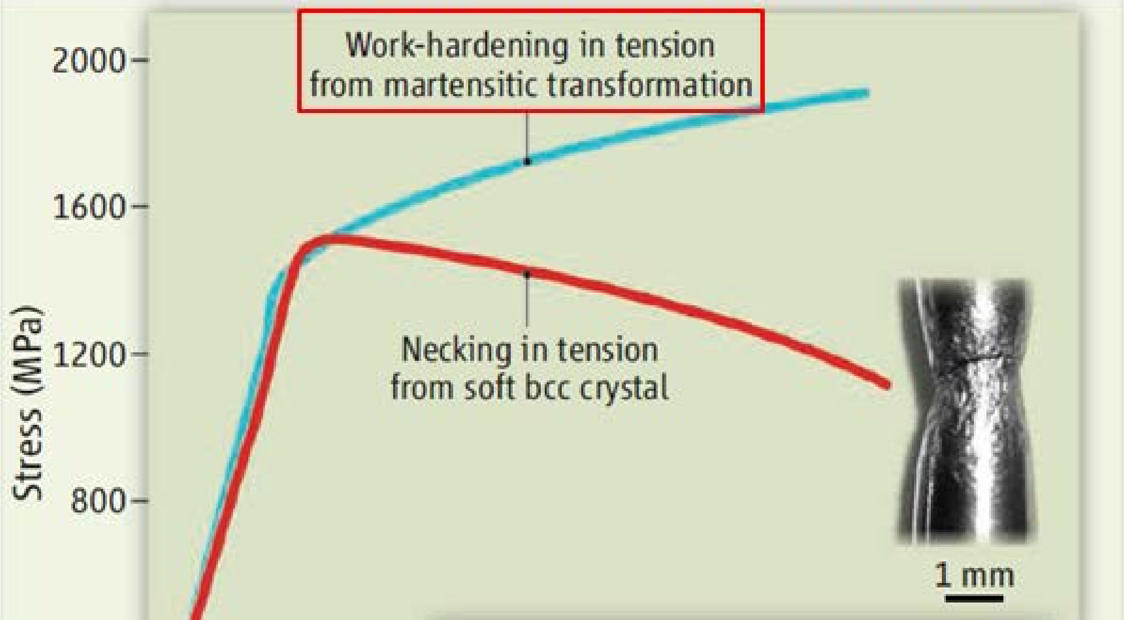

ZrCuAlCo	G (GPa)	ZrTiNbCuBe	G (GPa)
Cubic CuZr	29	bcc ZrTiNb	28
Glass	33	Glass	33

Development of a New Ti-based BMGC with High Work-hardenability

	Cu-Zr-Al system	Ti-Cu-Ni system
▷ Alloy system	Cu-Zr-Al system	Ti-Cu-Ni system
Secondary phase	CuZr Metastable B2 phase at RT "Shape Memory Behavior"	Ti-X Stable B2 phase at RT "Super-elastic Behavior"

Shape Memory Alloy (SMA)

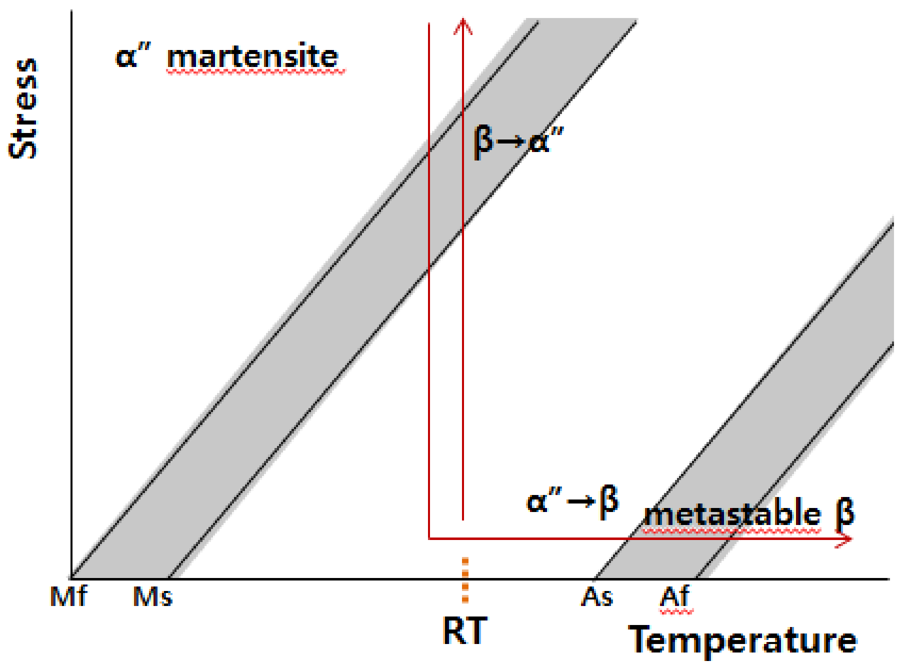

Super-Elastic Alloy (SE alloy)

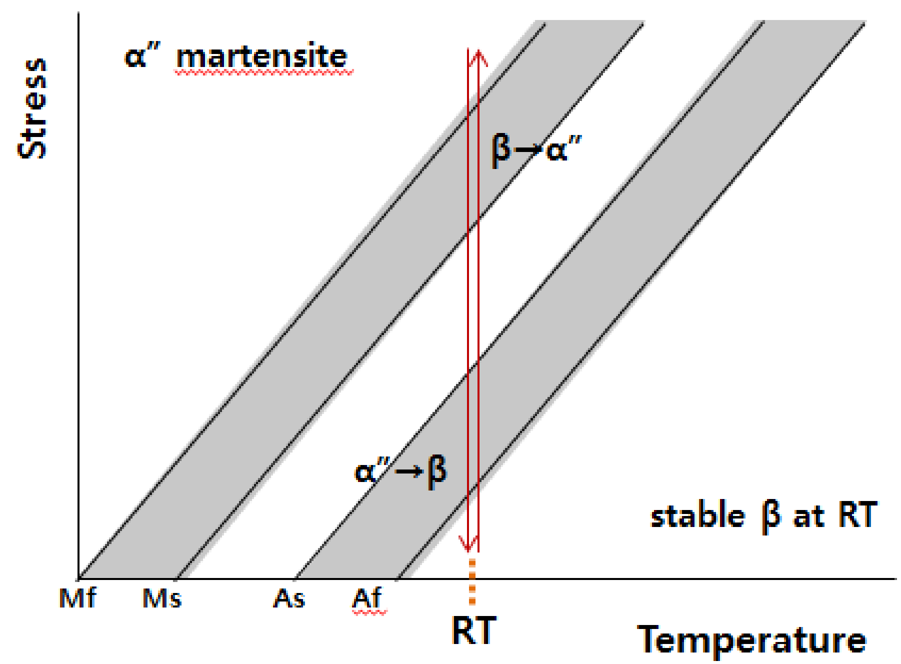

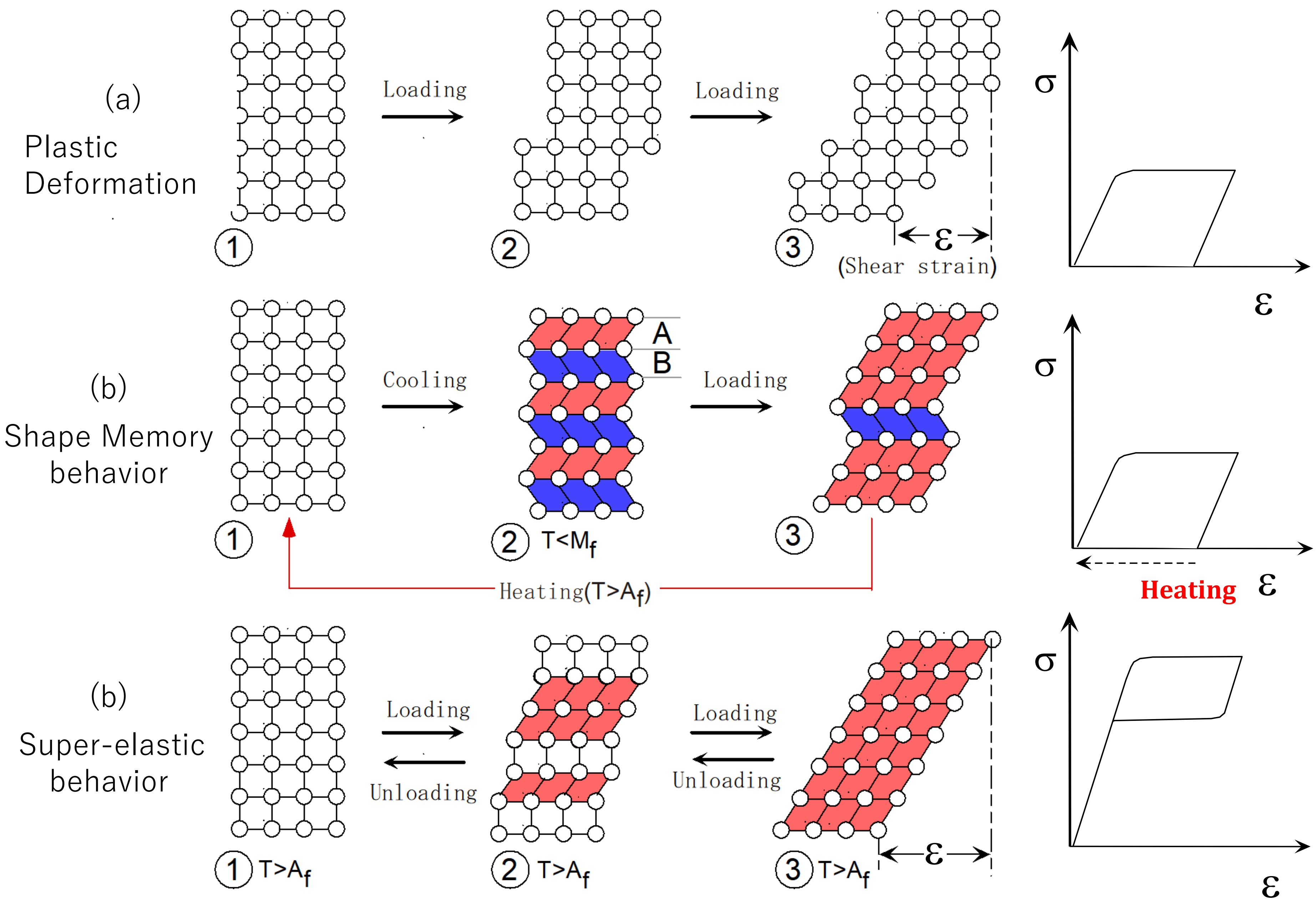

(a)
Plastic Deformation
Loading
Loading
(Shear strain)
σ
ε
(b)
Shape Memory behavior
Cooling
A
B
Loading
T<M_f
Heating(T>A_f)
Heating
(b)
Super-elastic behavior
Loading
Unloading
Loading
Unloading
T>A_f
T>A_f
T>A_f

Development of a New Ti-based BMGC with High Work-hardenability

▷ Alloy system	Cu-Zr-Al system	→	Ti-Cu-Ni system
Secondary phase	CuZr Metastable B2 phase at RT "Shape Memory Behavior"		Ti-X Stable B2 phase at RT "Super-elastic Behavior"

Ref: S.P. Alisova, et al, Russian Metallurgy, (5), 207-209 (1986)

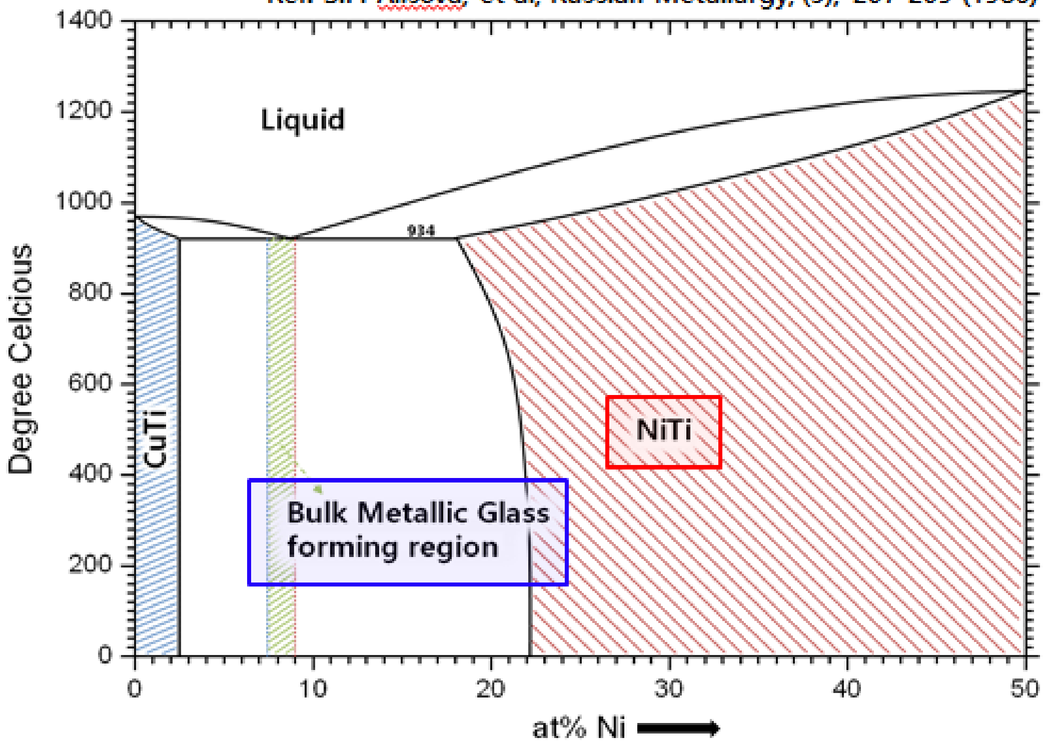

▷ TiCu-NiTi pseudo-binary eutectic

High glass forming ability ~ 1.5ϕ

+

NiTi ~ representative SMA

or

Ti-X ~ Superelastic alloy by phase transformable B2 phase

In-situ high energy X-ray diffraction under compression (APS 11-ID-C)

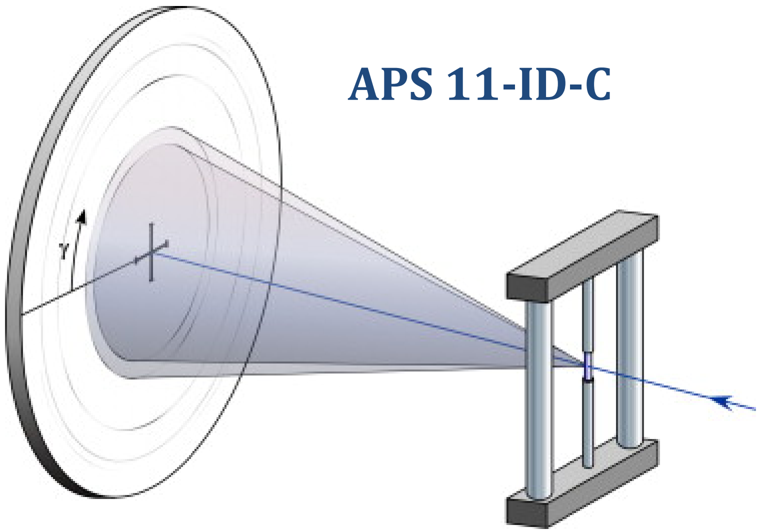

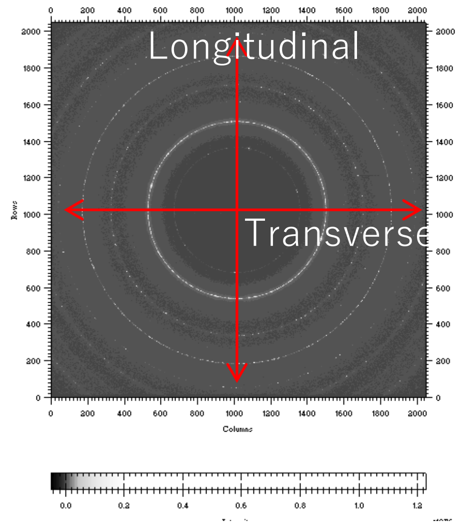

$(TiCuNiSnSi)_{98}Zr_2$

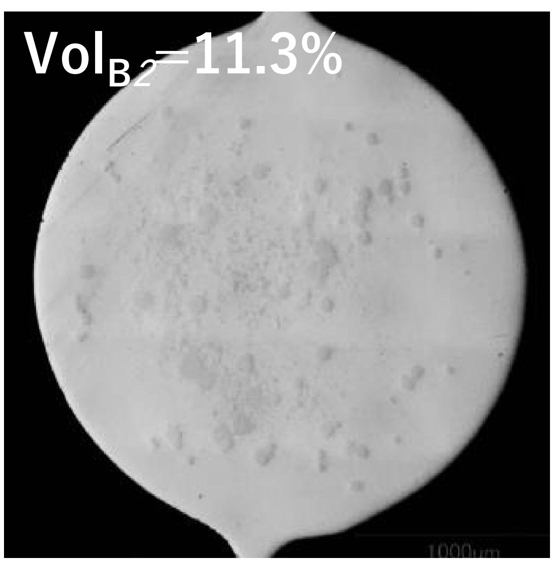

PT stress of 2nd phase ~ 850 MPa

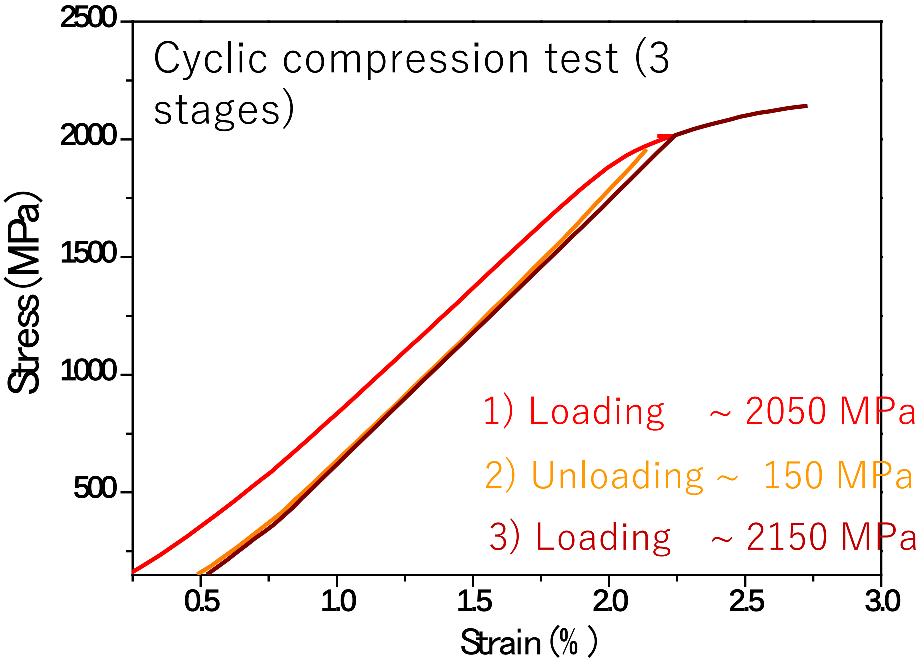

In-situ diffraction under compression: 1st loading ~ 2050 MPa

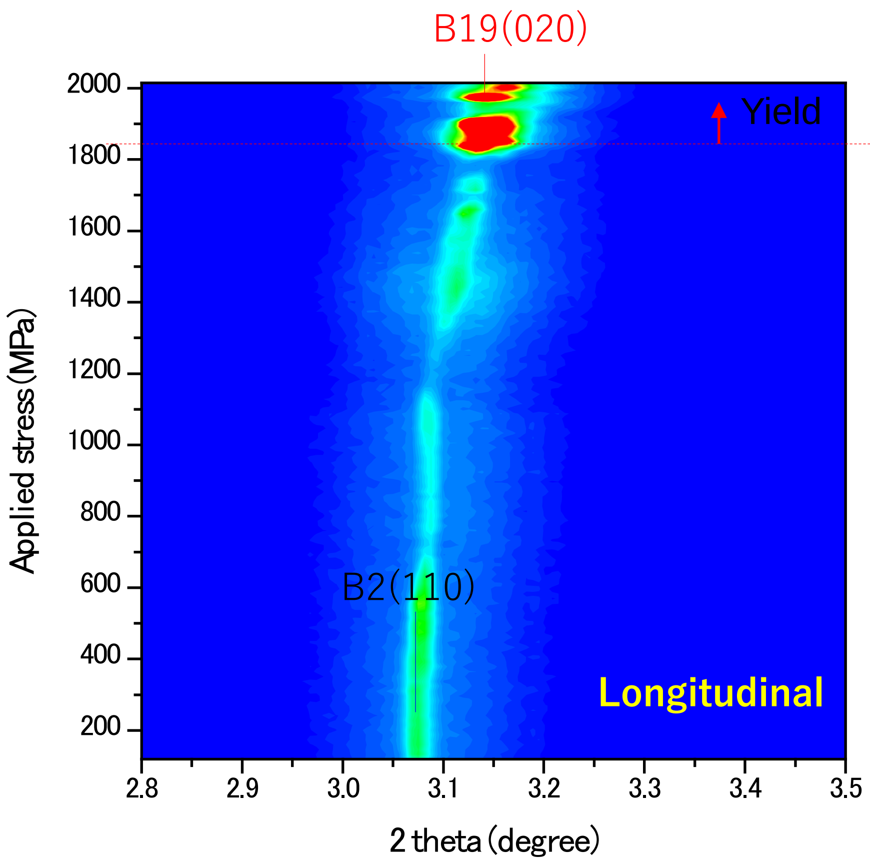

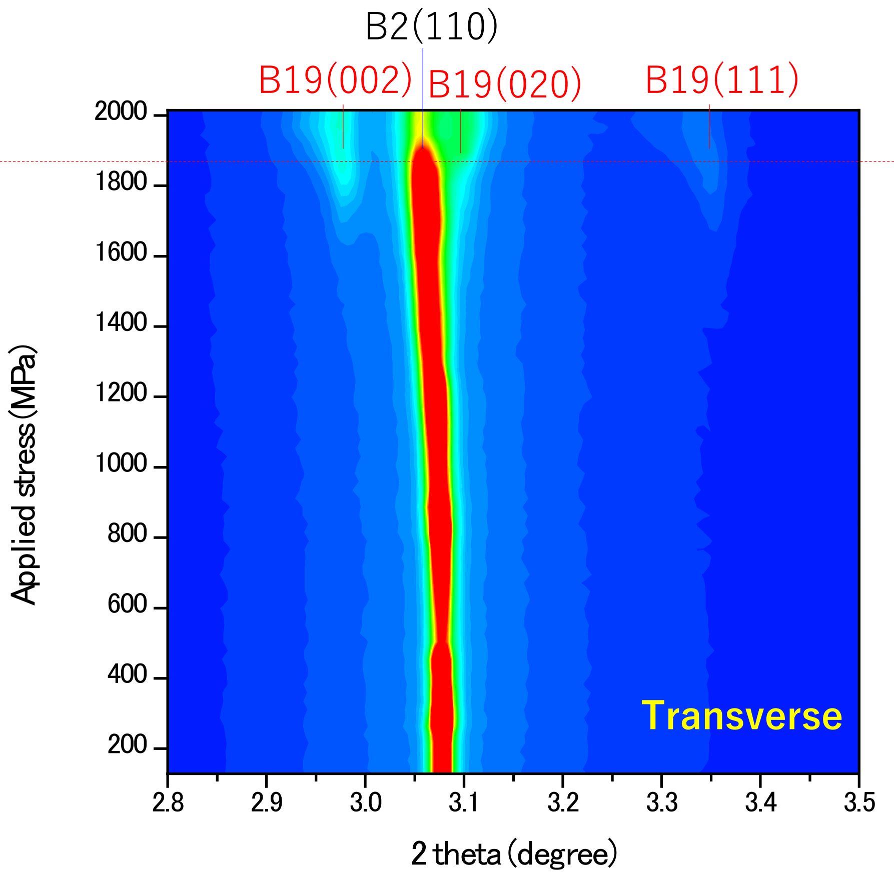

- M.T. is constrained by horizontal frame of MG matrix because of the imbalance of Poisson's ratio during M.T.(~0.5) with elastic loading of MG matrix (~0.33).
- Preferred orientation before deformation = B2 (110), Preferred orientation after deformation for Longitudinal direction = B19 (020) and for Transverse direction = B19(002), B19(020), B19 (111)

In-situ diffraction under compression: Unloading ~ 150 MPa

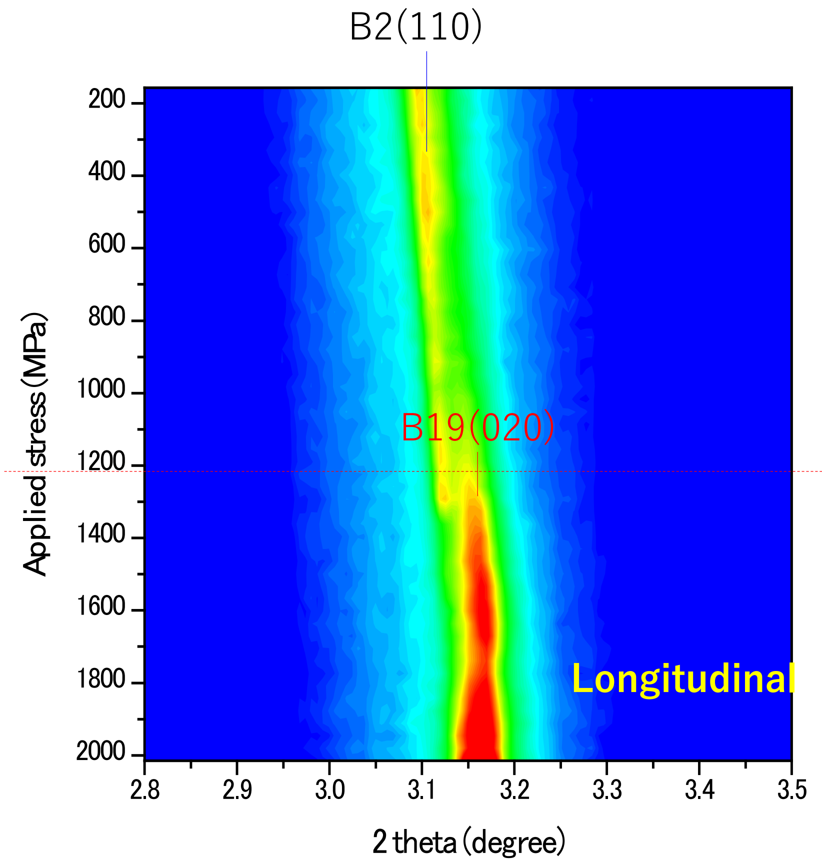

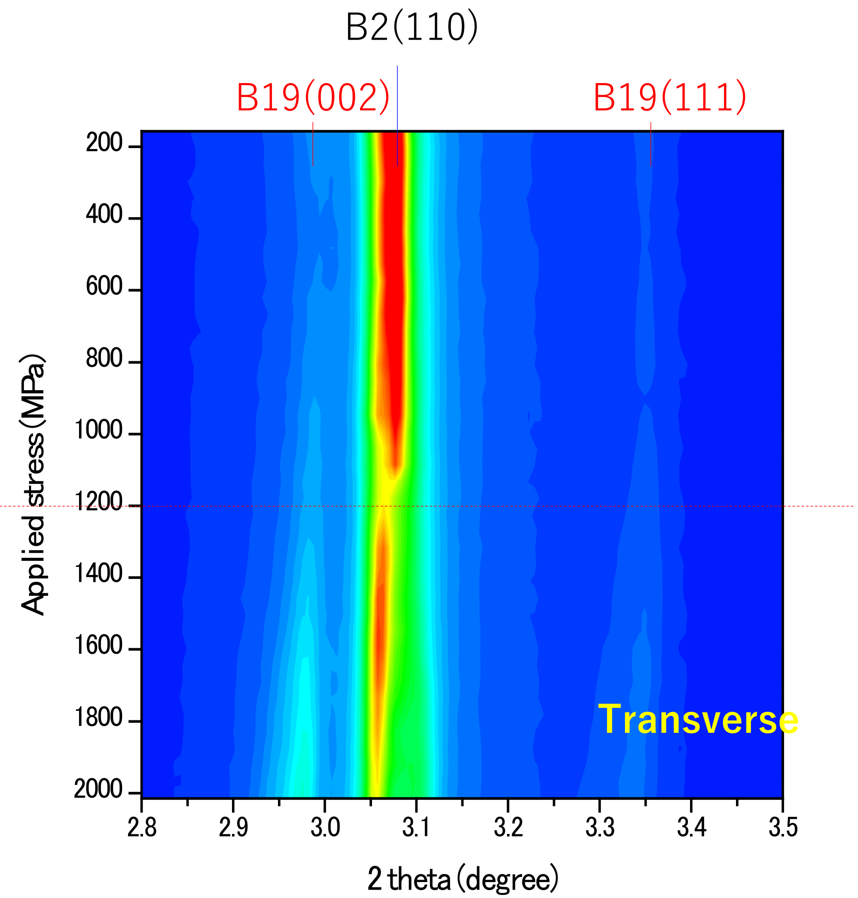

- After unloading down to ~150MPa, most of B19 reverse transformed to B2, but small fraction of B19(002) & (111) remained.
- Preferred orientation before deformation = B19 (020) / after deformation = B2(110)

In-situ diffraction under compression: 2^{nd} loading ~ 2150 MPa

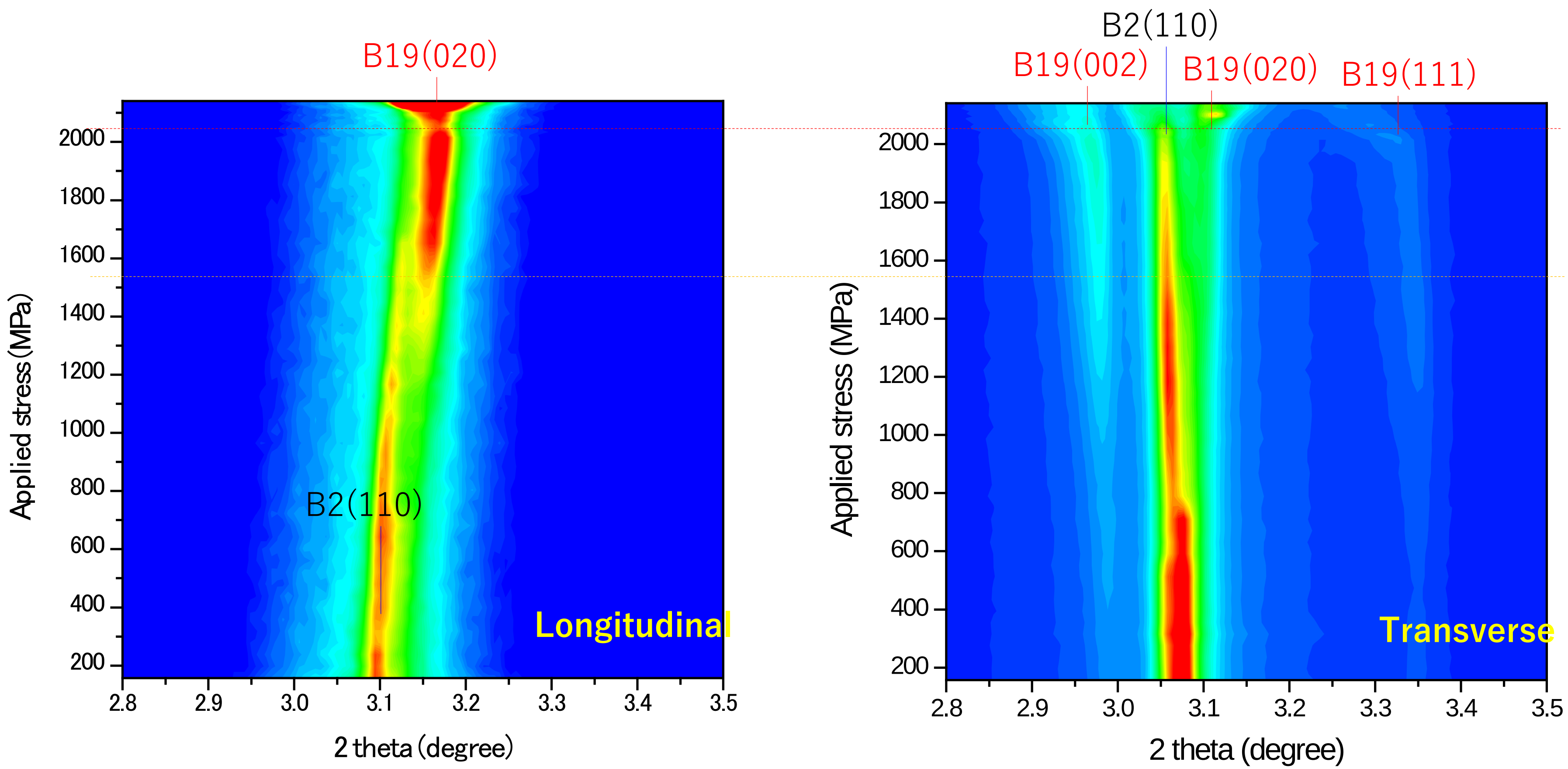

- M.T. is constrained by horizontal frame of MG matrix because of the imbalance of Poisson's ratio during M.T.(~0.5) with elastic loading of MG matrix (~0.33).
- Preferred orientation before deformation = B2 (110), Preferred orientation after deformation for Longitudinal direction = B19 (020) and for Transverse direction = B19(002), B19(020), B19 (111)

Origin for Improved work-hardenability in TRIP BMGC by SE 2nd phase

The observed work hardening in the CuZr based BMG composites cannot be solely attributed to the **1) intrinsic strain hardening of the B2 phases**, but also arises from 2) a constraining effect of the glassy matrix on the martensitic transformation and the subsequent deformation of the transformed phases. In theory, this constraint effect, also called *Eshelby back stress effect*, increases the elastic energy stored in the whole composite system, which leads to an increase in the applied stress and thus manifests as strain hardening in the BMG composite

Origin for Improved work-hardenability in TRIP BMGC by SE 2nd phase

1) "Strain hardening of transformable 2nd phase"

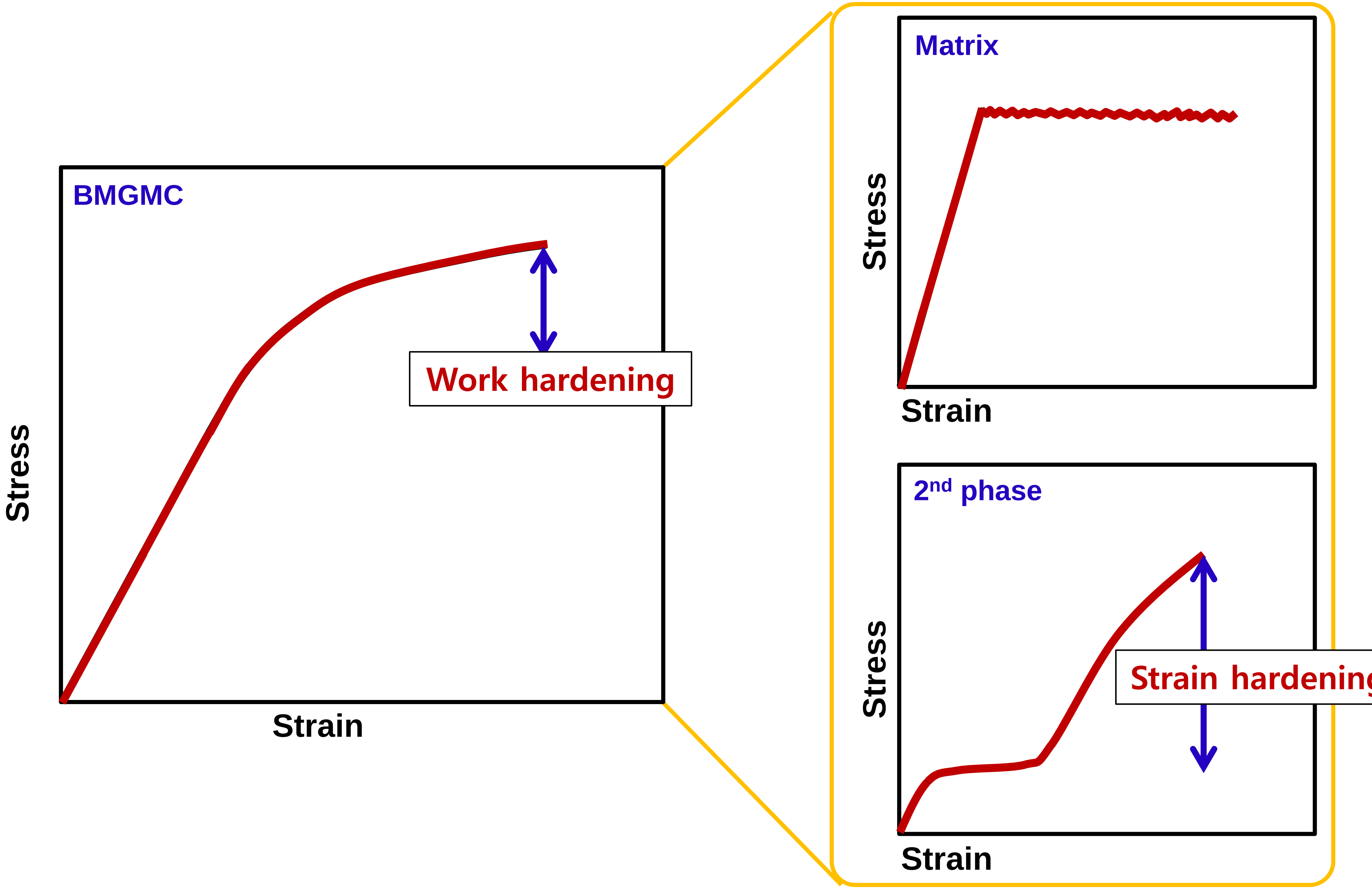

Origin for Improved work-hardenability in TRIP BMGC by SE 2nd phase

The observed work hardening in the CuZr based BMG composites cannot be solely attributed to the 1) intrinsic strain hardening of the B2 phases, but also arises from **2) a constraining effect of the glassy matrix on the martensitic transformation and the subsequent deformation of the transformed phases.** In theory, this constraint effect, also called ***Eshelby back stress effect***, increases the elastic energy stored in the whole composite system, which leads to an increase in the applied stress and thus manifests as strain hardening in the BMG composite

Origin for Improved work-hardenability in TRIP BMGC by SE 2nd phase

2) "Strong Eshelby back stress effect of transformable 2nd phase"

* Eshelby inclusion with elastic mismatch
→ Inhomogeneous stress/strain distribution
→ applying a effective transformation strain ϵ_{ij}^{T}

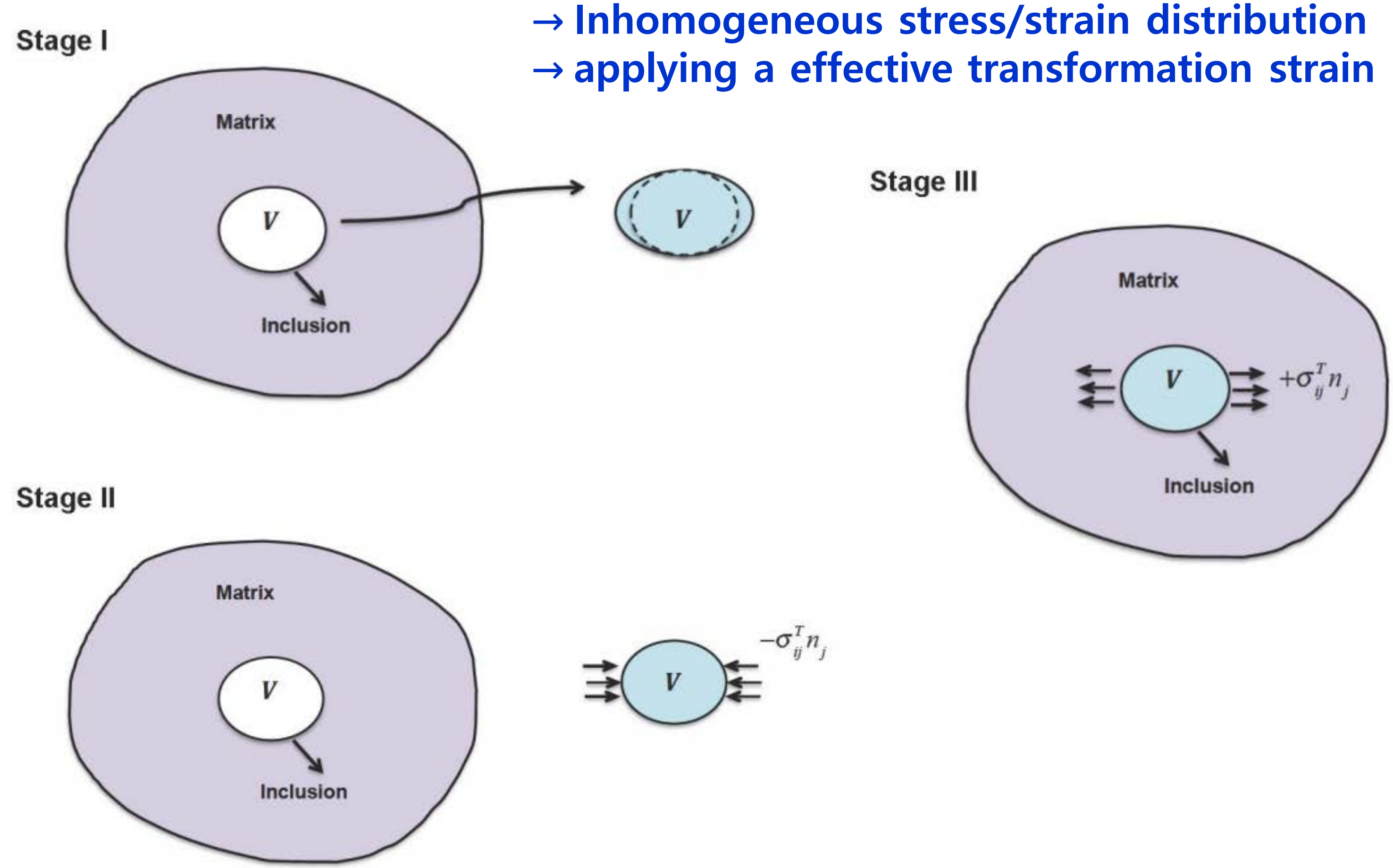

The schematic illustration of the three stages of Eshelby approach for solving the stress and strain fields due to the deformation of an inclusion in the matrix.

Origin for Improved work-hardenability in TRIP BMGC by SE 2nd phase

BMG composite with ceramic ZrC

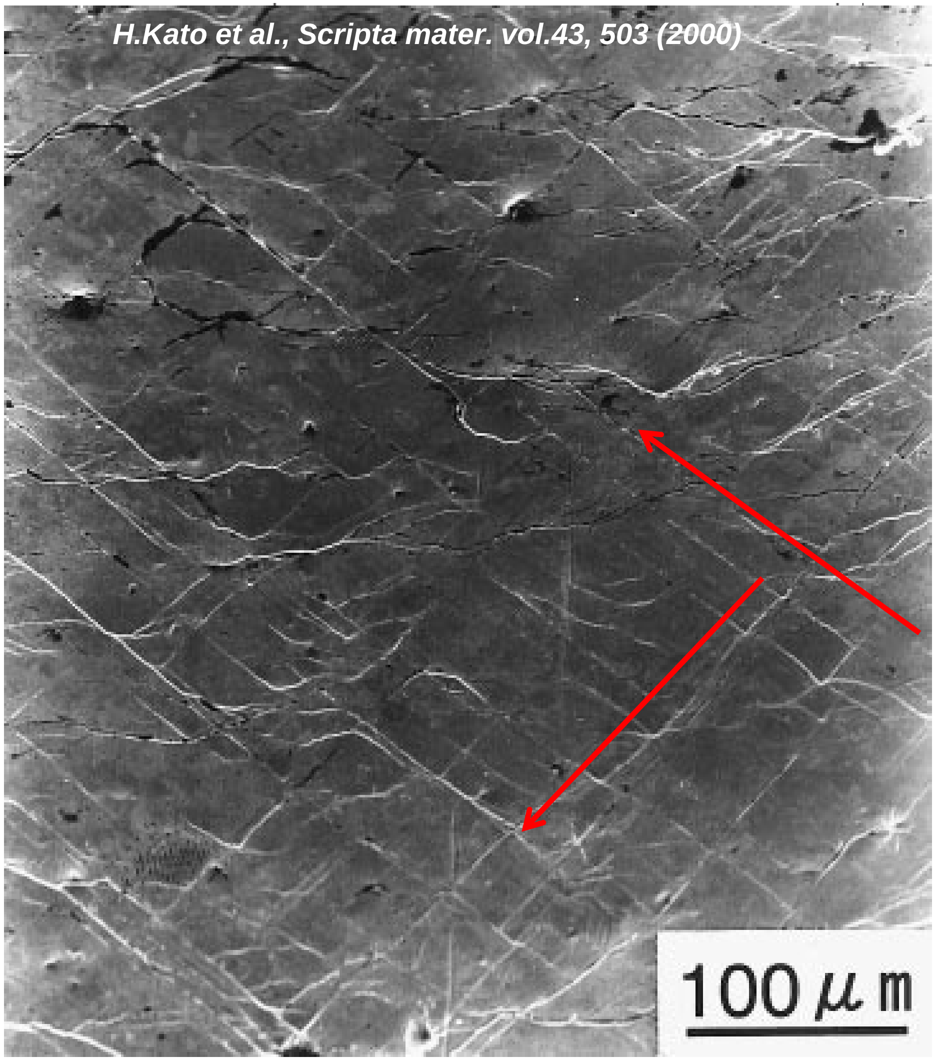

Origin for Improved work-hardenability in TRIP BMGC by SE 2nd phase

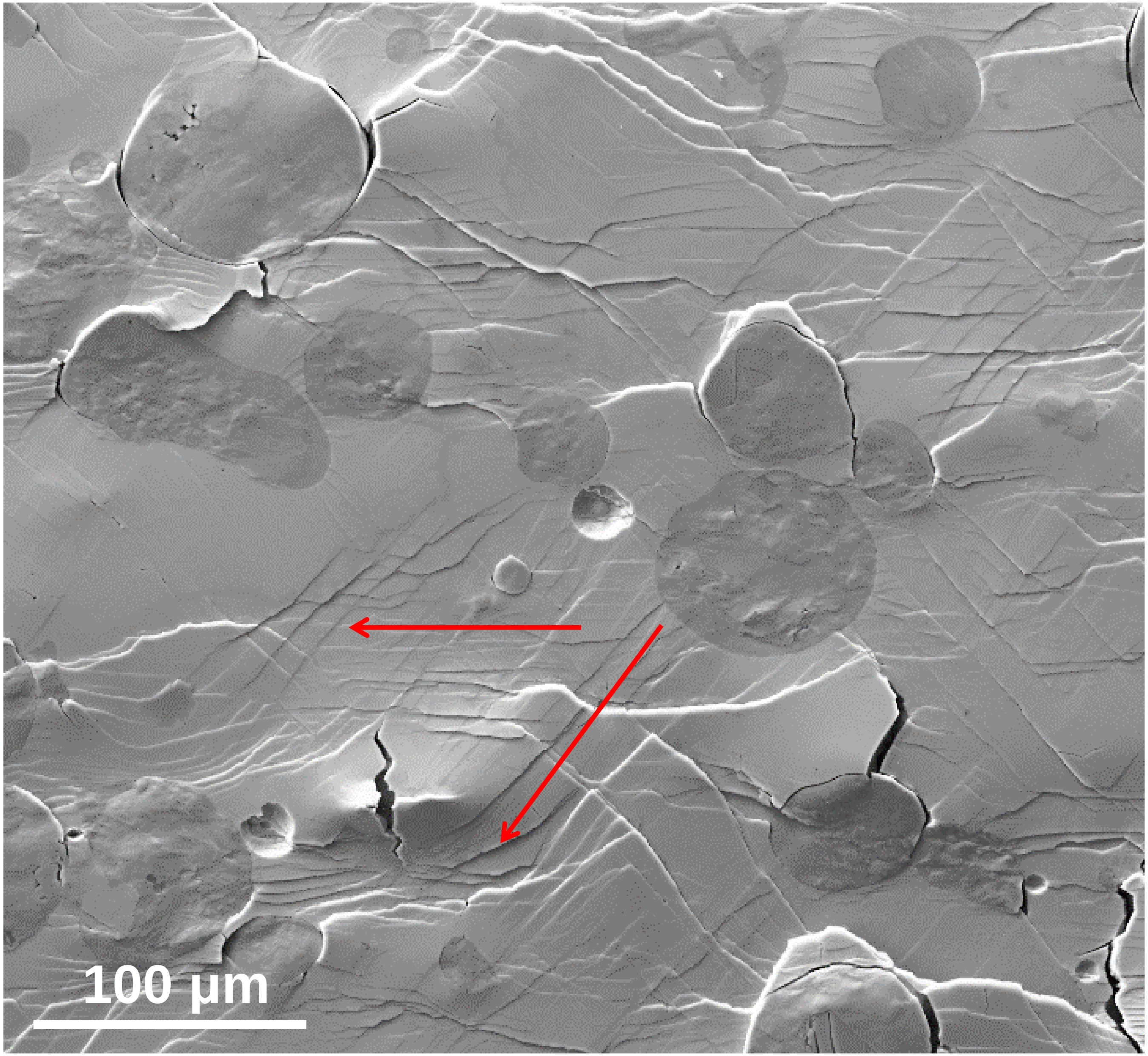

Origin for Improved work-hardenability in TRIP BMGC by SE 2nd phase

In-situ SEM test

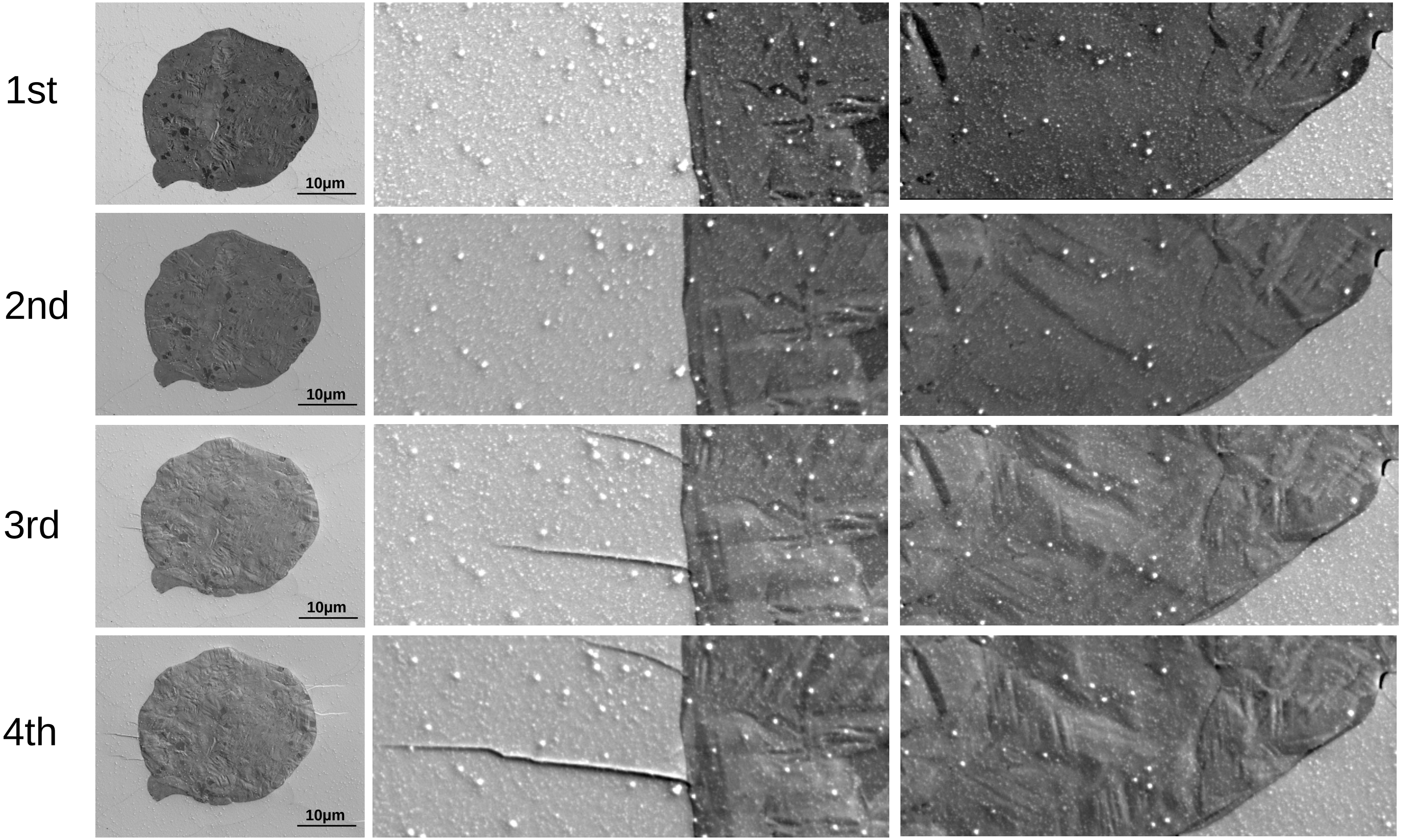

Martensitic transformation occurred during compressive deformation.

Direction of shear bands : perpendicular to the loading direction

In-situ synchrotron radiation _Advanced Photon Source (APS) 11-ID-C

In-situ compression

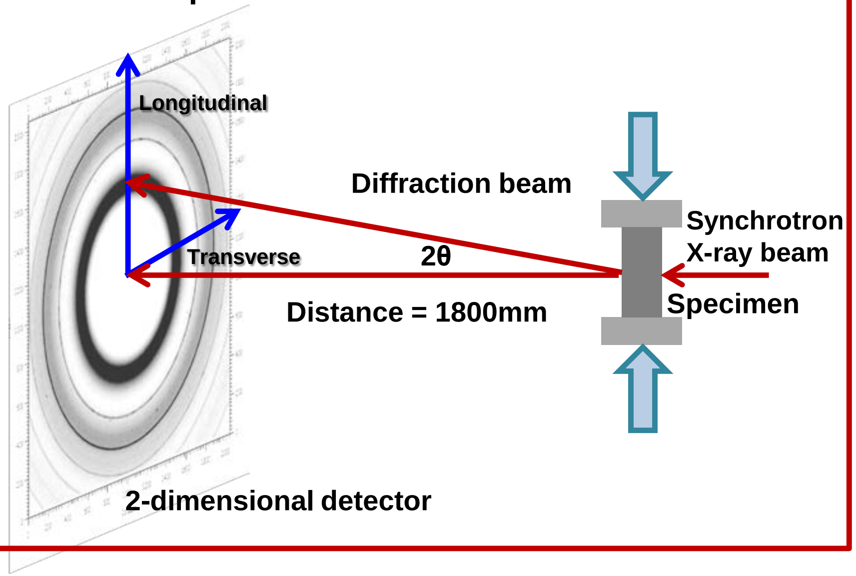

Rietveld refinement

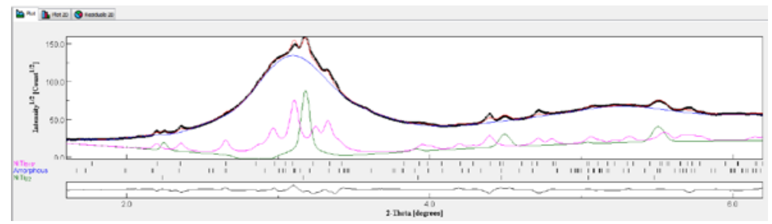

- Fitting at single azimuth angle
  Rwp : 5.81% (<10% is good fitting)
- Amorphous : Cu3Zr, orthorhombic, Pnma – Paracrystalline
  (small crystallite, large residual stress,
  Ref. M.Baricco, et al., J.Allo.Comp. 495, 377 (2010))
- NiTi_B2, NiTi_B19’

Fitting through whole azimuth angle

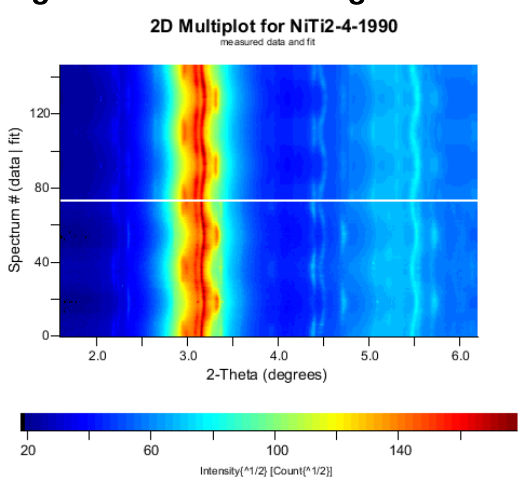

Lattice information, Phase fraction, Texture

Fitting through whole stress level

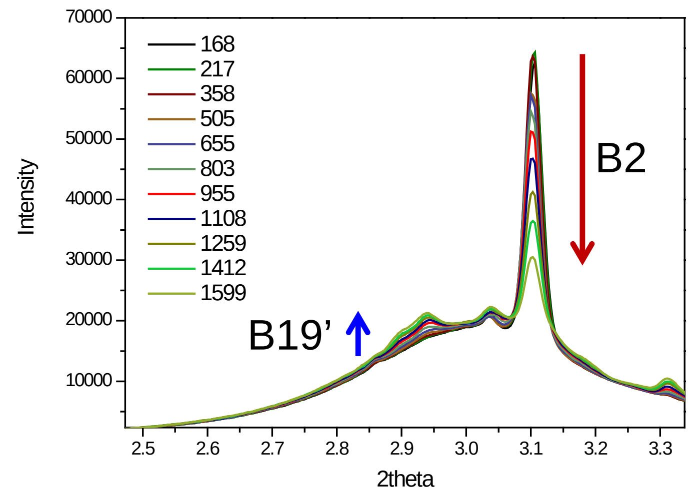

The fraction of martensitic transformation in elastic region

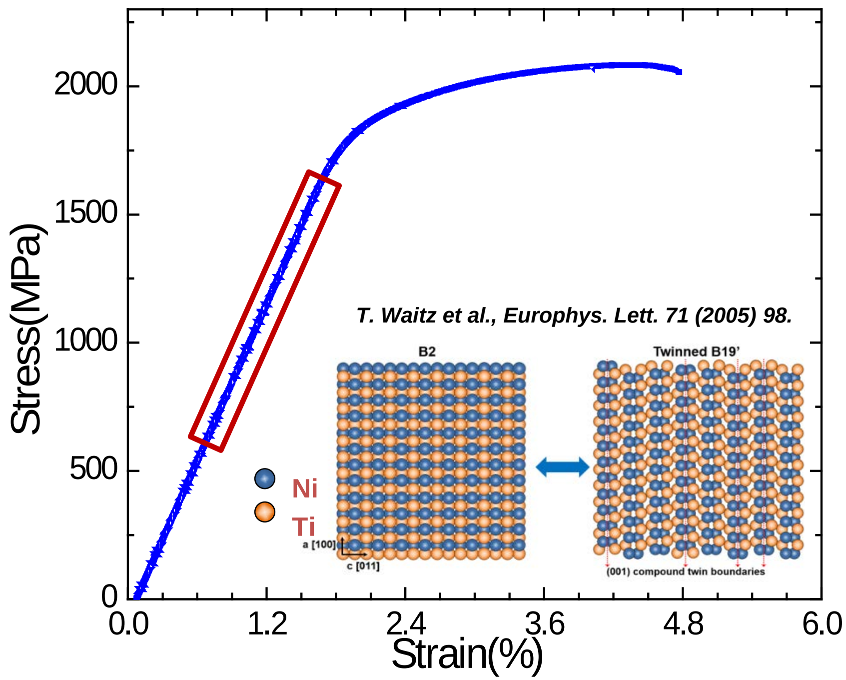

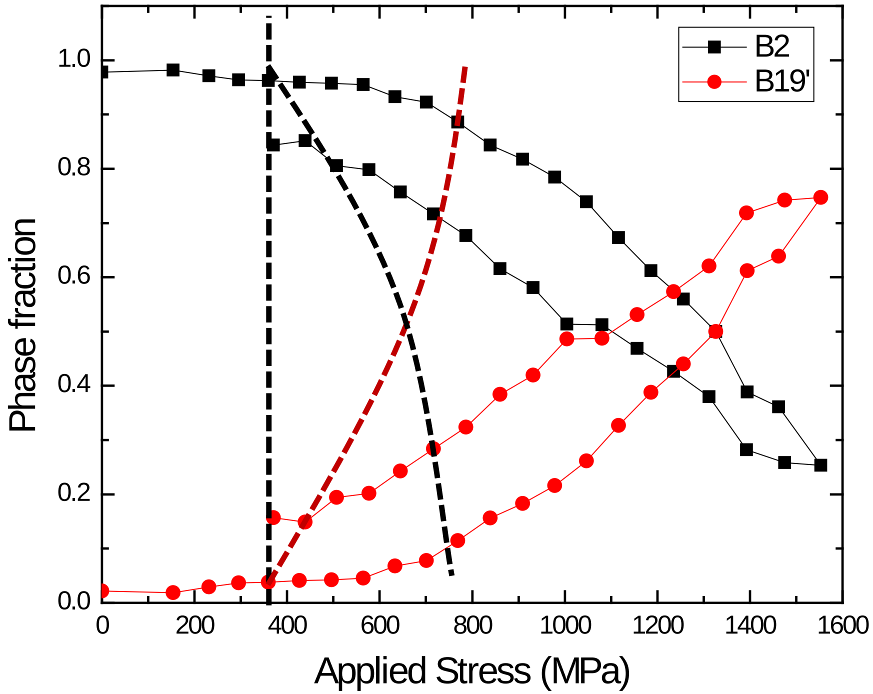

- **Martensitic transformation occurred gradually.**
- **Martensitic transformation is delayed by the interaction between 2nd phase and metallic glass matrix.** (Δmodulus btw matrix & 2nd phase >30GPa)

In-situ synchrotron radiation _Advanced Photon Source (APS) 11-ID-C

Phase fraction

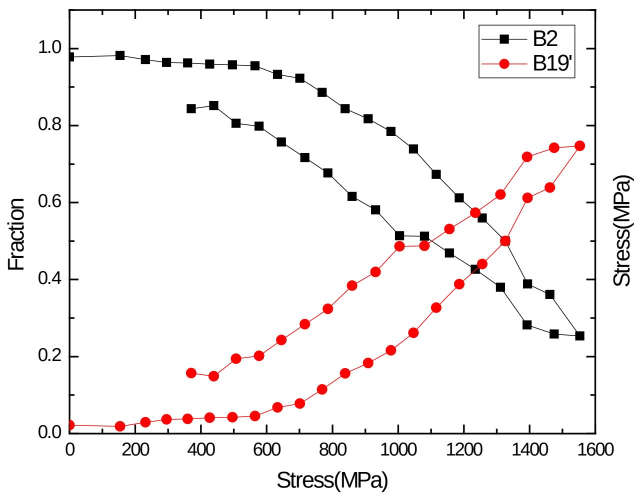

Lattice strain

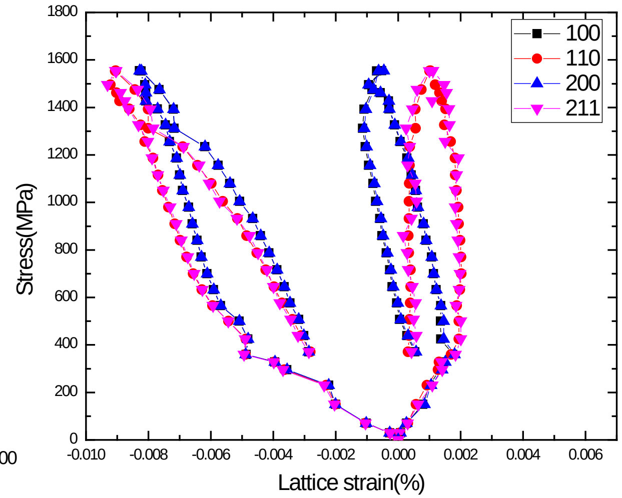

Effective stress

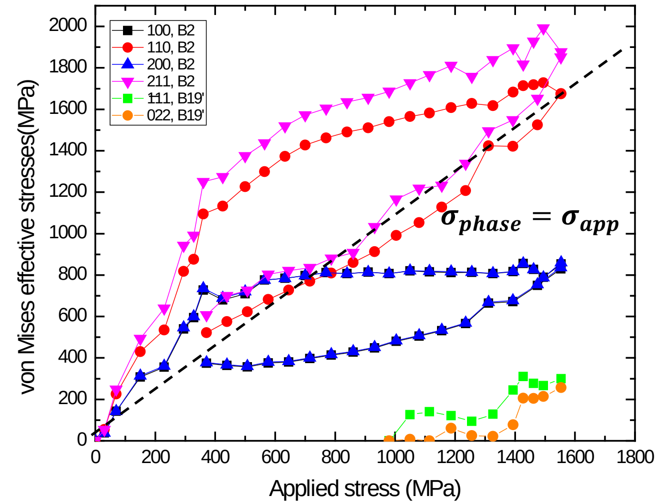

Texture of B2

Before load

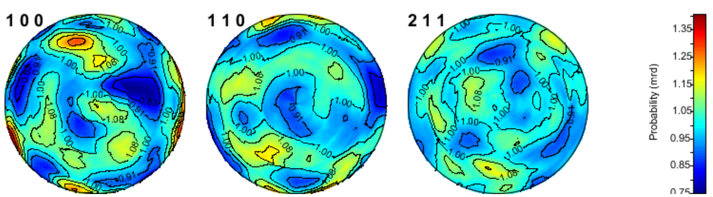

Maximum load

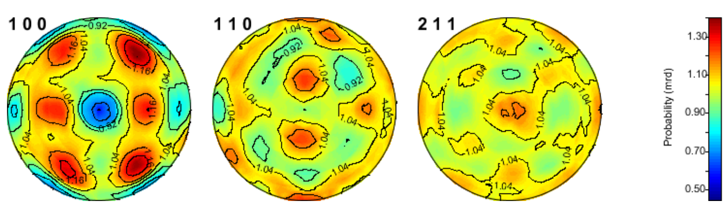

E100 = 143GPa
E110 = 216GPa
E211 = 240GPa

$$\sigma_1 = \sigma_3 = \frac{E}{1+\nu}\varepsilon_1 + \frac{\nu E}{(1+\nu)(1-2\nu)}(\varepsilon_1+\varepsilon_2+\varepsilon_3),$$

$$\sigma_2 = \frac{E}{1+\nu}\varepsilon_2 + \frac{\nu E}{(1+\nu)(1-2\nu)}(\varepsilon_1+\varepsilon_2+\varepsilon_3),$$

$$\sigma_{\mathrm{eff}} = \frac{1}{\sqrt{2}}\left[(\sigma_1-\sigma_2)^2+(\sigma_2-\sigma_3)^2+(\sigma_3-\sigma_1)^2\right]^{1/2}$$

1. Martensitic transformation occurred at <100> B2 crystallites.

Compare with soft crystalline 2nd phase

BMG composite with 10% Ta

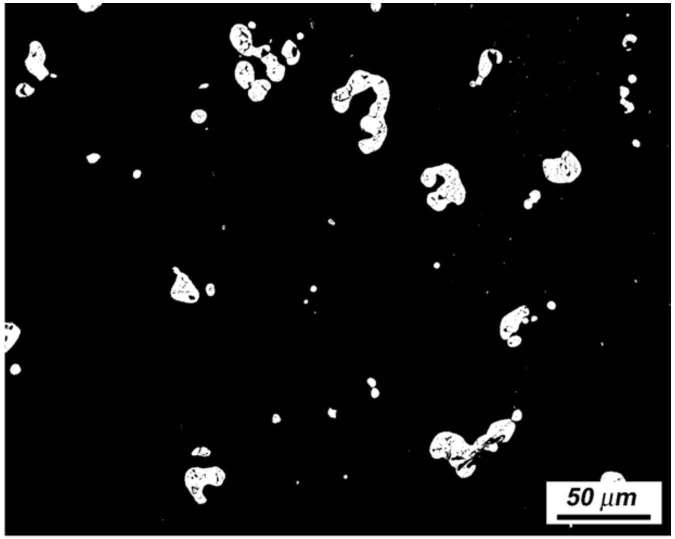

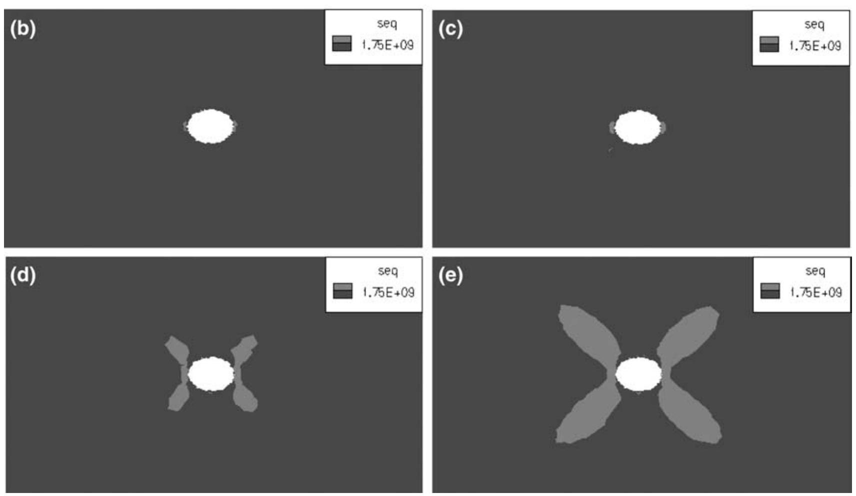

R.T. Ott et al. , Acta Mater. vol. 53, 1883 (2005)

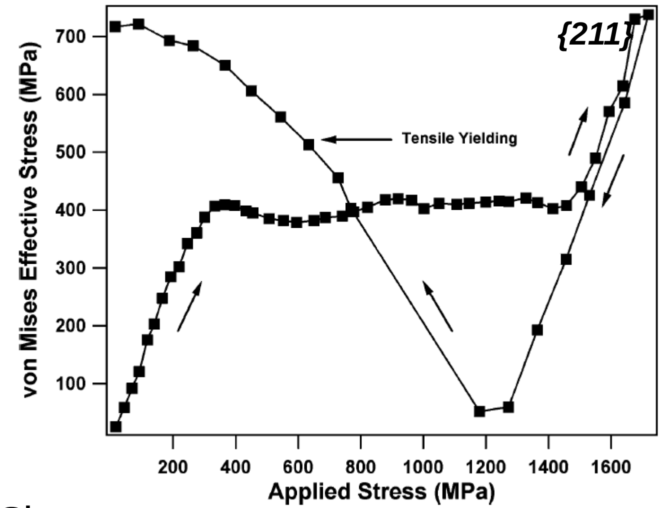

Shape memory

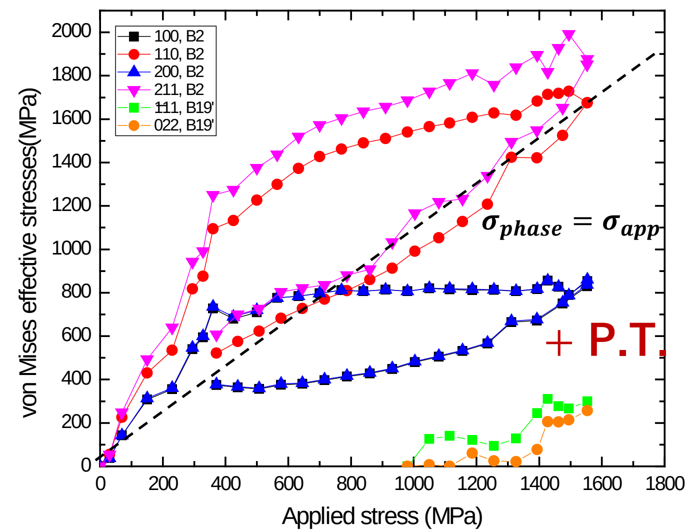

2. Misfit stress between matrix and 2nd phase become less pronounced by martensitic transformation of 2nd phase.

DFT-based MD simulation

Stress-induced phase transformation of NiTi in BMGC

Potential based MD simulation

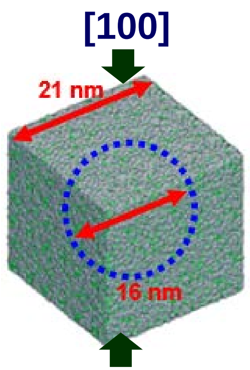

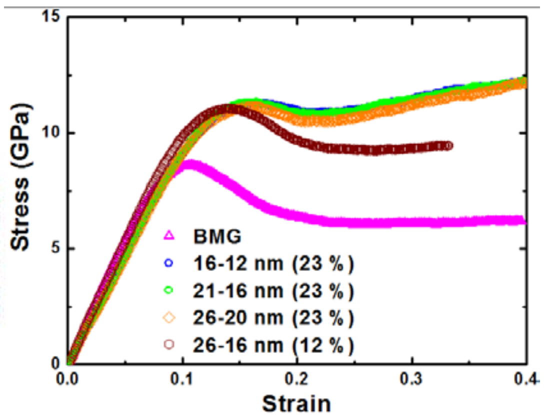

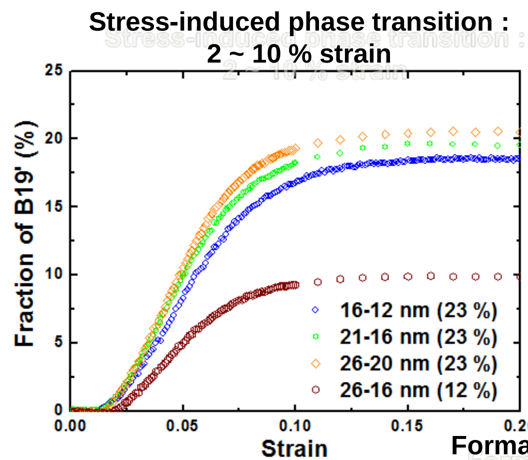

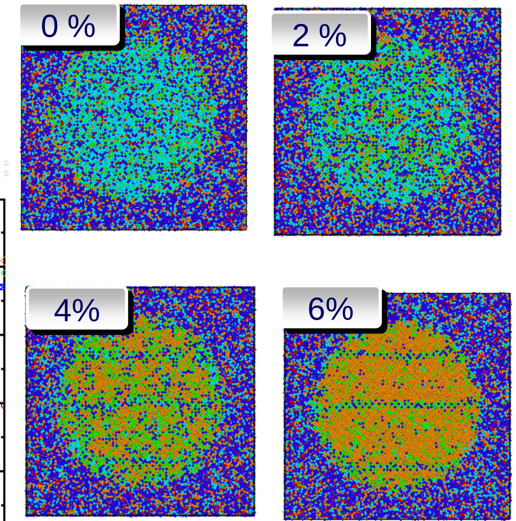

* Visualized based on the common neighbor analysis

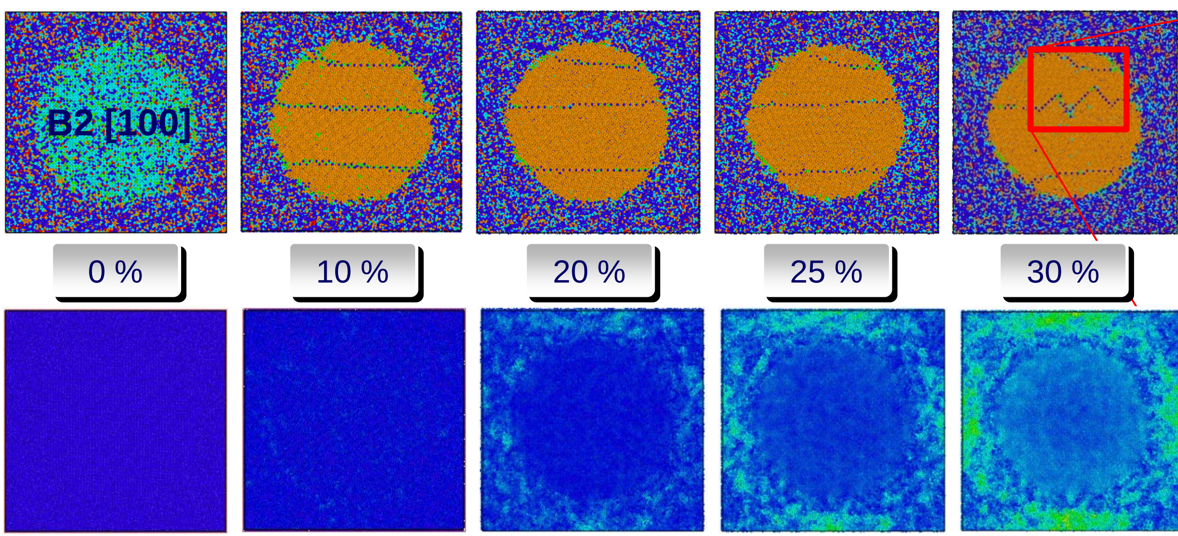

* Visualized based on the atomic strain analysis (min=0, max=0.9)

Formation of multiple martensite domains

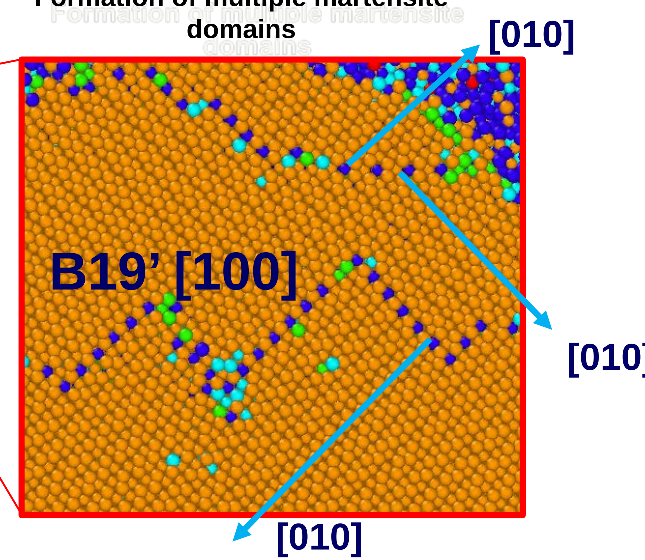

Formation of shear band along lateral directions

DFT-based MD simulation

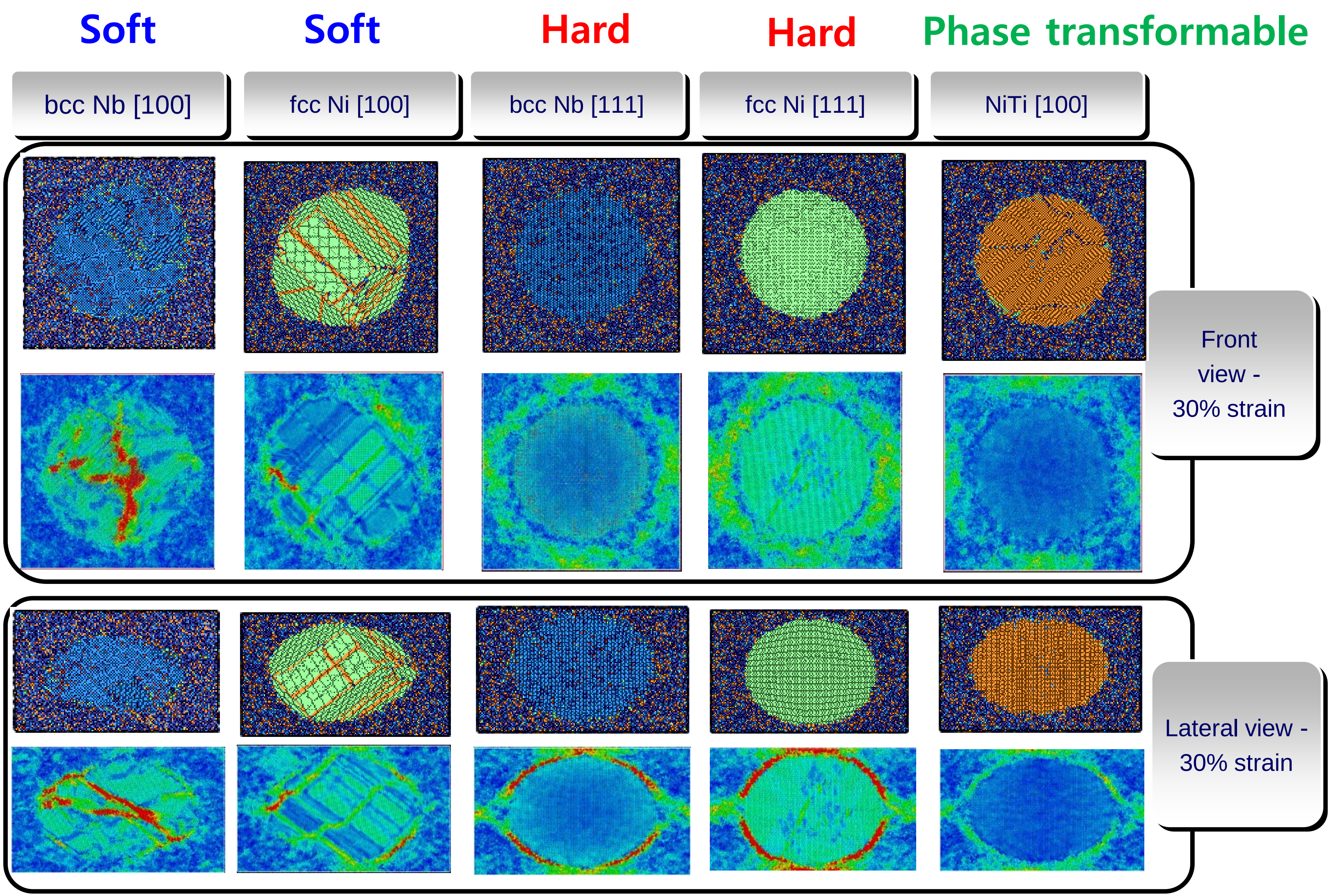

* Visualized based on the atomic strain analysis (min=0, max=0.9)

Strain localization of NiTi containing cell is less pronounced than other cases

Origin for Improved work-hardenability in TRIP BMGC by SE 2nd phase

Contribution to mechanical properties		Mono lithic	Soft	Hard	Transformable
Character of 2nd phase		no	elastic+ plastic	elastic	**elastic+ plastic+ TRIP**
1. Eshelby backstress effect		-	depends	weak	**Strong**
2. Damage management	Blocking shear band propagation	no	middle	middle	**Superior (reusable for SE phase)**
	Stress/strain localization	-	localized	localized	**Delocalized**

Soft crystalline

bcc Nb [100]

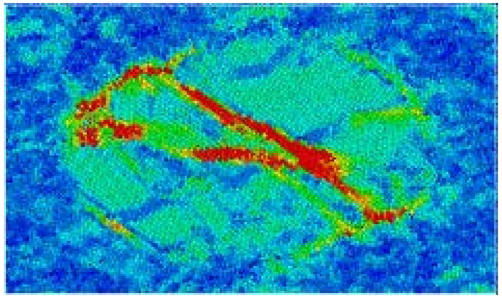

Hard ceramic

bcc Nb [111]

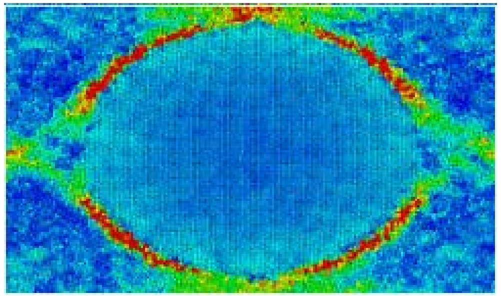

Transformable

NiTi [100]